Electrochemical Modulation of Sickle Cell Haemoglobin Polymerisation

Zeshan Iqbal

A thesis submitted in
partial fulfilment for
the degree of
Doctor of Philosophy

University College London
University of London
January 2008

ProQuest LLC
789 East Eisenhower Parkway
P.O. Box 1346
Ann Arbor, MI 48106-1346

بسم اللہ الرحمٰن الرحیم

Dedicated to my Parents

Acknowledgements

I'd like to thank Dr. Daren Caruana for all his support, encouragement and brain-storming discussions in his office over the last 4 years. It has been a pleasure to have worked with him as a colleague and known him as a friend over the last five years and his help in writing up this thesis has been immense. His enthusiasm and determination for all his work is an infectious and admirable quality.

I would also like to thank Profesor Mike Horton and Dr Rachel McKendry for their help and discussions regarding my work and for choosing me to participate in the National Institute of Material Science Conference in Tsukuba in Japan. Looking at the facilities in Japan and the work being done in the field of nanotechnology was an incredible experience, and climbing Mount Tsukuba in torrential rain whilst being "chased" by giant hornets is something I will always remember. Thanks also go to Dr Laurent Bozec for his discussions and analysis regarding the AFM experiments as well as training me on the Dimension AFM. A special thank you goes to Matthew Li who performed the mathematical modeling of oxygen depletion at the electrochemical cell and Dr Enrique Millan for his help with the direct electrochemistry experiments; his stories about Venezuela ensured the lab was never quiet over the summer months.

Special compliments are also due to Jim Stevenson in the technical workshop for his amazing manufacturing skills; the look on his face when I asked him to help manufacture the matrix electrode still brings a smile to my face, whilst thanks must also go to Dick Waymark for his incredible electronic skills, John Hughes for the consistently perfect glassware he made, and to the rest of UCL Chemistry Department technical support team.

A big thank you is also reserved for the wonderful people that I have worked with in G16 over the past 4 years: Bushra Chaudry, who I have known since the beginning of my undergraduate degree, for her help in study related and general matters over the last seven years, Emina Hadzifejzovic for her motherly nature in taking care of everyone in the lab and for the supplying me with fruits and daily encouragement, Jorge Sanchez for our daily discussions on the state of Spanish football as well as Katherine Knight, Katherine Holt and Estelle Bernard. I would also like to thank Moyu Watari, Dr Patrick Mesquida, Jaco Groot and Macarena Blanco all of whom I've had the pleasure

of working with at some point during my time at UCL and for funding I would like to thank the IRC and UCL Chemistry Department.

An immense thank you also goes to my friends and colleagues at Merck Sharpe and Dohme, Hoddesdon: to my manager Mukesh Solanki for letting me write up my thesis after hours at work; to Murtaza Kaderbhai and Ish Matharu for the laughs, jokes and tips and most importantly for keeping me sane during my time at MSD; to Neeta Camadoo who was my writing colleague in the office even if she was more interested in talking than studying; and to the rest of the guys there.

Finally, a special thank you and deep gratitude is reserved for my family; in particular to my wonderful parents for all their unconditional love, support, encouragement and prayers. I can never thank you enough or ever repay you for all you have done for me in my life and so it goes without saying that this thesis is dedicated to you both. I would also like to thank my brothers Osman and Ali for taking my mind off the long hours of writing by playing ProEvo Soccer and rightfully earning the title of "Champ of the House", and to my mother-in-law and brothers-in-law Haris and Hamza for their kind words and support. I would also like to thank Shiraz Malik, Zahoor Yousaf and the rest of the "ikhwa" for their encouragement and dua's and to Adil Hussain for covering my voluntary duties when I was writing up.

Lastly, an enormous thank you is reserved for my wonderful wife Sarah for all her love and endless patience in putting up with me during the writing period. Her kindness, generosity and regimental efforts in ensuring that I completed this thesis have been a sight to behold and I thank her from the bottom of my heart for bearing with me during the difficult periods.

And finally all Praise and Hamd is for Allaah Azzawajal (subhanahu wa'ta Allaah) without whom notihing is possible. I thank Him for giving me the strength and desire to complete my thesis and for the numerous blessing He's bestowed upon me and my family: "wa akhirana dawana Alhamdolillahi Rabbil Alameen".

Electrochemical Modulation of Sickle Cell Haemoglobin Polymerisation

Zeshan Iqbal
University College London, 2008

Abstract

Sickle cell haemoglobin differs from normal haemoglobin by a single amino acid in its β chain. This amino acid replacement, from glutamic acid to valine, causes polymerisation of proteins into defined long insoluble fibres with a typical diameter of 21.5 nm. The polymerisation is triggered by the formation of deoxyhaemoglobin from oxyhaemoglobin in low oxygen partial pressures, which results in a conformational change in the secondary structure of the protein. Pathogenesis in sickle cell disease depends on the polymerisation and gelation of deoxygenated HbS molecules.

In this work, an electrochemical method has been described to modulate the oxygen concentration in an optically transparent thin layer cell to produce deoxyhaemoglobin whilst monitoring the extent of polymerisation using turbidity measurements. The oxygen was depleted in the vicinity of the electrode and triggered the polymerisation. The dependence of protein concentration, temperature, pH and ionic strength on the nucleation and elongation of HbS polymerisation was characterised at the electrode surface and the kinetics of polymerisation was investigated using a model for fibrillogenesis describing a two-step process of nucleation followed by elongation. The rate constants, determined for a number of conditions, showed that nucleation is far slower than the growth whilst polymerisation at the surface was demonstrated to occur in three stages, with an initial time delay when no structures were observed followed by growth of fibrous hair-like strands and finally gel-like aggregation. An understanding of the factors which affect polymerisation at a surface and an insight into the dynamics and mechanism of polymer aggregation and the pathophysiology of sickle cell disease has been provided. A screening method for substances that effect the fibre nucleation and/or growth that could be valuable to the pharmaceutical industry for treating sickle cell disease is also presented.

Table of Contents

1 Introduction

2 Experimental Materials, Methods and Equipment

3 HbS Aggregation in Pt Coil Cell

4 HbS Aggregation in Au Micromesh Cell

5 HbS Aggregation in Pt Matrix Cell

6 Anti-Sickling Strategies

7 Direct Electrochemistry of HbS Polymers

8 Concluding Remarks

9 References

Appendices

Table of Figures

Table of Tables

Index of Abbreviations

AFM	= Atomic force microscopy
Au	= Gold
Ag	= Silver
CO	= Carbon monoxide
CO-HbS	= Carbon monoxide sickle cell haemoglobin
c_0	= Initial concentration
c_p	= Concentration of haemoglobin in the polymer phase
CE	= counter electrode
ΔC_P	= Polymerisation heat capacity change
c_{sat}	= Solubility
CV	= Cyclic voltammetry
D	= Diffusion coefficient
DeoxyHb	= Deoxygenated haemoglobin
DeoxyHbS	= Dexoygenated sickle cell haemoglobin
DIC	= Differential interference contrast
Δ	= Diffusion layer thickness
2,3-DPG	= 2,3-diphosphoglycerate
E	= Potential
$E_{initial}$	= Initial potential
E_{final}	= Final potential
Fe	= Iron
Fe (III)/Fe (II)	= Iron (III/II) redox couple
ΔG	= Polymerisation Gibbs free energy change

Glu	= Glutamic acid
γ	= Activity coefficient
H_2	= Hydrogen
ΔH	= Polymerisation enthalpy change
Hb	= Haemoglobin
HbA	= Adult haemoglobin
HbA_2	= Haemoglobin A_2
HbC	= Haemoglobin C
HbF	= Fetal haemoglobin
HbS	= Sickle cell haemoglobin
HCl	= Hydrochloric acid
He	= Helium
H_2O_2	= Hydrogen peroxide
HOPG	= Highly oriented pyrolytic graphite
H_2SO_4	= Sulphuric acid
IHP	= Inositol hexaphosphate
K	= Equilibrium constant
k_1	= Nucleation rate constant
k_1	= Elongation rate constant
KCl	= Potassium chloride
Leu	= Leucine
N_2	= Nitrogen
NaCl	= Sodium chloride
NaOH	= Sodium hydroxide
O_2	= Oxygen

O^{2-}	= Superoxide
OH^-	= Hydroxyl ions
OTE	= optically transparent electrode
OxyHb	= Oxygenated haemoglobin
OxyHbS	= Oxygenated sickle cell haemoglobin
PG	= Pyrolytic graphite
Phe	= Phenylamine
PLL	= Poly-L-lysine
Pt	= Platinum
R	= Rest state of heamoglobin
RBC	= Red blood cell
RE	= Reference electrode
s	= Seconds
SCA	= Sickle cell anaemia
SCD	= Sickle cell disease
T	= Tense state of haemoglobin
$T\Delta S$	= Polymerisation entropy change
Val	= Valine
WE	= Working electrode

Chapter 1: Introduction

1.1 Sickle Cell Anaemia

Sickle cell anaemia (SCA) is the most common type of a group of autosomal recessive disorders termed as sickle cell disease (SCD). It is a genetic disorder of the blood in which the red blood cells (RBC) curve into a sickle shape due to the production and, most importantly, polymerisation of mutant sickle haemoglobin (HbS). It is a disease which afflicts millions of people throughout the world, in particular those whose ancestors come from equatorial regions such as sub-Saharan Africa, Saudi Arabia, South America and India, and clinical manifestations include amongst others severe haemolytic anaemia, pain crises, stroke, and chronic damage to vital organs such as lungs, kidneys and liver.

The fundamental process of HbS polymerisation inside sickle erythrocytes has been studied by almost every physical technique of protein chemistry, including electron microscopy, single-crystal X-ray diffraction, nuclear magnetic resonance, circular dichroism spectroscopy, laser photolysis and temperature jump kinetics. A large part of the success in understanding this process can be attributed to the application of these many different techniques. However, even though the polymerisation of HbS has probably become the best understood of all protein self-assembly systems, SCA is still a major global health problem, with an estimated 120,000 to 250,000 affected infants born annually [1], and at present most clinical interventions can be classified as tertiary prevention, such as therapies to ameliorate anaemia, reduction of the frequency of pain crises, or prevention of stroke recurrences. As of yet, there are no preventative treatments.

In this chapter, recent advances into the study of HbS polymerisation, it's structural and physical properties as well as the critical conditions required for polymer formation, are described. Electrochemistry is also introduced and a summary of relevant visualisation techniques is reported.

1.1.1 Structure of Haemoglobin

Haemoglobin (Hb) is the iron-containing metalloprotein in the RBCs of mammals responsible for binding oxygen (O_2) in the lung and transporting the bound O_2 throughout the body where it is used in aerobic metabolic pathways. Vertebrate Hb consists of four polypeptide chains: two alpha (α) and two beta (β), with each subunit consisting of one haem group and one O_2 binding site per subunit. The maximum capacity of a single Hb molecule is four O_2 molecules.

An important aspect of the structure of Hb is the major conformational change it undergoes upon binding an O_2 molecule. In 1938, Felix Haurowitz found that crystals of deoxygenated Hb (deoxyHb) shattered when they were exposed to O_2 [2]. It was shown many years later through x-ray crystallographic studies that the deoxygenated and oxygenated forms of Hb differ drastically in quaternary structure. The quaternary structure of deoxyHb is termed the tense (T) state whilst that of oxygenated Hb (oxyHb) is termed the relaxed (R) state (figure **1.1**).

Figure 1.1: A schematic diagram of the T and R conformational states of Hb, showing that the T state has a larger cavity than the R state [3].

The R state or oxygenated molecule is more compact as the iron (Fe) atomic distance of the β chains decreases from 40 to 33 Å on oxygenation. However, the T form has a lower affinity for O_2 and is a more constrained molecule than its counterpart because of the presence of eight additional salt-links [4].

The mechanism for this T to R state switch is illustrated in figure **1.2**. In the T state, the Fe atom does not lie in the plane of the porphyrin ring but is about 0.4 Å out of the plane towards the proximal histidine. This causes the haem group to be domed in the same direction. On oxygenation, an O_2 molecule binds to the sixth

coordination site of Fe, displacing water (H_2O), which causes the Fe atom to move into the plane of the porphyrin and the haem group to become more planar.

Figure 1.2: The mechanism for T to R state switch upon oxygenation. In the deoxygenated state the Fe atom is not in the plane of the porphyrin rings causing the haem group to be domed. When an O_2 molecule attaches to the 6th coordination site the haem group becomes planar causing conformational changes through the whole molecule [3]

The movement of the Fe atom into the plane of the haem produces a level effect which causes a conformational change that is transmitted through the whole molecule. This allows the switch in quaternary structure from T to R state to occur. Thus, a structural change within a subunit is translated into structural changes at the interfaces between subunits. The binding of O_2 at one haem site is thereby communicated to parts of the molecule which are far away. The T to R state conformational change is an important aspect of the polymerisation of HbS, and therefore needs to be understood at the onset.

1.1.2 Polymerisation of HbS

HbS is a single point genetic mutation of normal adult haemoglobin (HbA) that results in a hydrophobic valine residue replacing hydrophilic glutamic acid in the sixth codon of each of the two β chains [5, 6]. X-ray diffraction studies have shown that the β6 glutamate residue is situated on the surface of the protein. Consequently, the substitution of a valine residue does not have a significant effect on the protein conformation, whilst the O_2 affinity and allosteric properties are also virtually unaffected by this change. However, this alteration markedly reduces the solubility of the deoxygenated but not the oxygenated form of HbS.

The key to HbS polymerisation is the interaction of a β6 valine residue with a sticky hydrophobic pocket formed by the β85 phenylamine and β88 leucine residues on a different tetramer. This donor-acceptor interaction, in which β6 valine is donated to the EF acceptor pocket, requires the T or deoxygenated state, as exposure of the pocket only occurs in this state [7]. Subsequently, this causes the association of HbS monomers to form a "Wishner-Love" double strand of deoxyHbS [8], as depicted in figure **1.3**. This is the first stage of polymer formation. See section **1.1.3** for further details on the structure of the deoxyHbS double strands.

Figure 1.3: (a) schematic depiction of the phenylamine and leucine hydrophobic pocket formed for 6β valine **(b)** crystal structure of the "Wishner-Love" double strands of dexoy-HbS, showing the lateral contacts and the axial contacts which occur during coupling [8].

It is important to note that the exposure of the hydrophobic pocket also occurs in HbA when in the T-allosteric state but charge and size effect prevent 6β glutamic acid from binding.

The second stage is the growth and polymerisation of the deoxyHbS double strands. At high concentrations (close to those found in RBCs), single double strands of deoxyHbS polymerise into long stiff insoluble rod-like fibres of 21.5 nm diameter and variable length. A fibre consists of six Wishner–Love double strands wrapped around a central strand in the form of a twisted rope with a pitch of 270 nm (see section **1.1.4**). These fibres form non-covalent cross-links with each other to create a gel, causing the RBC to become rigid, and as a result block blood flow in the capillaries. The polymerisation process therefore triggers a sequence of pathogenic consequences by altering the shape and rigidity of the RBC. On reoxygenation, the polymers disassemble and the cells usually resume their normal biconcave disk shape. Thus, the consequence of the mutation is a catastrophic change in the intermolecular interaction of HbS molecules, more so than in its structural or functional properties.

1.1.3 Structure of HbS Molecule

The major advance in the structural analysis of the HbS molecule came from single crystal X-ray diffraction studies, first at 5.0 A [8] and then at 3.0 A resolution [9]. Recently, the crystal structure of deoxyHbS has also been refined at 2.05 A resolution [10]. These studies have shown that the Wishner-Love double strand of Hb tetramers is the basic building block of the intracellular sickle cell fibre (figure **1.3**). The HbS molecules pack within the crystal as parallel strands which are stabilised by axial contacts within each strand and lateral contacts between strands that involve the mutated valine residue. In the crystal structure there are two crystallographically distinct axial contacts and two distinct sets of lateral contacts. The axial contacts involve the α_1 and β_1 subunits of one tetramer and the α_2 and β_2 subunits of a different tetramer directly above it in the same strand, whilst the lateral contacts involve the valine residue of one β-chain and the hydrophobic valine-binding site, made up of phenylamine, leucine and several haem atoms, of a β-chain in an adjacent molecule [11]. In all instances, the molecular interactions are predominantly of the Van der Waals type and there are only a small number of potential hydrogen bonds and specific ion pair interactions present.

1.1.4 Structure of HbS Polymers

The predominant polymeric structure formed from the addition of HbS double strands is a solid fibre having a diameter of 21.5 nm and a variable length [12, 13]. Electron microscopy studies have further established that the HbS fibre consists of seven double-strands twisting about a common helical axis. Figure **1.4** shows a cross-section of a single HbS fibre, showing the fourteen strands [14-16].

Figure 1.4: Cross section of the seven double-strand fibre model. There are fourteen strands in the fibre with a central double strand surrounded by six other double strands [14].

The molecular contacts which stabilise the HbS fibre are intra-strand contacts (axial and lateral) and intermolecular contacts. Intra-strand lateral and axial contacts are similar in each molecule of the fibre. However, unlike the lateral contact regions, the number of axial contact residues decreases as a function of the radial position of the strand. Twenty two residues are involved in the axial contacts at the fibre centre (strand 12), whereas only six are involved at the fibre periphery (strand 1) [17].

Intermolecular double strand contacts on the other hand involve largely different residues for each strand of the fibre. The number of residues per strand is small, ranging from five residues on strand 2 to thirteen on strand 10 and therefore the fibre is a relatively loose-packed and plastic structure [17, 18]. These can be distinguished as either contacts between parallel double strands or contacts between anti-parallel double strands.

1.1.5 Aggregated Forms of HbS

HbS can aggregate into a number of macroscopic forms. The physiologically relevant structure is believed to be a gel, formed through cross-linking and branching of HbS fibres, because it has the structural characteristics which form inside deoxygenated sickle cells. Some insight into the gel structure has come from observations with a polarising microscope in the course of kinetic studies [19]. These studies have shown that the organisation of HbS polymers in gelled solutions is generally found to be in the form of domains with the polymer long axes pointing in a radial direction. The largest domains are formed on a timescale of hours and these can be millimetres in diameter, whilst the smallest domains are typically microns or less in diameter and these are formed relatively rapidly. The size and number of these domains are therefore determined by the timescale over which polymerisation occurs. The detailed arrangement of these domains and the polymers within the domains are not yet known. However, it is known that it is the domains of single fibres and fibre bundles that cause deformation of the RBC into the characteristic sickle shape, which if not limited by the Hb in a single cell, would be much larger than the cell itself.

A closely related but physically distinct form of polymeric HbS structure is obtained by stirring deoxyHbS solutions while they are being heated to produce aggregation [20, 21]. A free flowing suspension of elongated fascicles, found by electron microscopy to be bundles of parallel fibres packed in square or hexagonal arrays, are obtained instead of a gel [16, 22]. If the stirring is continued for a long time, for example in 50 mM Tris buffer at pH 6.7, macrofibres are formed by the association of small, organised bundles of partially fused fibres. Whereas in a fibre, four of the seven double strands are antiparallel to the remaining three, macrofibres are composed such that adjacent rows are antiparallel. Microscopic crystals have also been observed to grow from gels formed in the absence of stirring or any other shear forces after periods of months [23-25].

1.2 Critical Conditions for Polymer Formation

1.2.1 O_2 Saturation

The physiological variable to which HbS polymerisation is most sensitive to is O_2, with polymer formation being inhibited by O_2 saturation. Conceptually, the simplest model for the effect of O_2 on polymerisation is a straightforward two-state allosteric model [26]. DeoxyHb packs in a T conformation whereas oxyHb packs in an R conformation. However, for HbS polymer formation the registry between polymer-stabilizing molecular contacts present in the T structure is absent when HbS assumes the R structure. Therefore, it is the structural changes accompanying oxygenation which prevent polymer formation.

Experimentally, $^{13}C/^{1}H$ magnetic double-resonance spectroscopy has been used to measure the amount of HbS polymer within sickle erythrocytes as a function of O_2 saturation. Measurements show that the amount of intracellular deoxyHbS polymer increases monotonically with decreasing O_2 saturation, whilst the polymer can be detected even at O_2 saturation values above 90% (figure **1.5**) [27].

Figure 1.5: The curve for polymer formation as a function O_2 saturation of unfractionated sickle cell RBCs at pH 7.65. ■ and ● is data obtained from samples of different individuals. O_2 saturation was varied by using equilibration in a tonometer with gas mixtures containing varying amounts of O_2 and was measured directly for each sample. Each data point represents 1024 spectral accumulations, X, □, ○ and Δ. The solid line represents the theoretical calculation for polymer fraction as a function of oxygen saturation with an allosteric model [27].

1.2.2 Effectors of O_2 Saturation

pH Level:

Studies have shown that the aggregation of HbS is markedly dependent on pH [28, 29]. One such study involved the measurement of the solubility (C_{sat}) of HbS solutions, dialysed exhaustively against 0.06 M phosphate buffers of pH 5.5 to 8.1, by ultracentrifugation and sedimentation methods. As shown in figure **1.6**, the solubility changes very little between pH 6 and 7, and then sharply increases at more acidic and basic values, whilst the minimum in the solubility-pH profile is seen at pH 6.5. This suggests that a significant effect of an increase or decrease in pH is destabilisation of the polymer through an increase in the net electrostatic repulsion between molecules. The pH dependence may also be due to the titration of histidines that form hydrogen bonds or ion-pair in intermolecular contacts [28].

Figure 1.6: effect of pH on solubility of HbS in 0.06 M sodium phosphate buffer at 25°C. Hb solutions were dialysed extensively against phosphate buffers of pH 5.5 to 8.1 [28].

Other effectors of O_2 Saturation:

2,3-diphosphoglycerate (2,3-DPG), inositol hexaphosphate and ATP all act in a similar manner. All of these molecules have a strong negative charge and bind in the central cleft of deoxyHb, and thus act by biasing the conformational equilibrium in Hb toward the deoxygented form, and favouring O_2 release. However, they interact at distinctly different sites, and therefore their effects can be additive. The effect of 2,3-DPG on HbS polymerisation is investigated in more detail in Chapter **4.7**.

1.2.3 HbS Concentration

The concentration of fully deoxyHbS is another factor that determines *in vivo* polymer formation. When deoxyHbS concentration exceeds the solubility, polymer formation begins. Therefore, increasing HbS concentration increases the extent of polymerisation. In understanding this concept it is important to appreciate the molecular crowding in a solution of Hb at concentrations typically found in a RBC. At 340 mg cm^{-3}, Hb molecules are 1.6 molecular diameters apart centre to centre, but only 1.1 molecular diameters apart edge to edge and their natural motion ensures that they will encounter each other every few nanoseconds. In concentrated solutions, HbS particles are greater in number and much closer and thus there is an increase in molecular collisions and more chance of a hydrophobic interaction occurring between the mutated valine residue of one HbS and the β-subunit of another [30]. High HbS concentrations normally required experimentally for the assembly of HbS fibres [30] poses a problem as an experiment can require more than 200 mg cm^{-3} of HbS protein per single experiment. However, numerous studies [31, 32] of the polymerisation of HbS in 1.5 M phosphate buffer have found that in high molarity buffer solutions polymerisation occurs at much lower concentrations (*ca.* 50 mg cm^{-3}).

Wang *et al.* [14] compared the structures of HbS fibres formed in high molar phosphate buffer (1.5 M) with low molar buffer (0.05 M) to determine whether the high buffer concentration affected the structure of the polymers being formed and found that in all cases the polymers formed in 1.5 M had the same structures as those formed in 0.05 M phosphate buffer. The general appearance, spacings and intermediates of the polymers from negative staining, imaged with cryo-electron microscopy and Fourier transforms, were used for the comparison.

The influence of non-HbS on the polymerization process needs to be discussed briefly aswell as HbS frequently occurs in red cells in combination with a large fraction of other Hb, such as HbA, fetal haemoglobin (HbF) and haemoglobin C (HbC) [33]. The fraction of HbS in red cells differs considerably among the various types of sickle cell disease. HbA and HbC have been shown to increase the solubility of deoxy-HbS in mixtures with HbS, whilst HbA_2 and HbF have an even greater sparing effect; a sparing effect is where normal or abnormal Hb that may be present along with HbS in human erythrocytes act to elevate its solubility under

conditions of partial or total desaturation [34]. The HbS molecular crowding is diminished with a variable intracellular Hb composition, and thus the molecular collisions between HbS particles are fewer [33]. Increased proportions of HbA, HbF or HbC therefore results in decreased clinical severity.

1.2.4 Temperature

Studies performed to see the effect of temperature on the solubility of deoxy-HbS have shown that polymer formation is favoured by elevated temperature. In a 0.15 M, pH 7.15 potassium phosphate solution, solubility of HbS decreases from about 320 mg cm^{-3} at 0 °C to a minimum of 160 mg cm^{-3} at about 35 °C, and then increases again (figure **1.7**) [35, 36].

Figure 1.7: Temperature dependence of deoxy-HbS solubility in a solution of 0.15 M phosphate buffer and 0.05 M sodium dithionite as an additional reducing agent [36].

Therefore, at total concentrations below 160 mg cm^{-3}, deoxyHbS solutions remain liquid between 0 °C to 45 °C; at concentrations above 320 mg cm^{-3}, the solution contains polymers at all temperatures; and between 160 mg cm^{-3} and 320 mg cm^{-3}, the solution undergoes reversible polymerisation and depolymerisation on heating and cooling [30, 36].

1.2.5 Experimental Conditions for Polymerisation of HbS

There is a wealth of literature concerning the formation of HbS aggregates *in vitro*, and a summary of the conditions used for HbS polymerisation in these studies is presented in table **1.1**. It is noticeable that a wide range of HbS protein concentrations have been used from low values of only 6 mg cm^{-3} to extremely highly concentrated ones of 940 mg cm^{-3} whilst the molarity of phosphate buffer used was dependent on the HbS concentration; high concentrations of HbS were associated with low buffer concentrations. Furthermore, solution pH was limited to the physiological pH range.

The method by which HbS polymerisation was initiated in each study is also summarised in table **1.1**. Heating of the protein solution, commonly referred to as the temperature jump method, has been favoured by many investigators to induce polymerisation because of its simplicity and compatibility with all the monitoring techniques. However, although the temperature jump method has many advantages, another being disassembly of the polymers by cooling, a major limitation is its non-applicability to high HbS concentrations. The shortest delay times which can be accurately measured are the thermal equilibration times of the order of 10 s which at 37 °C corresponds to a concentration of 230 mg cm^{-3}, slightly lower than those found in sickle RBCs [37].

Therefore many recent studies, especially those investigating kinetics of polymerisation, have employed a laser photolysis technique developed by Ferrone *et al.* in which the polymerisation reaction is initiated by rapid removal of carbon monoxide (CO) from a CO saturated HbS solution [30, 37]. The advantages of this technique are that polymerisation can be achieved extremely quickly and the experiment can be repeated many times as recombination of CO results in depolymerisation.

Electrochemistry has been used as the method of initiation in this present investigation. Electrochemical reduction of O_2 at an electrode surface in contact with HbS solution causes local deoxygenation, and thus induction of fibre formation. This removes the need to deoxygenate the whole solution as only deoxygenation at the surface is required.

Reference	HbS conc. (mg cm^{-3})	Phosphate buffer (M)	pH	Other conditions	Method of nucleation
10	120	0.03	7.0	HbS in buffer conc. to 120 mg cm^{-3}	polymerisation occurred in 2 days
14	25	1.5	6.7	- 25 °C	temp jump to 25 °C
20	20	0.1	7.0	IHP and EDTA; 25 °C	gentle stirring
37	440	0.15	7.35	Sodium dithionite	photolyse CO-HbS
38	55	1.8	7.3	Sodium dithionite	photolyse CO-HbS
39	240	0.1	7.2	25 °C	photolyse CO-HbS
40	240	0.1	7.2	25 °C	photolyse CO-HbS
41	9 – 35	0.15	7.35	humidified He	temp. jump to 37 °C
42	830	0.1	7.0	deoxygenated with sodium dithionite	temp. jump to 28 °C
43	6 – 12	0.05	7.5	Dextran added	incubation for 30 min at room temp.
44	68	1.8	7.4	2 °C	temp. jump to 30 °C
45	270	0.15	7.35	Sodium dithionite	photolyse CO-HbS
46	> 100	0.05	7.4	37 °C; glutaraldehyde	stirring under N_2
47	1350	0.1	7.2	25 °C	photolyse CO-HbS
48	240	0.05	6.7	stained with phosphotungstic acid	photolyse CO-HbS and temp.jump

Table 1.1: Conditions for HbS polymerisation and methods of nucleation initiation used in selected studies found in literature.

1.3 Thermodynamics and Kinetics of HbS Polymerisation

1.3.1 Thermodynamics of HbS Polymerisation

Thermodynamically, the simplest description of HbS polymerisation consists of the aggregation of HbS into helical polymers or three-dimensional crystals. A two component system consisting of a solution plus polymer phase is commonly referred to as a gel, and the overall process of forming a collection of domains of aligned polymers as gelation or polymerisation. Each of the two phases of the polymerisation model are distinct entities, in which the solution phase of the gel contains only HbS molecules of 64.5 kDa as the monomers, with no clear evidence for aggregation in this phase, whilst the polymer phase behaves like an ordered crystal in equilibrium with a solution of HbS monomers. Although, the crystal is the thermodynamically more stable structure, polymers always form first.

The separation of a gel into solution and polymer phases can be achieved by centrifugation [49, 50] and the concentration of HbS in each phase measured by sedimentation into a compact pellet. The concentration of HbS in the solution phase can be measured using an analytical sedimentation technique, and the results confirm the presence of singular HbS molecules as the sedimentation velocity profile only contains a single peak whose coefficient is very similar to that of Hb tetramers [29].

The concentration of HbS in the polymer phase is taken as a measure of the solubility of deoxygenated HbS, or in other words a measure of the intracellular HbS concentration in equilibrium with the polymer in solution. It can be approximately measured in solubility experiments in near-infrared spectrophotometry on the turbid pellets, from which the concentration of Hb in the pellet is calculated using mass conservation [51]. From these experiments the volume fraction of the solution phase is calculated to be 350 mg cm^3 and the concentration of deoxyHbS in the pure polymer phase is 690 mg cm^{-3} [51]. The solubility data can then be used to calculate the fraction of polymerised Hb, χ_p, at any temperature and the total concentration, c_o, using the mass conservation relationship [51]:

$$\chi_p = (1 - c_{sat} / c_o)/(1 - c_{sat} / c_p) \qquad \textbf{(1.1)}$$

where c_{sat} is the solubility and c_p is the concentration of Hb in the polymer phase (690 mg cm^{-3}). The equilibrium constant, K, for the polymer phase in the reaction Hb (solution) + nH_20 = $Hb(H_20)_n$ (polymer) is given by [51]:

$$K = 1 / a_{Hb} (a_{water})^n \quad \textbf{(1.2)}$$

where a_{Hb} is the activity of the Hb monomer and a_{water} is the activity of water in the solution phase. The activity of Hb is simply the product of the solubility and the activity coefficient ($a = c_{sat}\gamma$).

The polymerisation enthalpy change, ΔH, or the apparent molar heat of gelation is given as the heat absorbed per mole of Hb entering the polymer phase and can be obtained from the temperature dependence of the equilibrium constant using the van't Hoff equation:

$$d \ln K/d (1/T) = - \Delta H/R \quad \textbf{(1.3)}$$

A large decrease in the apparent ΔH with temperature is seen from the van't Hoff analysis of the solubility data and this is confirmed by direct calorimetric measurements [36, 52]. However, data obtained from scanning calorimetric measurements [36], the more sensitive of the two methods, gives values for ΔH which are in fair agreement with those obtained from the solubility data, but are lower by 0 to 12.6 kJ mol^{-1}. This difference may be due to some proton or ion-binding process which has not been included in the thermodynamic analysis.

1.3.2 Kinetics of HbS Polymerisation

The kinetics of fibre formation and polymerisation are extremely important and have played a central role in understanding the physical chemistry of HbS polymerisation as well as the pathophysiology of the SCA to subsequently improve therapeutic strategies

A large variety of techniques have been used to monitor the process of polymer formation, including nuclear magnetic resonance [53, 54], viscosity [55-57], turbidity [21, 51, 58], linear birefringence [25, 59, 60], light scattering [20, 60, 61] and transverse relaxation times [62], and the results from all of these techniques show the same basic kinetic features of polymerisation. A typical progress curve for polymerisation of an initially polymer-free solution is shown in figure **1.8** [35].

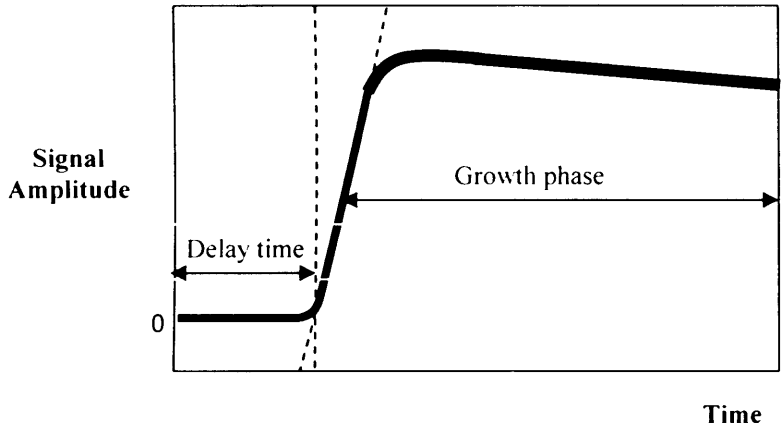

Figure 1.8: Time course of HbS polymerisation. This is a typical progress curve showing a two step mechanism for polymerisation in which there is a delay period initially, during which time no change in the signal is observed. This period corresponds to the time taken for nucleation to occur and so is also referred to as the nucleation time. This is followed by the appearance of the polymer and subsequently growth proceeds exponentially.

There is a marked delay in the initial part of the progress curve during which time no change in the signal is observed, and this corresponds to a period called the delay or nucleation time during which no polymer formation. The delay is followed by an explosive and highly autocatalytic formation of polymer [63, 64].

The length of this delay time is found to be strongly dependent on the inverse initial concentration of HbS to a very high power. This power is not constant but varies with the HbS concentration from 15 at 350 mg cm^{-3} [37] to as high as 35 to 50 at 250 mg cm^{-3} [63, 64]. Furthermore, the delay time is also found to be related

to the solubility of HbS, and thus dependent on the variables which alter the solubility of HbS such as extent of deoxygenation, temperature and pH. A simple empirical formula, called the supersaturation equation [65], relates the delay time, t_d, to the solubility:

$$1 / t_d = \lambda (c_o / c_{sat})^n \quad \textbf{(1.4)}$$

where t_d is the delay time, λ is the proportionality factor, n is found to be approximately 30-40 under physiological conditions and the supersaturation, (c_o / c_{sat}), is defined as the ratio of the initial HbS concentration to the equilibrium solubility.

1.3.3 Double Nucleation Mechanism

Originally it was thought that the dependence of the delay time on solution conditions could be explained by a simple one-step nucleation mechanism based on equilibrium nucleation and growth of individual polymers. However, this mechanism could not explain the existence of a delay period prior to polymer formation. Consequently, a double nucleation mechanism, in which all the experimental observations involving the kinetics of HbS polymerisation could be explained, was postulated by Ferrone *et al.* (figure **1.9**) [66].

Figure 1.9: The double nucleation mechanism of HbS polymerisation consisting of an initial nucleation phase known as homogeneous nucleation followed by growth of the polymer known as heterogeneous nucleation. The homogeneous nucleation consists of the sequential addition of thermodynamically unfavourable monomers until the aggregate reaches a certain size called the critical nucleus (depicted as nucleus in this diagram). The formation of the critical nucleus is the first signal seen in a progress curve after the delay time. Once the critical nucleus is reached further addition of monomers becomes thermodynamically favourable and so growth of polymers is fast and explosive. This autocatalytic growth is termed the heterogeneous nucleation [67].

This mechanism postulates that polymer formation is the result of two types of nucleation. In the first type, aggregation of HbS molecules occurs in the bulk solution to form the first polymer and this is termed as homogenous nucleation. This polymer grows by the addition of monomers to the ends. In homogenous nucleation, the sequential addition of monomers is a thermodynamically unfavourable random process initially as there is significant entropic loss for the monomer associated with aggregation. The substantial loss of translational and rotational freedom of the monomer is only partially compensated for by the

entropy gain from the centre of mass and torsional vibrations of the molecules in a polymer lattice. However, the reaction becomes increasingly favourable as the number of monomers increases due to an increase in stability associated with an increase in the number of bonds per molecule from 0.5 bonds in a dimer to 4.1 bonds in the infinite polymer. Monomer addition occurs till the aggregate reaches a certain size, termed as the critical nucleus, which in this context is the aggregate at which size the forward reaction becomes thermodynamically favourable. Consequently, the formation of the critical nucleus is the rate-determining step. Experimentally, the existence of the delay time is accounted for by the time taken to form the critical nucleus as there is no polymer formation till this stage, whilst, the energetic gain needed to form the critical nuclei is dependent on the initial concentration. The rate of growth of polymer in this stage is governed by the relationship [68, 69]:

$$\alpha = k_+ (\gamma c_o / \gamma_i c_i) \quad \textbf{(1.5)}$$

where α is the homogenous growth rate of polymer, k_+ is the monomer addition rate constant and γ is the activity coefficient of the monomer.

The second type of nucleation is termed heterogeneous nucleation and this step involves nucleation (i.e. homogeneous nucleation) on the surface of pre-existing polymers as well as growth of polymers. As more polymers form, the available surface area and thus the number of sites available for heterogeneous nucleation increases with time. As a result, there is a continuous increase in the rate of heterogeneous nucleation providing an explanation for the highly explosive and exponential growth observed in the progress curves. The contacts which create heterogeneous nucleation are a subset of the fundamental contacts within the double strand [66]. Another intriguing aspect of heterogeneous nucleation is the ability of the polymers to display considerable flexibility with intersection sites of newly generated polymers able to display maximum angular separation of 21° to 26° as well as polymer alignment [67].

The heterogeneous nucleation rate is proportional to the concentration of monomers already present in polymers, $g_o\Delta$, and thus rate is described as [70]:

$$g_o\Delta = (k_+\gamma)\, cc_j \quad \textbf{(1.6)}$$

where Δ is the concentration of monomers incorporated into polymers and c_j is the concentration of heterogeneous nuclei of size j.

Consequently, the rate of polymer formation for the complete reaction is given as [66]:

$$\omega = \alpha(c) + (c_o - c)g_o\Delta(c) \quad \textbf{(1.7)}$$

where $\alpha(c)$ is the rate of homogeneous nucleation and $g_o\Delta(c)$ is the rate of heterogeneous nucleation per concentration of the polymerised monomer.

1.3.4 Polymer Melting

Melting is the term used to describe the depolymerisation of HbS molecules upon oxygenation. If a cell containing polymers reaches the lungs, then oxygenation will lead to melting. However, if polymer melting is not complete by the time the cell enters the tissues where O_2 pressure is low then the remaining polymers promote rapid growth through heterogeneous nucleation, and if this time for melting is longer than the 1 second required to transit deoxygenated portions of the RBCs then obstruction of the microvasculature occurs [38, 70]. Consequently, the rates of depolymerisation could play a crucial role in the resolution of pathophysiological processes.

Unfortunately, the kinetics and mechanism of polymer melting have not been as widely studied as those of polymerisation and many early reports have provided conflicting data. Initially, the absence of a delay time observed during melting led to the prediction that melting upon reoxygenation at the lungs is fast [71]. However, other studies have indicated that this process is slow enough, on the order of tens of seconds that polymers persist during circulation, and thus contribute to occlusion [72]. In addition, it is also known that the process of depolymerisation occurs by shortening of individual fibres at their ends in the presence of CO, whilst the affinity of polymerised HbS for the ligands CO and O_2 is three to ten times lower than the affinity of solution T state HbS.

1.3.5 Nucleation and Growth of Fibres in Literature

Much of the literature on the nucleation and growth of HbS has focussed on the polymerisation of HbS in solution, and therefore been largely concerning homogeneous rather than heterogeneous nucleation. Homogeneous nucleation is the initiation of polymerisation through thermodynamically unfavourable random aggregation of HbS monomers, whilst heterogeneous nucleation consists of homogeneous nucleation and growth of polymers on the surface of existing polymers and other surfaces. Recent literature detailing the mechanistic steps of fibre formation and the techniques with which they have been visualised are summarised in table **1.2**.

Homogeneous and heterogeneous nucleation was originally postulated on the basis of macroscopic data from kinetic measurements. However, a short paper by Samuel *et al.* [42] described the observation of the nucleation, growth and interaction of HbS fibres in real time using non-invasive video-enhanced differential interference contrast (DIC) and dark-field microscopy. This provided, for the first time, the direct visualisation of the polymerisation process in detail. The reported images supported most aspects of the double nucleation mechanism. The first fibres were seen 12 minutes after the temperature jump and thus a delay was apparent before polymers were seen. The polymers then grew rapidly producing a resulting network which was highly branched and cross-linked to give a gel. Branching, arising from the thick regions of the fibre, was thinner than the parent fibre, whilst, the images of the gel showed that it was a dynamic and flexible entity [42].

Reference	Description of Study	Method of Nucleation	Visualisation Techniques
41	Liquid-liquid separation demonstrated in solutions of HbS and dense liquid droplets seen to act as nucleation centres for HbS spherulites	temp. jump (24-37 °C)	DIC microscopy and AFM
42	Observation of nucleation, growth and interaction of fibres in real-time demonstrated	temp. jump (2-28 °C)	DIC microscopy and dark-field microscopy
43	Investigation of the structure, solubility behaviour and phase distributions with dextran upon HbS polymerisation	incubation for 30 min at room temp	electron microscopy
45	Determination of rates of induction times of homogenous nucleation of HbS fibres	photolyse CO-HbS	DIC microscopy
46	Determination of the content and orientation of aligned HbS polymer	humidified nitrogen	differential polarisation imaging microscopy
47	Observed individual events and structures in the development of gel domains	photolyse CO-HbS	DIC microscopy
48	Mechanisms of depolymerisation of HbS fibres	photolyse CO-HbS and temp. Jump	DIC and electron Microscopy

Table 1.2: A description of the techniques used for the visualisation and monitoring of nucleation and growth of HbS polymers from studies found in literature.

Another study by Briehl and co-workers [73] enhanced the use of DIC microscopy to observe individual HbS fibres in gels, and showed not only that gels and fibres were fragile and easily broken by mechanical perturbation, but breakage resulted in vast acceleration of gelation kinetics due to the creation of new, growing fibre ends (figure **1.10**). Since gelation kinetics is critical in inducing microvascular obstruction, the acceleration of gelation upon breakage may have important implications *in vivo* to the pathogenesis of sickle cell crises.

Figure 1.10: DIC microscopy images showing fracture of a single HbS fibre and rapid filling of the field with numerous new fibres after fracture (fracture induced as a result of mechanical perturbation due to a tap on the slide): **(a)** before fracture only single fibre visible; **(b)** after fracture fibre fragments visible (arrow indicates point of fracture); **(c, d)** fragments grow and cross-link till field is densely filled with fibres. Hb concentration was 12.4 mmol L^{-1} (heme) at 25'C and fibre formed 56 minutes after the temperature increase. The width of the field is 24 pm. DIC microscopy produces images many times larger than small objects; hence, fibers are much thinner than the DIC images shown [73].

Figure **1.10** shows the time-course of a polymer initiated by a temperature increase. It can be seen that after the resulting fibre was fractured to create new growing ends polymerisation was rapid and the field filled in quickly with fibres to produce a large mass of polymers. The first fibre appeared 56 minutes after the temperature jump, but after the fracture the growth of newer fibres was far quicker. In other words, the overall rate of polymer formation in the gel was increased due to the creation of new fibre ends.

DIC microscopy coupled with ligation control, through the use of photolytic epi-illumination, has also been used to define the structure and development of gel domains and to demonstrate the mechanism of fibre melting. Changes in photolytic intensity were seen to alter domain growth rates and domain structure with fibres growing slowly and radially without branching at low laser intensity, and growing faster and forming highly cross-linked, dense domains at high intensity [47]. Depolymerisation, on the other hand, occurred at two sites on the fibres. At low

CO partial pressures the dominant mechanism of dissolution was depolymerisation at fibre ends at rates of approximately 1 μm s^{-1}, whereas at high CO partial pressures the dominant mechanism was rapid dissolution, complete in one second or less, along fibre sides. A model has been postulated to describe the mechanisms of end and side-depolymerisation [48].

1.4 Electrochemistry

1.4.1 Electrochemical Reduction of O_2

The O_2 reduction reaction is a complex multi-electron process that may include a number of elementary steps involving different reaction intermediates. In general, however, the mechanisms are of two types, with a modified Wroblowa *et al.* [74] scheme the most effective in describing the complicated reaction pathway by which O_2 is reduced at metal surfaces, see figure **1.11**:

Figure 1.11: The O_2 reduction reaction scheme. O_2 can be electrochemically reduced either directly to H_2O in a 4 electron reduction reaction governed by the rate constant k_1 or via the intermediate H_2O_2. In this case, O_2 is initially adsorbed on the electrode surface and is converted to H_2O_2 through a series 2 electron reaction from which it is reduced to H_2O. It is important that O_2 is reduced directly to H_2O as the peroxide has a detrimental effect on Hb [74].

Based on this reaction scheme, O_2 can be electrochemically reduced either directly to water (H_2O) in a "direct" 4 electron reduction (k_1) or to intermediate hydrogen peroxide (H_2O_2), termed as a "series" $2e^-$ reduction. Subsequently, the adsorbed H_2O_2 can be electrochemically reduced to water with the rate constant k_3 ("series" $4e^-$ pathway), chemically decomposed on the electrode surface (k_4) or desorbed into the bulk solution (k_5). Indeed, in some conditions the reaction only proceeds to the intermediate H_2O_2 stage, for example at mercury, O_2 is reduced in two well defined steps separated by up to 1V [75]. The "direct" $4e^-$ reduction of O_2 implies that cleavage of the O-O bond by dissociative adsorption occurs at an early stage in the reduction, whilst in the "series" $4e^-$ pathway the first step is the reduction of O_2 to superoxide, O^{2-} (or HO^{2+} to HO_2) [76].

Rotating ring-disc electrode experiments may be used to distinguish the two pathways and to provide an estimate of the relative importance of the pathways

under conditions where they co-exist. O_2 is reduced at a rotating disc of the active material, and the formation of H_2O_2 is monitored on a ring electrode surrounding the disc. Studies have provided at least fourteen different reaction pathways [77] for O_2 reduction and thus reliable kinetic parameters cannot be obtained nor can comparisons between electrode materials be made, especially where products and mechanisms may be different. Even so, the reduction of O_2 is always a slow reaction [78].

A qualitative example of the rotating disc electrode can be seen with the Pt disc electrode. Current – voltage curves at the Pt disc show only a single reduction wave, implying a complete $4e^-$ reduction. On the other hand, the response on the ring, whose potential is held at a value where the H_2O_2 oxidises, proves that some H_2O_2 is formed during the rising region of the curve, and that at Pt the O_2/H_2O_2 and H_2O_2/H_2O processes must occur at very similar potentials [77]. This is confirmed by recent studies which have suggested that a series pathway via an $H_2O_{2,ad}$ intermediate may be operative on Pt and Pt bimetallic compounds [76]. In either case, however, the rate-determining step appears to be the addition of the first electron to $O_{2,ad}$.

As with HbS polymerisation there is a pronounced effect on O_2 reduction with pH; a gradient of pH with distance from the electrode surface is present with a higher pH at the electrode than in the bulk solution. This effect is apparent in phosphate buffer of pH 7.0 where the wave for O_2 reduction is steep and the half-wave potential is 300 mV positive to that for O_2 reduction for 0.1 M NaOH. In contrast, the wave is drawn out and the half-wave potential is approximately 150 mV in unbuffered systems. This can be readily understood in terms of the pH change as a result of O_2 reduction itself. In the very foot of the wave, the pH close to the surface of Pt is identical to that in the bulk, whilst in the limiting current regions, the four electron protonation reactions of reduced O_2 species will cause the hydroxyl (OH^-) ion concentration and thus the pH at the surface to increase to *ca.* 11. Therefore, both the thermodynamics and kinetics of O_2 reduction will change as the pH increases [77].

Furthermore, it is also now well established that the reaction rates of the O_2 reduction reaction on Pt surfaces are structure sensitive. These arise due to structure sensitive adsorption of spectator species such as OH^- and HSO_4^-, both of which inhibit the reduction of molecular O_2 by blocking the initial adsorption. In

addition, O_2 reduction in Cl^- containing solutions is accompanied with peroxide formation implying that within the same potential limits H_2O_2 is formed as an intermediate. This effect seems to manifest itself in the Pt(110) and Pt(100) structures but not in Pt(111) [76].

In contrast with Pt, Au supports mainly the 2 x $2e^-$ step reduction of O_2 ("series" $4e^-$) in acid media, a feature that can be used for the electrochemical synthesis of hydrogen peroxide. The trends in half-wave potential and shape of the first $2e^-$ reduction of a Au microdisc electrode are similar to that of Pt but the shape of the second wave is different because OH^- ions are generated during the first stage of reduction. The subsequent reduction of H_2O_2 on these electrodes is very slow and the mechanism of H_2O_2 reduction is strongly dependent on surface orientation. In alkaline solution, reduction proceeds only by the series mechanism with HO^{2-}_{ad} as an intermediate in the reduction process. The formation of HO^{2-} does not involve the cleavage of the O-O bond as isotopic experiments on various surfaces provide strong evidence that all the peroxide oxygen originates from the O_2 [78]. Furthermore, as at Pt the pH dependence is noticeable whilst current-potential curves show that hydrogen evolution commences at a potential expected for an alkaline environment [76].

The reduction of O_2 at Pt and Au was of particular interest in our system because these were the electrodes employed in the investigations. The importance of the reaction proceeding to completion is paramount so that firstly no H_2O_2 is formed as peroxide has a detrimental effect on Hb, whilst secondly a relatively fast reduction of O_2 is achieved.

1.4.2 Chronoamperometry

The study of the variation of the current response after a single potential step under potentiostatic control is called potential step chronoamperometry. In a potential step experiment the potential is stepped at a time t_0 from an initial potential $E_{initial}$ to final potential E_{final} corresponding, respectively, to no electrolysis and to complete conversion of reactants to products at the electrode surface (figure **1.22**).

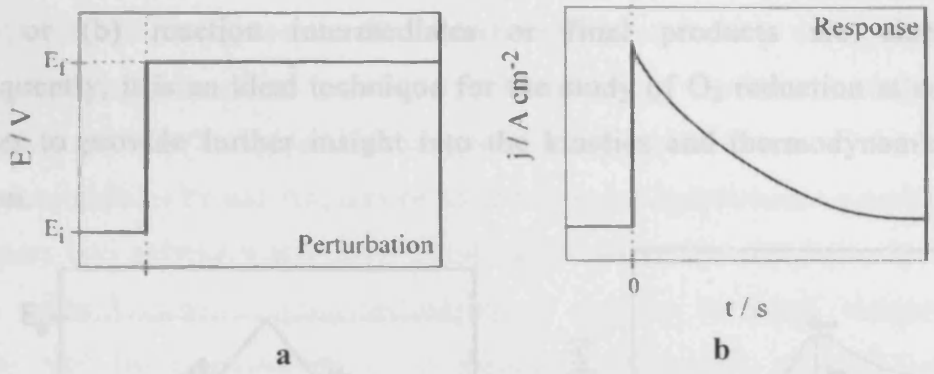

Figure 1.22: Figures showing **(a)** the excitation waveform for a single potential step experiment **(b)** the current density evolution response over time for the same electrochemical technique [79].

Immediately after the potential step, a large current is detected which decays steadily with time. This arises since the magnitude of the current is controlled by the rate of diffusion of the reactant to the electrode. As the reactant is converted to the product due to the heterogeneous electron transfer reaction, the reactant is depleted close to the surface, and a depletion zone is formed. Consequently, the concentration gradients shortly after the step are extremely large, since there has been little time for any depletion of electro-active species, and the currents are also very large. Gradually, as depletion occurs, the diffusion layer thickness increases and the current decreases. The thickness of this depletion zone or diffusion layer, Δ, is governed by the equation:

$$\Delta = \sqrt{2Dt} \qquad (1.8)$$

where D is the diffusion coefficient and t is the time taken for the reaction. In some experiments it is advantageous to monitor charge, instead of the current, as a function of time and this technique is referred to as chronocoulometry.

1.4.2 Chronoamperometry

The study of the variation of the current response after a single potential step under potentiostatic control is called potential step chronoamperometry. In a potential step experiment the potential is stepped at a time t_0 from an initial potential $E_{initial}$ to final potential E_{final} corresponding, respectively, to no electrolysis and to complete conversion of reactants to products at the electrode surface (figure **1.22**).

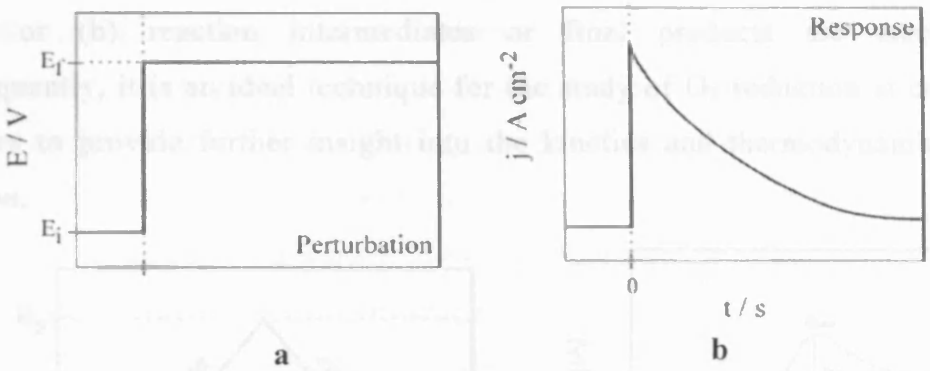

Figure 1.22: Figures showing **(a)** the excitation waveform for a single potential step experiment **(b)** the current density evolution response over time for the same electrochemical technique [79].

Immediately after the potential step, a large current is detected which decays steadily with time. This arises since the magnitude of the current is controlled by the rate of diffusion of the reactant to the electrode. As the reactant is converted to the product due to the heterogeneous electron transfer reaction, the reactant is depleted close to the surface, and a depletion zone is formed. Consequently, the concentration gradients shortly after the step are extremely large, since there has been little time for any depletion of electro-active species, and the currents are also very large. Gradually, as depletion occurs, the diffusion layer thickness increases and the current decreases. The thickness of this depletion zone or diffusion layer, Δ, is governed by the equation:

$$\Delta = \sqrt{2Dt} \qquad (1.8)$$

where D is the diffusion coefficient and t is the time taken for the reaction. In some experiments it is advantageous to monitor charge, instead of the current, as a function of time and this technique is referred to as chronocoulometry.

1.4.3 Cyclic Voltammetry (CV)

The most common technique to study electrode reactions, and perhaps the most versatile electroanalytical technique for the study of electroactive species, is CV. It involves applying a triangular potential ramp (figure **1.13 (a)**), where the potential of the working electrode (WE) is swept forward oxidising the sample in question, and subsequently the electrode potential is scanned back to its original value. The potential scan can be used to define whether (a) the product of electron transfer is stable or (b) reaction intermediates or final products are electroactive. Consequently, it is an ideal technique for the study of O_2 reduction at conducting surfaces to provide further insight into the kinetics and thermodynamics of this reaction.

Figure 1.13: Figures showing **(a)** a triangular potential ramp is applied in CV; **(b)** CV of a reversible redox couple with the parameters of the voltammogram depicted: E_{pc} cathodic peak potential; i_{pc} cathodic peak current; E_{pa} anodic peak potential; i_{pa} anodic peak current [80].

A CV is obtained by measuring the current at the WE during the potential scan and the shape of the voltammogram depends on the reversibility of the redox couple. The important parameters of a voltammogram are shown in figure **1.13 (b)**. Small peak to peak separation and a well-defined peak are characteristic features of a reversible electron transfer reaction, i.e. a redox couple in which both species rapidly exchange electrons with the WE This is because in a reversible electron transfer reaction current flows as soon as the reduction becomes thermodynamically viable because of the rapid electrode kinetics associated with the reaction. However, slow electron transfer at the electrode causes the peak to peak separation to increase. In these reactions, no current flows until an overpotential has been applied to drive the reduction or oxidation of the sample.

1.5 Summary

As the introduction has shown, much of the pioneering work in this field has established the basic structural, biochemical and biophysical properties of HbS polymerisation, and in this regard this process is extremely well understood. However, only recently have investigations been performed on manipulating the nucleation and growth of fibres and gel formation in order to open new avenues for the inhibition of HbS polymerisation or any associated pathogenic events.

Presented in this thesis are results concerning the nucleation and growth of HbS aggregates formed at a number of conducting surfaces using a novel electrochemical method. Local deoxygenation of HbS solution at the surface of electrodes, such as Pt and Au, can be used to trigger hydrophobic coupling of HbS monomers into polymers and gels. These structures can be subsequently visualised *in-situ* using various imaging techniques to gain an in depth insight into the kinetics and thermodynamics of nucleation and growth of HbS aggregates. Consequently, the visualisation and monitoring of the protein growth using optical, UV-visible spectroscopy and scanning probe microscopic techniques are also described. Furthermore, the utilisation of this method to provide an assessment of the effectiveness of current therapies that exist for SCD is presented. In this thesis, the basis for a methodology is presented that may be used as a screening method for substances that effect the fibre nucleation and or growth, one which could be valuable to the pharmaceutical industry for treating SCD.

Chapter 2: Experimental Materials, Methods and Equipment

2.1 General Experimental

In this chapter, the experimental details and methodologies common to all experiments will be discussed and a general outline of the materials and instrumentation utilised will be provided. Furthermore, the preparation procedure and electrochemical techniques used to probe the protein solutions will be described.

However, it is important to note that this chapter only serves to outline a general experimental. Data analysis methodologies and the construction of thin layer electrochemical cells specific to each chapter will be detailed in the relevant chapters.

2.2 Materials

HbS and HbA were purchased from Sigma chemical company (Poole, UK) and used as supplied. The supporting electrolyte was 1.5 M (pH 7.0) potassium phosphate buffer solution which was prepared by mixing stock solutions of dihydrogen potassium phosphate and dipotassium hydrogen phosphate (Avocado, UK) to achieve a solution with pH 7.0. Changes to the stock solutions ensured correct buffer concentrations and pHs were obtained for experiments where the pH and molarity of the phosphate buffer solution varied. H_2O used in experiments and for cleaning purposes was de-ionised H_2O from a Millipore Milli-Q gradient® (18.2 MΩ cm, < 0.05 S cm^{-2} at 25 °C) water system. Sodium chloride (NaCl) was obtained from BDH AnalaR whilst other chemicals were of analytical reagent grade. Sodium dithionite was obtained from Sigma chemical company (Poole, UK).

Ethylenediaminetetraacetic acid (EDTA), 3,5-dichloro-2-hydroxybenzenesulfonic acid (DHSA), horseradish peroxidise and 4-aminoantipyrene, used for the spectrophotometric assay of H_2O_2, as well as vanillin, 5-hydroxy-2-furfural (5HMF) and 2,3-DPG for the anti-sickling experiments were obtained from Sigma chemical company (Poole, UK). 3-mercapto-1-propenesulfonic acid, 2-mercaptoethanol, 1-butanethiol and cystamine dihydrochloride (Aldrich, UK) were used as the thiol compounds. Free haemin, poly-L-lysine and iota carrageenan were used for modifying electrodes for direct electrochemistry experiments.

Electrodes were all obtained from Advent Research Materials Ltd, Oxford or Johnson Matthey, Cambridge. The electrodes used for each specific cell are described in the relevant experimental section of each chapter. Quartz cuvette (1 mm pathlength) and glass microscope slides were obtained from Hellma, UK. For the AFM experiments, 3% glutaraldehyde was obtained from Sigma chemical company (Poole,UK) and mica and silicon nitride contact and tapping mode were obtained from Veeco (Santa Barbara, Ca). Other materials such as silver conductive paint, epoxy resin, parafilm and epphindorfs were obtained from RS (UK), pipettes were obtained from Fluka whilst argon (Ar) and nitrogen (N_2) gas cylinders were received from BOC gases (UK).

2.3 Instrumentation

Electrochemistry techniques, specifically chronoamperometry and CV, were carried out in a conventional three electrode system comprising a working (WE), reference (RE) and counter electrode (CE) connected to a PC operated potentiostat (μAutolab Type II, Eco Chemie B.V. supplied by Windsor Scientific Ltd, UK), controlled by GPES software (version 4.7, Eco Chemie B. V. Utrecht, Netherlands). The WE is the electrode at which the electrochemical process of interest takes place, whilst the role of the RE is to provide a fixed potential to which the potential of the WE is referred. The RE is also sometimes called the ideal nonpolarisable electrode. The purpose of the CE is to supply the current required by the WE, without limiting the measured response of the cell. In this sense, it should not impose any characteristics on the measured data, and as consequence it should have a large area compared to the working electrode. In our three-electrode system an optically transparent electrode (OTE) was used as the WE, a Pt coil served as the CE whilst all potentials were given versus the quasi-reference electrode (Ag/AgCl).

An optical microscope (Jenalab; Carl Zeiss, Germany) connected to a video camera (TK-1085E; JVC, Japan) with PC data collection (Presto Video Works Ver 4.1 Rev 6; Newsoft Technology Corp, Taiwan) was used for image collection and processing and images were analysed using Presto Video Works PC data collection software and CorelDraw (version 8.232). Absorption spectra were recorded with an Agilent 8453 UV-visible spectrophotometer (Agilent technologies) on plain glass microscope slides (0.80 mm x 1.00 mm thick) or quartz cuvettes (pathlength 1.0 mm) using UV-visible ChemStation software (Rev. A. 09. 01, Agilent technologies) in kinetic mode (i.e. spectra acquired at regular or increasing time intervals over a period of time). The spectrophotometer experiments run time ranged from 1000 s to 4500 s with spectra being recorded at intervals of 2 s or 10 s. The wavelength acquisition range was from 200 – 1100 nm and time traces at 600, 650, 700 and 800 nm were monitored.

The temperature was controlled with the use of a small peltier device (Thermo Electric Cooler Type DT1069; Marlow Industries Inc., USA) and measured with a home-made thermocouple. The copper plate above the peltier device allowed for efficient heat transfer between the peltier device and the microscope slide or quartz

cuvette. Temperature manipulations were carried out using programmable water bath (Grant LTD6 waterbath, Grant Instruments Ltd, Cambridge) with a temperature range of – 20 °C to 100 °C. A digital pH meter (PH215, Denver Instruments, Germany) was used to produce solutions of different pH.

2.4 Construction of Thin Layer Electrochemical Cells

A series of robust and easily constructed thin-layer cells were designed specifically for optical and spectroelectrochemical measurements. The Pt coil electrochemical cell (chapter **3**) was used exclusively for imaging with the optical microscope whilst the Au micro-mesh electrochemical cell (chapter **4**) and Pt matrix electrochemical cell (chapter **5**) were used to monitor protein growth with the UV-visible spectrophotometer. The fabrication of each cell is detailed in the relevant chapters.

Cleaning of the electrochemical cell followed a general procedure, termed as experimental procedure **1**. The cell was soaked in pure water and medical wipes (Kimberley-Clarke, UK) were used to draw the solution out. This was performed as many times as was necessary until the red colouration of the protein disappeared. The electrodes were electrochemically cleaned by cycling in 0.1 M sulphuric acid until there was no further change in the voltammetric response. Two sets of thirty CV cycles were generally performed, with new acid solution being used after the first thirty cycles and the electrochemical cell was finally rinsed with copious amounts of H_2O.

2.5 HbS Polymerisation

Three main techniques were used to achieve polymerisation of HbS: *in-situ* electrochemical deoxygenation, *ex-situ* temperature jump method and *ex-situ* salting out method. The *ex-situ* techniques were generally used for those experiments where imaging could not be performed immediately due to further preparation, such as in AFM experiments (chapter **3**) or for the direct electrochemistry experiments (chapter **7**).

In situ Electrochemical Deoxygenation: Polymerisation using Electrochemistry:
HbS polymerisation was primarily achieved using electrochemical means by electrochemical O_2 reduction of a small volume of HbS solution within a purpose built electrochemical cell using step potential chronoamperometry. This is termed experimental procedure **2** and is described in more detail in section **2.6**.

Polymerisation using temperature jump method:
This method (experimental procedure **3**) is a slight modification of the procedure described by Adachi *et al.* [81]. A solution of HbS protein dissolved in 0.1 ml phosphate buffer (1.5 M, pH 7.0) was degassed thoroughly by passing a stream of Ar gas over the top of the solution for 1 hour and was subsequently placed into a cuvette of pathlength 1 cm under an inert atmosphere. A further 1.0 ml degassed H_2O was added to the HbS solution and the cuvette was placed in a waterbath set at 2 °C for 30 minutes. The temperature jump was obtained by quickly transferring the cuvette to a water jacketed cuvette holder at a temperature of 38 °C positioned in front of the spectrophotometer light beam. The jacketed cuvette holder was also at a temperature of 38 °C. All spectra's were examined to ensure a significant increase in the absorbance was seen to indicate formation of HbS aggregates. If no such increase was seen then the solution was not used for any further experiments. All solutions were stored under Ar in the fridge until use and used within one day of initial preparation.

Polymerisation using Isothermal salting out method:

This procedure [82] (experimental procedure **4**) involved degassing a solution containing 2.4 ml phosphate buffer (2.52 M, pH 7) in a cuvette (1 cm pathlength) for 1 hour. Sodium dithionite (10 mg ml^{-1}) was added in some cases to ensure buffer solution remained O_2 free. Sodium dithionite would have been all used up scavenging buffer O_2 before coming into contact with any protein. The cuvette was sealed with parafilm and placed into a waterbath set at 38 °C. At the same time, a solution of HbS dissolved in low molarity 0.025 M phosphate buffer solution was placed in an epphindorf vial, deoxygenated thoroughly by passing a stream of Ar over the top of the solution, and placed into the waterbath at 38 °C. Once both solutions had equilibrated to the waterbath temperature, the cuvette was placed in a water jacketed holder positioned in the spectrophotometer and HbS solution was quickly added causing HbS protein aggregates to be formed. The HbS polymer formation, as a result of salting out at isothermal conditions, was followed spectrophotometrically. Spectra which did not show an increase in the absorbance were not used any further. All solutions were stored under Ar gas in the fridge until use and used within one day of its initial preparation.

2.6 Electrochemistry

The two electrochemical methods mainly used were step potential chronoamperometry and CV. Deoxygenation of the HbS solution was performed by electrochemical reduction at the electrode surface using step potential chronoamperometry. The HbS solution was held at a potential E = 0 V for 3 s initially and then stepped to E = - 0.55 V versus the quasi-reference electrode. The time of the step potential experiment varied from 1000 s to 6000 s. A typical chronoamperometric scan observed in our experiments is shown in figure **2.1**. These were similar to the characteristic current density evolution response seen in figure **1.22**; initially a large current was detected which steadily decayed with time.

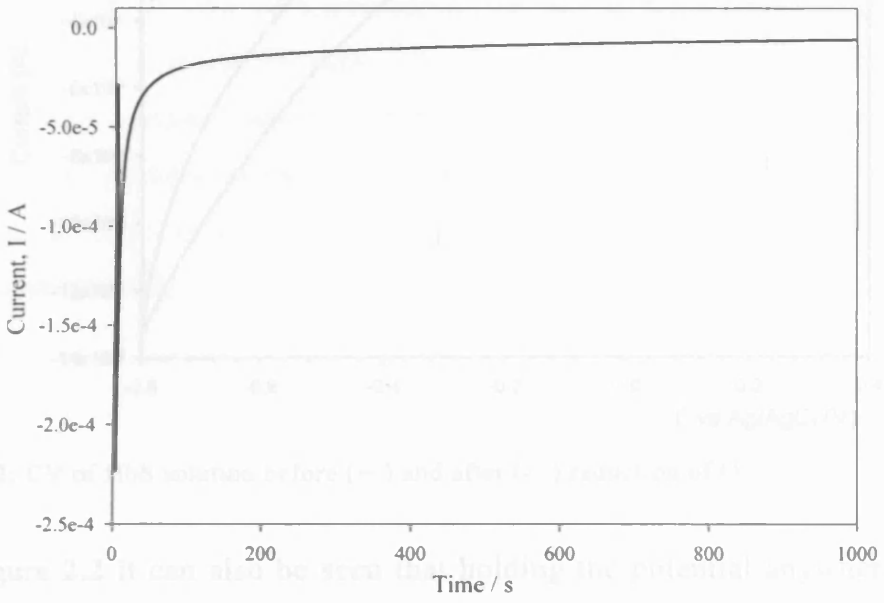

Figure 2.1: A typical current density evolution response seen in our HbS polymerisation potential step experiments.

A thorough CV study was performed on the HbS protein solution consisting of 1.5 M (pH 7.0) phosphate buffer and 0.5 M NaCl, before every experiment to ascertain the electrochemical potential window of O_2 in solution at the particular electrode being used (this varied when using different electrode materials). CV potentials ranged from + 0.5 V to – 0.8 V for the forward and reverse cycle and were scanned at a rate of 25 mV s^{-1} versus the quasi-reference electrode.

CVs were also performed before and after the chronoamperometry experiments to monitor the extent of O_2 reduction and to confirm electrochemically that complete

reduction of O_2 had been achieved. This was an important step to ensure that the electrode surface environment was conducive to maximal HbS polymerisation and growth. Figure **2.2** demonstrates a pair of CV plots performed on HbS solution before and after the potential step experiment and it can be seen that the CV performed prior to O_2 reduction (solid line) has a large shoulder, attributable to O_2 presence, in the potential range -0.25 V to -0.8 V. This shoulder is not present in the CV (dotted line) after the reduction process meaning that O_2 had been largely removed giving an anaerobic environment.

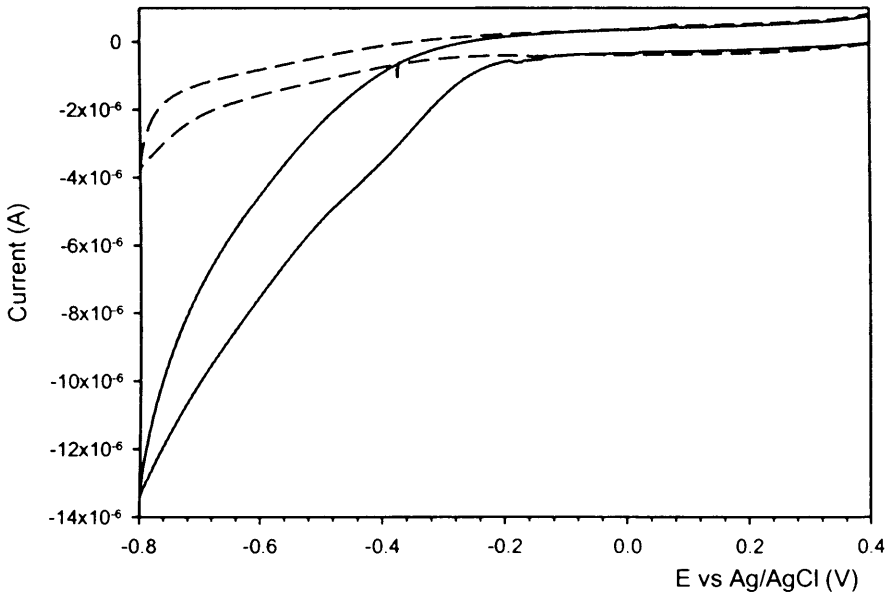

Figure 2.2: CV of HbS solution before (—) and after (---) reduction of O_2.

From figure **2.2** it can also be seen that holding the potential anywhere in the O_2 shoulder range of -0.3 to -0.8 V would cause O_2 reduction and therefore a potential of -0.55 V versus the quasi-reference electrode was chosen. Furthermore, complete deoxygenation was confirmed electrochemically by comparing the minimum charge needed to remove all O_2 from a cell with the actual experimentally obtained value. This electrochemical method of polymerisation induction by O_2 depletion is referenced as experimental procedure **2**.

2.7 Optical Microscope Experiments

The potentiostat was coupled with the optical microscope to allow the ensuing HbS polymerisation process to be followed *in situ*. A solution of HbS and 0.5 M NaCl, added as supporting electrolyte to increase the ionic strength, was dissolved in air-saturated 1.5 M phosphate buffer (pH 7) and pipetted under the coverslip. The cell was placed on the optical microscope stage and the electrodes were connected to the potentiostat and a CV was performed on the background solution of 1.5 M, pH 7 phosphate buffer and 0.5 M NaCl before every experiment. A Jenalab optical microscope connected to a JVC video camera was used to focus upon either a section of the electrode or the whole electrode before the start of the experiment and deoxygenation was performed by electrochemical reduction at the electrode (E = -0.55 V) using chronoamperometry methods (see experimental procedure **2**). Changes at the electrode were monitored and images were collected and analysed using Presto Video Works PC data collection software. CV was performed straight after the chronoamperometric experiment to confirm disappearance of the O_2 shoulder. The electrochemical cell was cleaned as described in experimental procedure **1**. The optical microscope experimental will be referred to as experimental procedure **5** in discussions further in this thesis.

2.8 Spectroelectrochemistry Experiments

A potentiostat was coupled with the UV-visible spectrophotometer so that changes in turbidity as a result of formation of protein aggregates could be monitored *in situ*. Hb protein was dissolved in a solution containing both 1.5 M phosphate buffer (pH 7) and 0.5 M NaCl and 50 µl ± 10 µl of the Hb solution was introduced into the cell. High molarity phosphate buffer and NaCl were used to increase the ionic strength and thus increase conductivity of the solution. The electrochemical cell was fixed vertically on to the back of the thermostat stage which was clamped in position in front of the spectrophotometer light beam. Fixing the cell onto the thermostat allowed relatively easy control and access of the HbS solution temperature within the cell.

Both the potentiostat and the UV-visible spectrophotometer were started simultaneously. Absorption spectra were recorded in kinetic mode with spectra being taken every second or every 2 s whilst deoxygenation of Hb solution was performed electrochemically (E = -0.55 V versus the quasi-reference electrode). In experiments where electrochemistry was not performed, solutions of phosphate buffer were thoroughly degassed with a continuous supply of Ar prior to the experiment. CVs of the initial solution were recorded before and after every experiment (+ 0.5 to - 0.8 V versus quasi-reference electrode at a rate of 25 mV s^{-1}) and the time of the experiments varied from 1000 s to 6000 s. All solutions were used within a day of their preparation. The cell was cleaned as described in experimental procedure **1**. The spectroelectrochemistry procedure will be referred to as experimental procedure **6** in future discussions.

2.8.1 R to T State Conversion of Hb

Absorption spectroscopy was used to ascertain whether conversion of oxyHbS to deoxyHbS had occurred. It was important to spectroscopically demonstrate the mechanistic R to T state flip as exposure of the hydrophobic pocket by which HbS molecules aggregate only occurs in the T state. The spectroscopic set-up could also be utilised to check the efficiency of deoxygenation at specific points during the experiment. Figure **2.3** shows the conversion of oxyHbS to deoxyHbS at the WE. HbS concentration of 10 mg cm^{-3}, dissolved in a salt solution comprising 1.5 M potassium phosphate buffer and 0.5 M NaCl, was used and the electrode was held at - 0.55 V for 1000 s. Characteristic peaks at wavelengths 540 nm and 580 nm seen at 0 s indicated the presence of oxyHb [83], whilst the reduction of O_2 through potential-step chronoamperometry allowed the T state of Hb, characterised by the replacement of the two peaks by a single peak at 560 nm, to be formed within 200 s. Consequently, all spectra were checked after each experiment to ensure complete conversion had taken place.

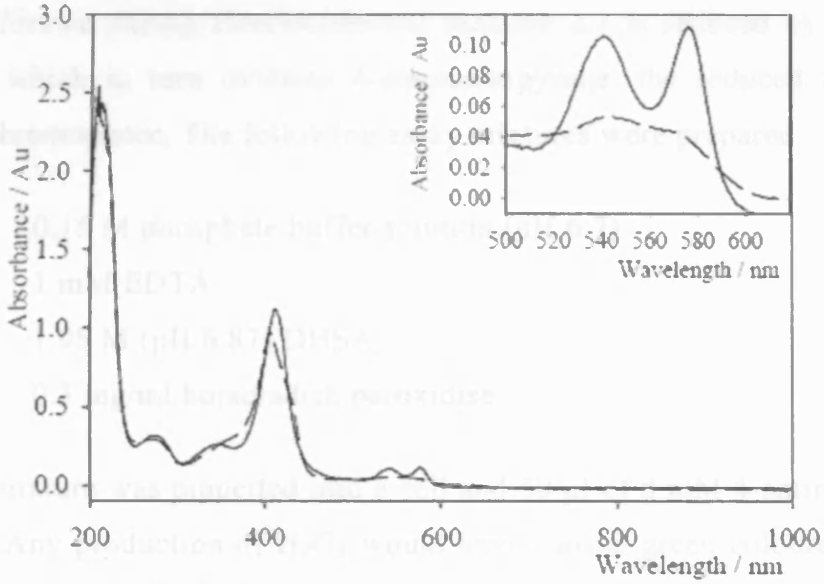

Fig. 2.3: *In situ* spectroelectrochemistry experiment showing the conversion of oxyHbS to deoxyHbS, before electrochemical depletion of oxygen (—) and after 1000 s (---). The insert shows the absorbance between 500 to 620 nm for the same spectra; a conversion of two peaks at 540 nm and 580 nm to a single peak at 560nm is observed. Experiment conditions: HbS concentration 10 mg cm^{-3}; 1.5 M pH 7.0 phosphate buffer; 0.5 M NaCl; E = -0.55 V vs Ag/AgCl for 1000 s.

2.8.2 Spectrophotometric Assay for H_2O_2

A spectrophotometric assay method was also employed to ensure that changes in absorbance were directly attributed to the formation of HbS aggregates. It was paramount that the O_2 reduction reaction proceeded to completion to avoid any production of H_2O_2, which can cause Hb cell degradation and heme loss. As described earlier, the O_2 reduction reaction at a metal surface is a complex multi-electron process involving different reaction intermediates, with O_2 either being electrochemically reduced directly to H_2O or to intermediate H_2O_2. Consequently, the production of H_2O_2 in the HbS solution during the course of the reduction experiment was assayed by a spectrophotometric technique based on an enzyme linked detection system first described by Barham and Trinder in 1972 [84]. Essentially the reactions that take place in this system are as follows:

$$O_2 + HbS_{(oxidised)} \rightarrow H_2O_2 + HbS_{(reduced)} \quad \textbf{(2.1)}$$

$$H_2O_2 + \text{4-aminoantipyrene}_{(reduced)} + \text{Peroxidase} \rightarrow \text{4-aminoantipyrene}_{(oxidised)} \quad \textbf{(2.2)}$$

Any H_2O_2 formed during electrochemical reaction **2.1** is reduced by horseradish peroxidase which in turn oxidises 4-aminoantipyrene, the reduced acceptor, to produce a chromophore. The following assay mixtures were prepared:

1.55 ml	0.15 M phosphate buffer solution (pH 6.7)
1.55 ml	1 mM EDTA
0.20 ml	1.95 M (pH 6.87) DHSA
0.20 ml	0.3 mg/ml horseradish peroxidise

The above mixture was pippetted into a cell and 50 µl of 8 mM 4-aminoantipyrene was added. Any production of H_2O_2 would have caused green colouration around the WE. The rate at which this chromophore appeared was monitored at 520 nm and assays were carried out in all thin-layer electrochemical cells, both in the background salt solution and in the HbS solution. Run time of this experiment varied from 60 s to 1000 s. The detection limit of this assay was estimated, in a homogeneous cell, to be 1×10^{-7} M. All assays confirmed that there was no H_2O_2 formation.

Chapter 3: HbS Aggregation in Pt Coil Cell

3.1 Introduction

In this chapter, the fabrication of the first in a series of three robust electrochemical cells used to house the previously explained HbS coupling reaction is described. The modulation of HbS fibrous growth at the electrode surface and the conditions for reproducible growth of HbS aggregates in the Pt coil electrochemical cell are presented whilst the visualisation of aggregates using optical microscopy is described. The fabrication of an electrochemical cell was required to perform electrochemical deoxygenation on small volumes of Hb and monitor the ensuing effects on protein aggregation, and therefore the methods by which optimisation of O_2 depletion was achieved in the Pt coil electrochemical cell are also explained. Furthermore, experiments depicting the imaging of HbS aggregates with atomic force microscopy (AFM), using a number of imaging surfaces and *ex-situ* procedures are described.

3.2 Experimental

3.2.1 Materials, Instrumentation and Procedures

The optical microscope experiments were performed according to experimental procedure **5**. HbS protein was dissolved in air-saturated 1.5 M (pH 7.0) phosphate buffer and 0.5 M NaCl was added as supporting electrolyte to make the polymerising solution. All experiments were performed at room temperature unless otherwise stated. HbA was used for the control experiments and the mixtures were prepared in the same way as HbS solutions. HbS concentrations of 50 mg cm^{-3} and 300 mg cm^{-3} were primarily used as protein concentration needed to be high enough for aggregation to occur but also low enough so that protein use was minimised. Pt wire (diameter 0.1 mm, hard temper, 99.99 % purity) and silver (Ag) wire (grade 1, diameter 0.05 mm) were employed as the electrodes (chapter **3.2.2**). The general experimental and all apparatus for the above techniques are described in chapter **2**.

Ex-situ AFM experiments were performed using the Dimension 3100 AFM (Veeco Instruments, Santa Barbara, Ca.) controlled by Nanoscope version 6.12 software for image collection. Silicon nitride cantilevers were used for both contact mode imaging (DNP-S, Veeco, Santa Barbara, Ca.) and tapping mode imaging (OMCTL, 280kHZ, Veeco, Santa Barbara, Ca) whilst images were analysed using offline Nanoscope version 6.13r1 software and WXSM software.

HbS aggregates for AFM imaging were produced using the *ex-situ* isothermal salting out method (experimental procedure **4**). A solution of 10 mg cm^{-3} HbS protein was added to pH 7.58, 2.52 M phosphate buffer for the stock and dilutions of 1:50, 1:500 and 1:5000 were made. No sodium dithionite was added. Freshly cleaved mica stuck on a small piece of glass was dipped into the HbS fibre solution stored under an inert atmosphere. The solution was left to incubate on the mica for 10 s and then fixed using 3% glutaraldehyde solution by slowly adding and removing the solution from the surface of the mica. The fixative was left to set for 15 minutes and the mica was washed by slowly immersing into pure water (3 x 200 µl) and nitrogen dried.

3.2.2 Construction of Pt Coil Thin Layer Electrochemical Cell

A glass microscope slide (25 mm x 50 mm) was used as the base of the electrochemical cell. Three electrodes (100 μm diameter coiled Pt wire WE, 100 μm coiled Pt wire CE and 50 μm Ag wire RE) were fixed onto the slide and connected to copper electrical wires using silver conductive paint. Epoxy sealant was applied for electrical insulation and stability and a coverslip was fixed on top of the electrodes by carefully seeping epoxy resin. Only one edge of the coverslip was fixed to allow diffusion of atmospheric O_2 into the cell and pressure was applied when fixing the coverslip to ensure a thin layer was obtained. A schematic representation of this cell is shown in figure **3.1**.

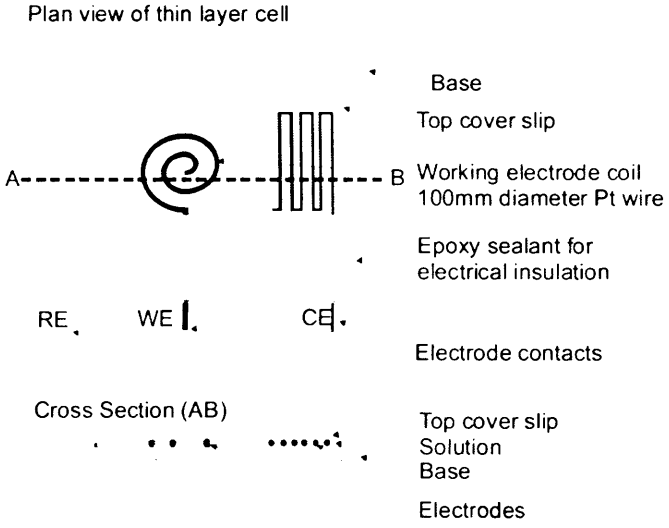

Figure 3.1: Plan view of Pt coil thin layer electrochemical cell incorporating a three electrode system with a 100 μm diameter coil shaped Pt wire as the WE, a 100 μm coil shaped Pt wire as the CE and a 50 μm Ag wire as the RE. The WE coil was composed of five turns, whilst the CE coil was composed of ten turns. The Ag wire was anodised with AgCl prior to use. A microscope slide was used as the base of the cell and a glass coverslip was placed on top to obtain a thin layer. Epoxy sealant was applied for electrical insulation. Not to scale.

To obtain good electrochemical measurements the RE was positioned close to the WE whilst the area of the CE was twice that of the WE. This was achieved by doubling the number of coils in the counter electrode. All materials used in the fabrication of the cell were thoroughly cleaned prior to its construction using acetone.

3.3 Electrochemical Cell Design

Two essential features of the electrochemical cell, necessary for monitoring the growth of HbS aggregation at an electrode, were optical transparency and the capacity to perform electrochemistry on small volumes of oxygenated HbS solutions (i.e. a thin-layer). Optical transparency was essential so that any physical or structural changes occurring at the electrode or in the bulk solution surrounding the electrode could be easily identified and followed through optical or spectroscopic means. This was primarily achieved by incorporating an OTE as the WE. Even though the Pt coil electrode was not an OTE by definition, it could essentially be classed as one due to the compact coil geometry of the electrode allowing changes to be followed at different points along the surface. Transparency was also achieved by using a non-conductive glass microscope slide as the base of the cell and a plastic transparent coverslip.

Use of the coverslip also ensured small solution volumes. A thin layer of solution was necessary as it enabled minimal use of protein material in the solution reaction as well as caused the diffusion rate of electro-generated species moving into the bulk solution to be increased. In some electrochemical cells, small solution volumes were achieved by housing the electrodes in 1 mm pathlength cuvettes.

Another essential attribute was the geometry of the WE. The incorporation of a WE whose geometry allowed a more efficient electrochemical reduction of O_2 ensured faster HbS polymerisation kinetics. Originally, a single Pt wire was used as the WE but by changing the geometry to a coil, an improved arrangement for O_2 depletion within the thin layer electrochemical cell was achieved, see chapter **3.4**. The fabrication of all electrochemical cells in this thesis followed similar design specifications.

3.4 Optimisation of the Pt Coil Cell

The original design of the electrochemical cell incorporated a single Pt wire (25 μm diameter and 10 mm length) as the WE and not a coil. After unsuccessful attempts with this cell, it was thought that the electrical conductivity of the WE was not high enough to remove all of the O_2 in the cell combined with the O_2 diffusing into the system (D = 1.97 x 10^{-5} cm^2 s^{-1}). Therefore, the diameter of the Pt wire WE was changed from 25 μm to 100 μm. An increase in the diameter of the electrode not only increases the current passing through it thereby increasing the conductivity but it also increases the surface area exposed to the solution and with it the volume of HbS solution being reduced (conductivity, $\varepsilon = 1 / (RS / l)$, where R is the resistance, l is the length and S is the cross-sectional area of a uniform specimen of the material). However, although the conductivity and exposed surface area increases, the thickness of the O_2 reduction diffusion layers from the material remains uniform, as thickness is given by $\Delta = \sqrt{2Dt}$, and therefore does not depend on the dimensions or properties of the material.

Results were finally obtained when the geometry of the WE was changed from a single Pt wire to a compact Pt coil structure of 100 μm diameter with a set number of turns (figure **3.1**). This was performed to increase the O_2 reducing ability and achieve more efficient electrochemical O_2 depletion of the solution present within the coil, not distinguishing between solution directly in contact with the electrode or that present in the bulk within the coil. The main advantage of this WE, compared to the Pt wire, was that instead of having a uniform O_2 reduction diffusion thickness, this geometry ensured that O_2 reduction efficiency increased as you moved into the middle of the coil. However, as the electrode was coiled manually, a major drawback of this geometry was the inability to control the exact dimensions of the coil such as the number of turns and the size and the compactness of the coil. This meant that reproducibility of results was difficult to achieve. In chapter 4, the fabrication of a Au micromesh cell, built to overcome this problem, and its use in obtaining kinetic rate constants for the nucleation and elongation of HbS aggregates is described.

3.5 Growth of HbS Fibrous Structures at Pt Coil Cell

Electrochemical techniques were used to investigate the growth of HbS aggregates in a thin layer optical cell to establish the conditions which would allow reproducibly fast HbS nucleation and polymerisation to occur. The geometry of the electrodes was found to be essential for the growth of HbS fibrous structures as the first structures were only seen when the WE was of a coiled geometry. The many experiments performed prior to using a coil did not give any results.

Figure **3.2** shows the changes in structure morphology on the surface of the Pt coil working electrode when a solution of 33 mg cm^{-3} HbS dissolved in 1.5 M, pH 7.0 potassium phosphate buffer was reduced (E = - 0.70 V). 5 mM sodium dithionite was also added and the solution was degassed for an hour and then stirred for a further four hours before any electrochemistry was performed on the solution.

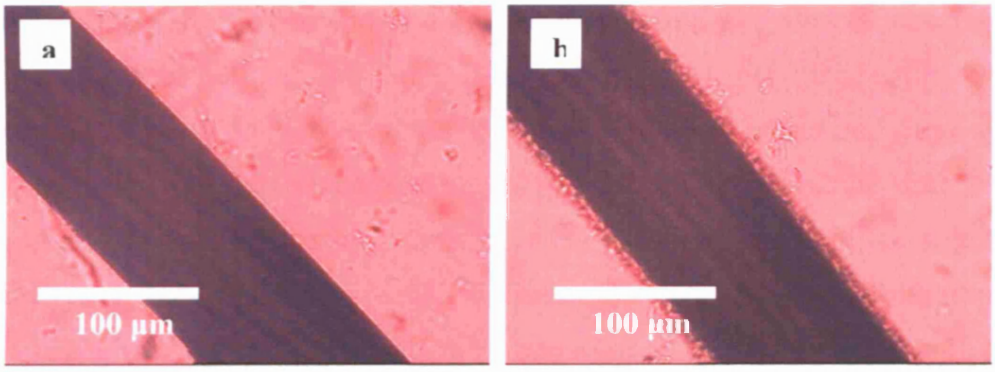

Figure 3.2: Optical images of a section of the Pt coil WE at **(a)** time = 0 s; **(b)** time = 344 s showing the initial stages of HbS aggregate formation at the electrode surface. Experiment conditions: HbS concentrations 33 mg cm^{-3}; 1.5 M pH 7.0 phosphate buffer; 5 mM sodium dithionite; N_2 degassing (1 hr); stirring (4hrs); E = - 0.70 V *vs.* Ag/AgCl for 4000 s.

The fur-like structure, evident in figure **3.2 (b)**, was the first time structural changes at the surface had been seen after electrochemical reduction of O_2. The initiation of these aggregated structures occurred at time = 344 s and the structures subsequently grew in length as the experiment proceeded. However, due to many limitations of this preparation, such as the sporadic and non-uniform growth of the structures across the coil, inconsistent reproducibility of results and the long time taken for initiation of the structures, changes were made to the conditions to overcome these problems. The time taken for the structures to appear can be thought of as the "delay time" and was dependent on the rate of deoxygenation and

rate of nucleation of aggregation. Consequently, the HbS concentration was increased from 33 mg cm^{-3} to well above saturation concentrations of 300 mg cm^{-3}, whilst more importantly 0.5 M NaCl was added to increase the ionic strength and thus the conductivity of the solution. A high molarity phosphate buffer was originally used as studies have shown that high buffer concentrations are associated with polymerisation at much lower protein concentrations (see chapter **1.2.5**) [31, 32], however, it was found that using buffer lower than 1.5 M did not produce any results even when the HbS concentration was significantly increased. Further changes included doubling the number of turns on the coil from five to ten turns to try to maximise depletion of O_2, whilst the chronoamperometric potential of the electrode was also changed to - 0.55 V *vs.* the quasi-reference electrode, instead of - 0.70 V, as H_2 gas evolution was observed at potentials higher than - 0.60 V.

Figure **3.3** shows the surface morphology of the coil WE at different time intervals when a solution of 300 mg cm^{-3} HbS dissolved in 1.5 M, pH 7.0 phosphate buffer was reduced (E = - 0.55 V *vs.* Ag/AgCl). 0.5 M NaCl was added and there was no degassing or stirring performed and no sodium dithionite added. At time = 0 sec the Pt electrode was bare but at time = 163 s the first formation of aggregated structures was seen. In other words, the onset of HbS aggregate formation was seen at 163 s, whilst also visible was the elongation of aggregates after 3570 s.

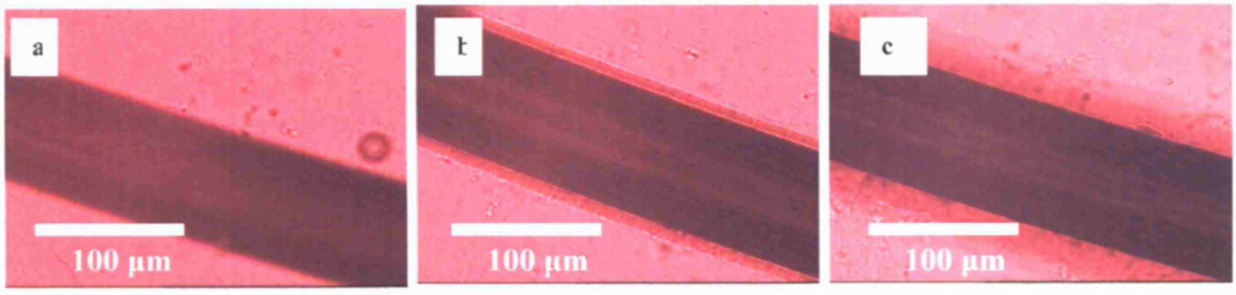

Figure 3.3: Optical images of a section of the Pt coil working electrode at **(a)** time = 0 s; **(b)** time = 163 s; **(c)** time = 3570 s showing the nucleation and growth of HbS aggregates. Experiment conditions: HbS concentrations 300 mg cm^{-3}; 1.5 M pH 7.0 phosphate buffer; 0.5 M NaCl; E = - 0.55 V *vs.* Ag/AgCl for 6000 s.

A significant decrease in the delay time to 163 s was apparent in this experiment. This was primarily due to the addition of NaCl which increased the ionic strength

of the solution and had a pronounced effect on the induction times of HbS aggregate formation. The high ionic strength also provided a salting out effect for solubility purposes and thus, the use of NaCl as an additive was present in all further experiments. Ionic strength and salt type have been shown previously to influence aggregation and growth of HbS fibres in other experimental systems [85]. These measures decreased the delay times of nucleation and increased the growth rate through an increase of factors which affect polymer formation and hence improved experimental reproducibility.

In vivo Hb concentration per red blood cell (MCHC) is 320 mg cm^{-3} to 360 mg cm^{-3} [86] and the ionic strength of blood plasma is 0.16 M [87]. The choice of 300 mg cm^{-3} as the protein concentration allowed a direct comparison to be made with polymerisation *in vivo*. However, a system where lower ionic strength solution can be used still needs to be developed. Furthermore, it was also noticeable that the aggregated structures present in the optical microscope images in figure **3.3** did not look fibrous (unlike the single fibres observed in figure **1.10** in chapter **1.3.5)**. This was primarily due to the low resolution available with the optical microscope as well as possibly an increased gelation effect occurring with the use of electrochemistry and thus obscuring individual fibres. Thus, the exact nature and structure of these aggregates could not be distinguished using the optical microscope and further studies will need to be performed using AFM to elucidate the exact structural nature of the electrochemically modulated aggregates.

3.6 Control Experiments

The control experiments performed in this investigation consisted of substituting HbA for HbS under the same electrochemical conditions in the thin layer cell. Once O_2 was removed, there was no aggregation of HbA observed on or near the coil at the end of an experiment over a period of 6000 s, figure **3.4 (b)** versus **3.3 (c)**. The only difference between HbA and HbS is a single amino acid (β6 glutamic acid to valine); HbA monomers do not tend to aggregate even though exposure of the hydrophobic pocket occurs in HbA when in the T allosteric state as charge and size effects prevent 6β glutamic acid from binding. Therefore any differences seen in the results performed with either protein was directly attributable to this single amino acid variation. This provided the most compelling evidence that those structures seen on the electrodes were HbS polymers and higher order aggregated structures and not as a result of other factors, such as salt precipitation. Furthermore, aggregated structures whose growth had been modulated electrochemically were also seen to disappear once the potential had been switched to open circuit and O_2 had been allowed back into the cell. This reversibility displayed upon reoxygenation is not only specific to our system but also occurs physiologically in the blood vascular system [88].

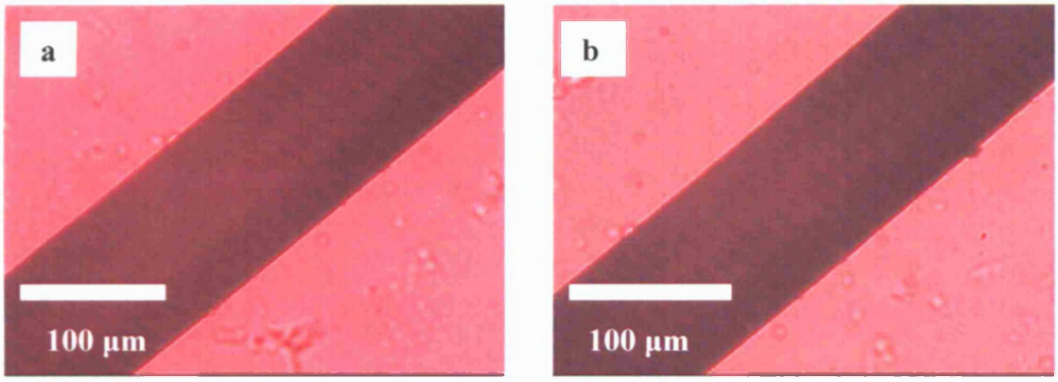

Figure 3.4: Optical images of a section of the Pt coil we when HbA solution was electrochemically deoxygenated. No fibre formation is seen at **(a)** time = 162 s; or **(b)** time = 5280 s. Experiment conditions: HbA concentration 310 mg cm^{-3}; 1.5 M pH 7.0 phosphate buffer; 0.5 M NaCl; E = - 0.55 V *vs.* Ag/AgCl for 6000 s.

HbA was an excellent control protein to use due to the high degree of similarity between the structures of HbA and HbS on the one hand but the contrasting

polymerising behaviour on the other. Consequently, HbA control experiments consisting of the same conditions and procedures were used in all subsequent experiments including those performed with the Au micromesh cell, Pt matrix cell aswell as the direct electrochemistry experiments (data not shown for all control experiments).

3.7 Stages of Growth

Another aspect which was investigated was the nature and rate of growth of these optically visualised aggregated structures over the time-course of the experiment. The optical microscope images showed three distinct stages of HbS growth. The first stage, occurring from 0 s to 200 s, was the time delay where no growth was observed. This was followed by early stage growth consisting of single hair-like strands protruding out of the electrode and these structures were apparent from the initiation of growth till approximately 2000 s (figure **3.3 (b)** and figure **3.5 (a)**). Finally, late stage growth occurred from 2000 s to 6000 s and showed structures which were gel-like, consisting of domains and cells rather than hair like fibres, protruding into the bulk solution (figure **3.5 (b)**). This was an interesting aspect present in all HbS aggregation experiments observed with the Pt coil cell.

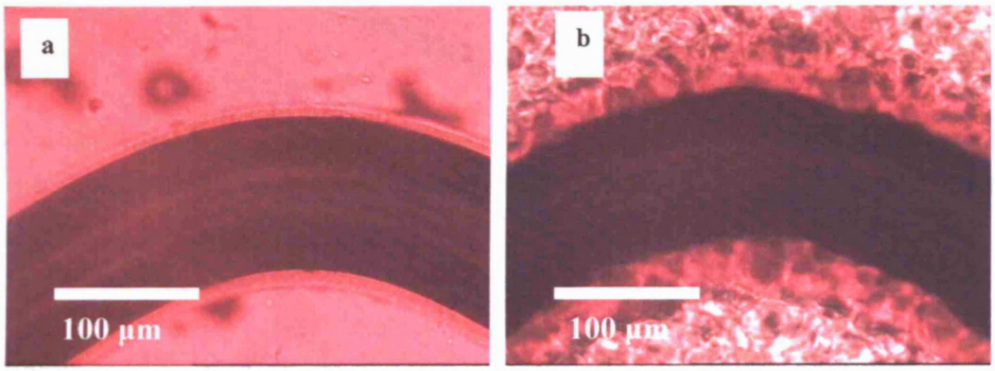

Figure 3.5: Optical images of the Pt WE in **(a)** the early stage growth, time = 338 s; **(b)** the late stage growth, time = 4047 s. Experiment conditions: HbS concentrations 350 mg cm^{-3}; 1.5 M pH 7.0 phosphate buffer; 0.5 M NaCl; E = - 0.55 V *vs.* Ag/AgCl for 5000 s.

Furthermore, optical images also showed that the formation of these aggregated structures initially occurred only at the electrode surface and not in the bulk solution (figure **3.6 (a)**). The geometry of the WE indicated that complete O_2 reduction of the HbS solution present within the coil should be achieved, whether it was the solution directly in contact with the electrode or that present in the bulk within the coil. Therefore, protein aggregation should have occurred at the electrode surface and in the bulk solution inside the coil simultaneously, but this was not seen. This was probably because growth at the surface was thermodynamically more favourable than growth in solution, due to the fact that the surface fixed molecule orientation, contributed to alignment and most

importantly acted as an anchor for the attachment of HbS molecules. The conducting electrode surface itself could be thought of as an existing polymer on which growth of new polymers occurred. Once aggregation had occurred at the electrode, further nucleation on existing polymers, diffusion of aggregated structures away from the electrode and fibre breakage led to fibres in the bulk solution acting as nucleating centres, along with dirt or salt molecules, for the initiation of more polymers (figure **3.6 (b)**)

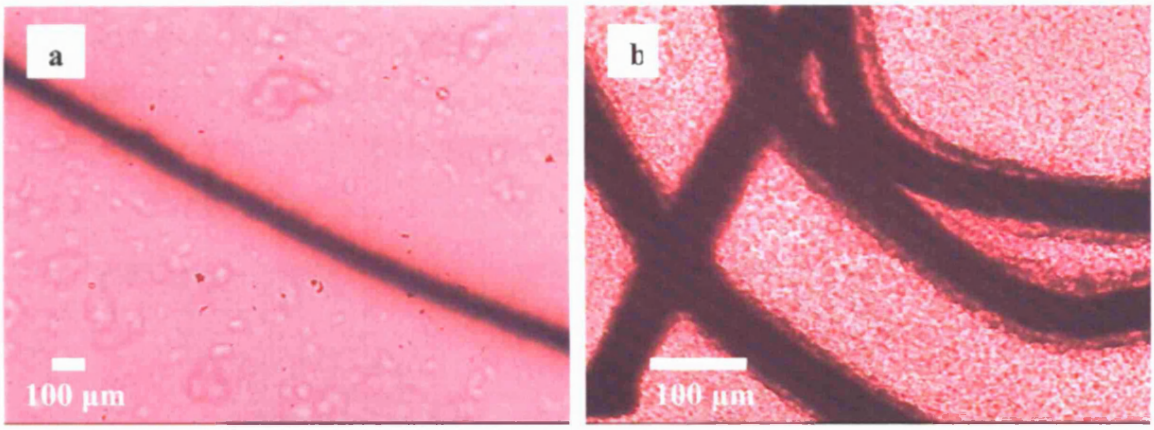

Figure 3.6: Optical images of the Pt WE in **(a)** time = 1276 sec ; **(b)** time = 4989 sec. Experiment conditions: HbS concentrations 350 mg cm^{-3}; 1.5 M pH 7.0 phosphate buffer; 0.5 M NaCl; E = -0.55 V *vs.* Ag/AgCl for 5000 sec.

The growth of HbS aggregates as seen with the optical images suggested that HbS aggregation occurs through a three step mechanism at the surface. The first step is the time delay before any growth is observed, followed by two distinct stages of growth as seen in figures **3.5 (a)** and **(b)**. This is in contrast to the traditional double nucleation model for HbS polymerisation consisting of homogeneous nucleation, which exhibits a delay time before the formation of polymers, and heterogeneous nucleation, which involves the exponential growth and branching of polymers on existing polymers. Further experiments with UV-visible spectroscopy were conducted to distinguish the mechanism of growth at the surface compared to growth in solution (see chapter 5).

It was also seen from the optical experiments that the nature of the electrochemically modulated aggregated structures on the electrode surface was different when differing additives were used. Figure **3.7** shows the late stage growth of two experiments, one where 5 mM sodium dithionite has been used and another in which 0.5 M NaCl was added. The optical image where sodium

dithionite was employed is noticeably distinct from the one in which NaCl had been used. The presence of granular structures in the solution surrounding the electrode is noticeable with sodium dithionite, whilst the fibres protruding from the electrode with sodium dithionite are also more compact and less domain-like than its counterpart. Sodium dithionite is a highly unstable reducing agent which scavenges residual O_2, even being consumed by reducing atmospheric (as opposed to solution and HbS bound) O_2. Furthermore, H_2O_2 results, if all the dithionite is not used up, which damages the protein. Consequently, the differences in structures seen in these images could have been as a result or a combination of these factors. The granular structures and non-domain like structures present in figure **3.7 (a)** could be pockets of protein damage present in the solution due to the presence of peroxide.

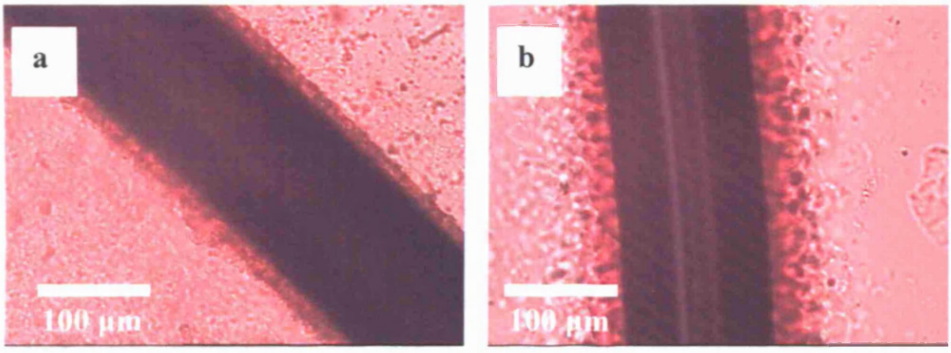

Figure 3.7: Optical images of the Pt WE showing the differences in growth when different additives **(a)** 5 mM sodium dithionite; **(b)** 0.5 M NaCl were used. Experimental conditions: HbS concentrations 300 mg cm^{-3}; 1.5 M pH 7.0 phosphate buffer; E = - 0.55 V *vs.* Ag/AgCl for 5000 s.

3.8 Growth Rate

A video clip of the growth of HbS aggregation at a bare Pt coil electrode was made by performing an experiment in which optical images of a small section of the Pt coil electrode was taken every 20 s over a period of 6000 s and the images were linked together using image processing software. The video showed the change in protein morphology from a strand like to a globular cell like structure on the surface of the electrode. Figure **3.8** shows a single image of the Pt electrode at 240 s (the film clip of the growth of protein fibres at the Pt electrode is available online as electronic supplementary information [89]).

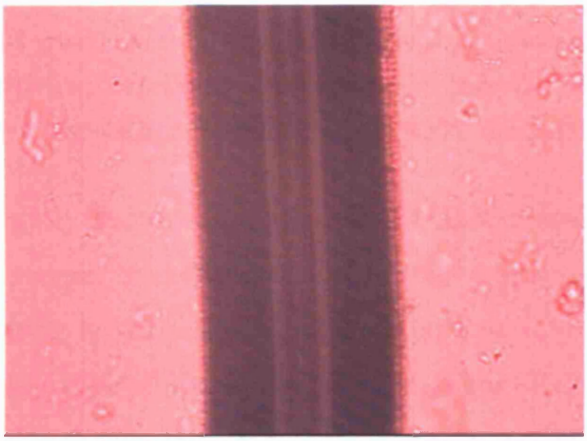

Figure 3.8: A single optical image of a section of the Pt coil WE taken at 240 s as part of a video clip showing growth of HbS aggregates at the surface. Experiment conditions: HbS concentrations 354 mg cm^{-3}; 1.5 M pH 7.0 phosphate buffer; 0.5 M NaCl; E = - 0.55 V *vs.* Ag/AgCl; run time 6000 s.

The growth rate of the HbS fibres shown in the video clip was ascertained by measuring the length of the hairy fibrous structures in each image and plotting a graph of growth length versus time, figure **3.9**. For the growth rate measurements a time period of only 2200 s rather than the full 6000 s was used as after 2200 s the structures became highly globular making it very difficult to accurately obtain a definite length measurement.

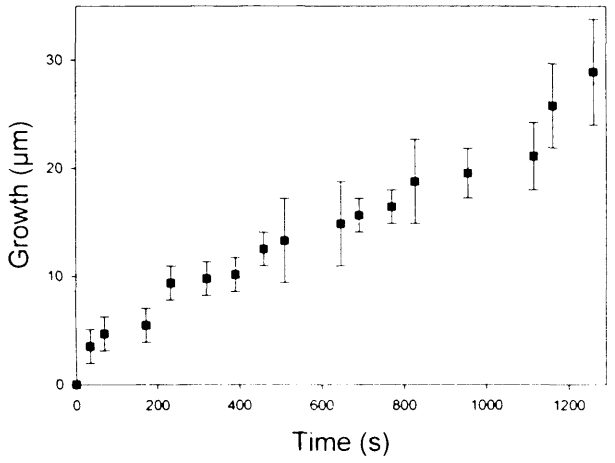

Figure 3.9: Graph of HbS growth (µm) *vs.* time (s) depicting the growth of fibrous structures over an experiment lasting 2200 sec. Experiment conditions: HbS concentrations 354 mg cm^{-3}; 1.5 M pH 7.0 phosphate buffer; 0.5 M NaCl; E = - 0.55 V vs. Ag/AgCl; run time 2200 s out of 6000 s.

The plot shows a slightly sigmoidal relationship with the initial period of growth (0 s to 150 s) being steeper than the rest of the plot indicating that the delay time was a major contributing factor to the kinetics of polymerisation. The growth rates of the first and second phase of the bi-phasic relationship were calculated to be 67 (± 8) nm s^{-1} and 40 (± 5) nm s^{-1} respectively and the average growth rate at this section of the Pt coil electrode was calculated to be 54 (± 9) nm s^{-1}.

Table **3.1** shows the average growth rate of HbS fibres formed free in solution [42] compared with the fibre growth rate at a Pt coil electrode (figure **3.9**). Electrochemical modulated fibre growth was seen to be slower than those formed free in solution, however, the time lines for the different sets of experiments were not taken into account as the electrochemically grown protein aggregates could only be measured up to 2200 s and not the full 6000 s. Fibre growth rate values of between 0.1 µm s^{-1} and 2 µm s^{-1}, determined in another study [73], through observation of the growth of cut end fibres were in accordance with the values for growth rates seen in table **3.1**.

	HbS conc. (mg cm^{-3})	Temperature (° C)	Average growth rate (μm s^{-1})
1	830	28.0	0.116 (± 0.007)
2	850	28.0	0.363 (± 0.128)
3	870	25.3	0.289 (± 0.079)
4	354	25.0	0.054 (± 0.009)

Table 3.1: Average growth rates of HbS fibres formed free in solution (rows 1, 2 and 3) taken from a study performed by Samuel *et al.* [42] compared to the average growth rate at a Pt coil electrode (row 4). Growth of HbS fibres formed free in solution were determined from serial video frames shown by video-enhanced DIC microscopy: HbS concentration 830 mg cm^{-3}, 850 mg cm^{-3} and 870 mg cm^{-3} dialysed into 0.1 M potassium phosphate (pH 7), deoxygenated at 2 °C in an anaerobic glove box with 50 mM sodium dithionite. Solutions were kept on ice and polymerisation was induced with a temperature jump to temperatures of 28 °C, 28 °C and 25.3 °C respectively. The first fibres were seen 102 minutes after the temperature jump. Experimental conditions for HbS aggregates grown at a Pt coil electrode see figure **3.9**.

3.9 AFM

AFM, a high-resolution scanning probe microscopy technique, consists of a microscale cantilever with a sharp tip which is used to probe the surface of the specimen and can be used to image the growth of individual HbS fibres (of diameter 21.5 nm) at specific points in the polymerisation cycle. When the tip is brought into the proximity of a sample surface, forces between the tip and the sample lead to a deflection of the cantilever and the deflection is measured using a laser spot reflected from the top of the cantilever into an array of photodiodes. This technique can be used to investigate the fundamental properties of nucleation and growth of HbS at a surface, such as induction times and growth rates whilst AFM also allows fibre spacing and length measurements to be carried out accurately enabling the kinetics and dynamics of polymerisation as well as the orientation of growth to be investigated. For delicate or soft samples such as proteins the tapping mode is used, as in contact mode the cantilever drags across the surface at constant force which can result in surface damage to the sample.

A number of *ex-situ* and *in-situ* AFM experiments, using contact and tapping mode in air and liquid, were performed to try to visualise the HbS fibrous and polymeric state of aggregated deoxyHbS. However, even though a number of procedures, including a variety of fibre formation techniques, and a range of conditions such as different protein concentrations, pHs and temperatures were attempted, only one image was obtained which showed the presence of fibre-like structures. The lack of HbS fibre images were most likely due to the sensitivity of the system to O_2 as even small amounts of O_2 could have caused fibres to dissolve, especially at the low protein concentrations being used, whilst numerous salt effects also became apparent when using the liquid tapping mode of the AFM.

Figure **3.10** shows an AFM image of HbS protein on mica and the presence of two fibre-like structures can be seen in the image (shown by arrows). In this experiment, 10 mg cm^{-3} HbS protein was used and the HbS polymer solution was dip coated onto the mica surface and incubated for 10 s. As the imaging was performed in air a fixative (glutaraldehyde) was used to fix any fibres onto the surface before any interaction with O_2 occurred.

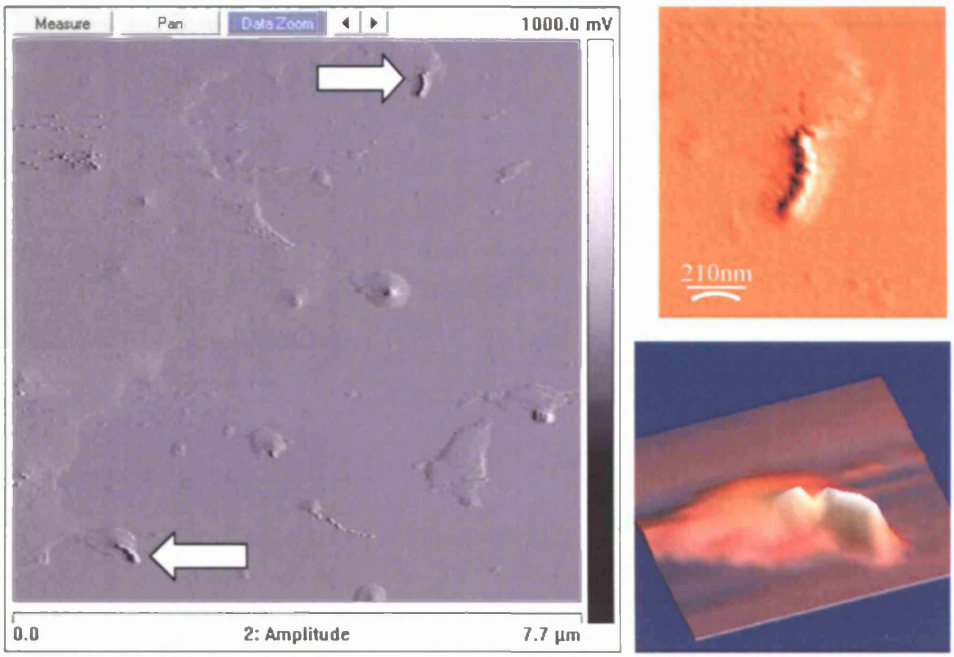

Figure 3.10: Dimension AFM imaging of HbS protein aggregates on freshly cleaved mica (scan size 10 µm; *z* height 75 nm; amplitude 1.0 V; drive amplitude 153.4 mV; silicon nitride tips (1 Ω)); HbS aggregates were formed with 10 mg cm^{-3} HbS protein in pH 7.58, 2.52 M phosphate buffer using experimental procedure 4. Mica surface was dip coated with the HbS aggregate solution stored under an inert atmosphere, incubated for 10 s and fixed using 3% glutaraldehyde solution.

The height of these two structures (height = 35 nm to 45 nm) seen in the image were measured to be similar to the diameter of a single HbS fibre (figure **3.11**), whilst these structures were also seen to be protruding from nodes and situated right on the edge of the protein and mica interface. However, it cannot be conclusively stated that these structures were HbS fibres as there was also a possibility that it could have been due to the presence of impurities in the system before the fixative was applied. Most of the experiments performed with HbS fibre solution deposited on mica and imaged in air showed a thick protein crust on the surface and the presence of nodes which could have been nucleating sites for the formation of HbS polymers. However, many experiments showed no images of fibres probably due to leaking of O_2 into the system. *In-situ* experiments were performed using an electrochemical cell but no fibres were seen.

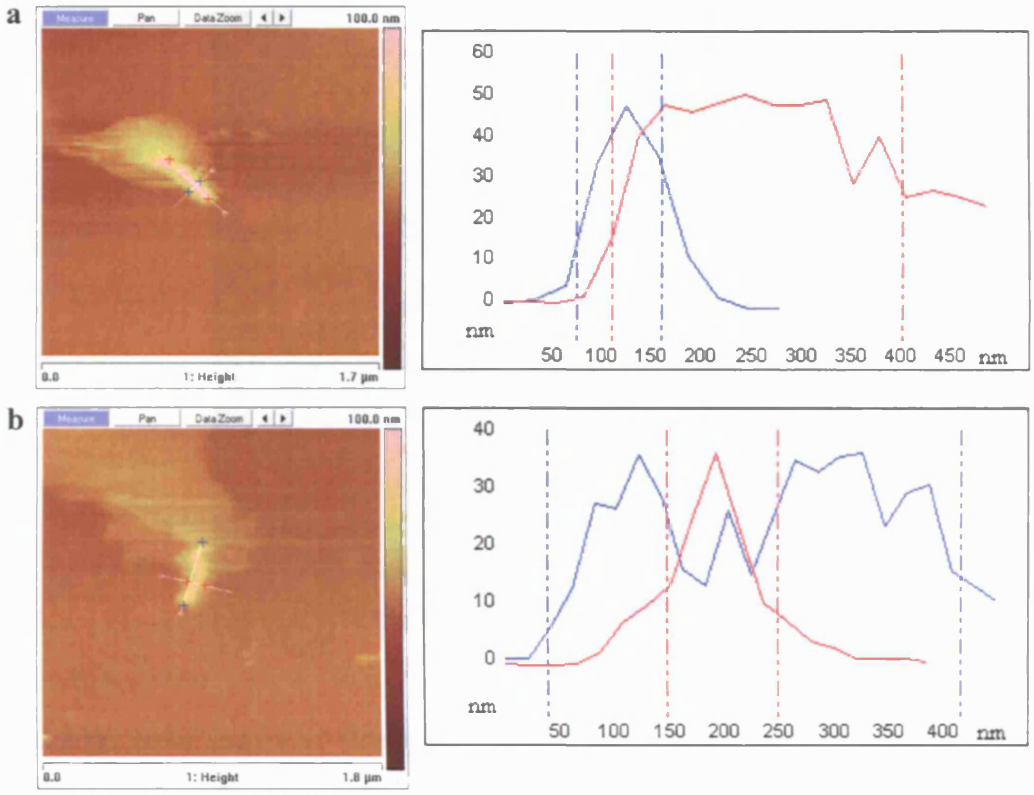

Figure 3.11: Figure showing the dimensions of the two fibre like structures seen in figure **3.10**. For **(a)** the length = 300 nm, width = 75 nm, height = 45 nm; **(b)** the length = 350 nm, width = 100 nm, height = 35 nm. For experimental conditions and image parameters see figure **3.10**.

Studies involved in monitoring the events associated with HbS polymerisation have generally used DIC microscopy as the main visualising tool, as explained in chapter **1**. This is because DIC microscopy allows structures to be viewed in real time without the limitations of invasive preparatory methods, thus allowing the kinetics, gel rheology and pathogenesis to be related to the underlying gel structure. However, AFM obviously has the great advantage of being able to image at far lower resolutions thus making it possible to image the growth of single HbS fibres. To date, only one set of AFM images on HbS fibres can be found in the literature [41], shown in figure **3.12**, because gelation of the solution due to polymerisation makes imaging of the surface extremely difficult. Further work is required to produce a working system for the *in-situ* and *ex-situ* imaging of HbS fibres.

Figure 3.12: AFM images of deoxyHbS polymers showing a variety of polymeric structures formed at 35 °C in a 220 mg cm^{-3} concentrated HbS solution: **(a)** Low-resolution image showing a variety of polymeric structures; **(b–d)** Higher resolution images showing thicker fibres consist of thin polymers of 22 nm diameter. The fibres were cross-linked with glutaraldehyde solution [41]

3.10 Conclusions

It was found that polymerisation of HbS could be observed by O_2 depletion using electrochemical reduction in a thin layer cell. The geometry of the WE was found to be essential for the growth of HbS aggregates as previous attempts with a Pt wire electrode did not produce any results. HbS polymerisation was visualised in a Pt coil electrochemical cell with an optical microscope and the conditions for reproducible growth of HbS aggregated structures at the Pt coil electrode was shown to be: HbS concentration of 300 mg cm^{-3} in 1.5 M, pH 7.0 phosphate buffer with the addition of 0.5 M NaCl and the electrode held at a potential of E = - 0.55 V versus Ag/AgCl. The use of high concentration buffer, and more importantly the addition of NaCl increased the ionic strength and the conductivity of the solution, and also provided a salting out effect for solubility purposes.

It was also demonstrated that three stages of polymerisation were seen from the optical images. The first was a time delay when no structures were observed and this could be thought of as the nucleation step. This was followed by two growth stages of HbS polymerisation, firstly growth of fibrous hair-like strands at the electrode surface and secondly globular and gel-like aggregation in the latter stages of the experiment. Furthermore, formation of the aggregated structures was seen to occur only at the electrode surface initially and not in the bulk solution showing that growth at the surface was thermodynamically more favourable than in solution. The average growth rate at a section of the bare Pt coil electrode, calculated to be 54 (± 9) nm s^{-1}, was in accordance with those presented in literature. Control experiments performed with non-polymerising HbA instead of HbS did not show growth of any structures at the electrode surface. Overall, an electrochemical technique was developed using an optimised thin layer Pt coil cell and the conditions for reproducible HbS aggregate growth and the different stages of polymerisation were characterised.

Chapter 4: HbS Aggregation in Au Micromesh Cell

4.1 Introduction

In this chapter, HbS aggregate formation at the surface of another in-house built thin layer electrochemical cell, a Au micromesh cell, is described. A methodology for the monitoring of HbS aggregation at the Au micromesh electrode by detecting turbidity changes as a result of light scattering caused by the polymerisation of HbS is presented. The kinetics of polymerisation using a model for fibrillogenesis describing a two-step process of nucleation followed by elongation is described, and the rate constants for two concentrations of HbS monomer, 50 mg cm^{-3} and 300 mg cm^{-3}, have been determined. The nature of protein growth from optical microscope images is also compared with the Pt coil cell whilst the effect of DPG, a negatively charged allosteric effector is explored for further optimisation of HbS polymerisation conditions.

4.2 Experimental

4.2.1 Materials, Instrumentation and Procedures

The UV-visible spectroelectrochemistry experiments were performed according to experimental procedure **6**. HbS or HbA were dissolved in 1.5 M (pH 7.0) phosphate buffer solution and NaCl was added as supporting electrolyte. For DPG experiments, 3 mM, 5 mM and 100 mM concentration of DPG was added to a solution containing Hb protein, 1.5 M (pH 7.0) phosphate buffer and 0.5 M NaCl and the UV-visible spectroelectrochemistry experiment was performed in the same manner described previously. All experiments were performed at room temperature unless stated otherwise. The electrodes used for constructing the cell were Au micromesh (aperture size 250 μm, plain weave wire diameter 60 μm, 82 grids per inch, 99.99 % purity) as the WE, Pt wire (diameter 100 μm, hard temper, 99.99 % purity) as the CE and silver (Ag) wire (grade 1, diameter 25 μm) as the RE. Au wire (diameter 250 μm, hard temper, 99.99 % purity) was used as the connection between the WE and the copper wire. The general experimental and all apparatus for the above techniques are described in chapter **2**.

4.2.2 Construction of Au Micromesh Thin Layer Electrochemical Cell

A robust and easily constructed thin-layer cell was designed specifically for spectroelectrochemical measurements in a similar way to the construction of the Pt coil cell. Figure **4.1 (a)** shows a schematic representation of this cell and figure **4.1 (b)** shows an actual image of the cell. Three electrodes - Au micromesh (3.0 mm by 4.0 mm) WE, 100 μm coil shaped Pt wire CE and 25 μm Ag wire RE - were placed in a quartz cuvette (1 mm pathlength) which had been cut in half to minimise the volume and connected to copper electrical wires using silver conductive paint. Au wire (diameter 250 μm) was looped through one of the apertures and used as the connection between the micromesh and the electrical wire and the connections were covered with epoxy resin to provide stability as well as to provide an impervious and non-conductive layer. A thin layer of typical total volume of 100 μl ± 10 μl was produced (measured by the volume of solution required to completely fill the cell). Black tape was used to blank most of the cuvette from the light beam, except for a small window on the Au micromesh electrode (1.0 mm by 1.5 mm). All materials were thoroughly cleaned prior to its construction using acetone.

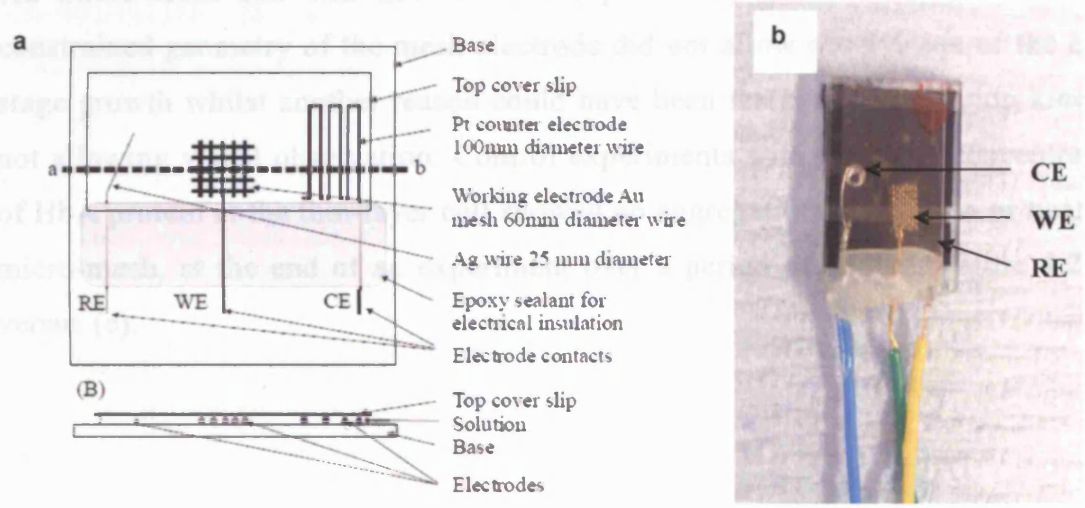

Figure 4.1: Figure showing **(a)** Schematic of the plan view (not to scale) **(b)** Actual image of the Pt micromesh thin layer electrochemical cell incorporating a three electrode system with a Pt micromesh (aperture size 250 μm) as the WE, a 100 μm coil shaped Pt wire CE and a 25 μm Ag wire RE. The Ag wire was anodised with AgCl prior to use. The electrodes were housed in a cuvette. Figure (b) shows the black tape covering the back of the cuvette used to blank the light beam.

4.3 Growth of HbS Aggregated Structures

Figure **4.2** shows the change in morphology of the Au micromesh surface when HbS solution of concentration 300 mg cm^{-3} was electrochemically deoxygenated. At time = 0 s the Au electrode was bare and at time = 1458 s the first formation of 'globular structures' at the electrode was seen (Figure **4.2 (b)**) which subsequently grew as the experiment proceeded (Figure **4.2 C**). However, no fibrous strand-like structures were seen. The time taken for the structures to appear was again dependent on the rate of deoxygenation and rate of nucleation of aggregation.

The main difference between the growth of HbS protein aggregates at the Pt coil and Au micromesh, as seen from the optical images, was the lack of any hair-like strands present. Whereas growth of HbS fibrous structures at the Pt coil electrode was seen to occur in a three step mechanism, going from an initial delay to the formation of hair-like strands protruding from the surface of the electrode and finally to the formation of globular cell-like structures. The formation of protein aggregates at the Au micro-mesh electrode occurred with the establishment of the globular structures straight after the time delay. No hair-like strands were noticeable from any of the images.

Although the reasons behind the lack of early stage hair like fibrous growth in the Au micro-mesh cell was not clear, one possibility could have been that the constrained geometry of the mesh electrode did not allow observation of the early stage growth whilst another reason could have been faster polymerisation kinetics not allowing visual observation. Control experiments with the same concentration of HbA protein at the thin-layer cell showed no aggregation of HbA, on or near the micro-mesh, at the end of an experiment over a period of 4500 s, Figure **4.2 (d)** versus **(e)**.

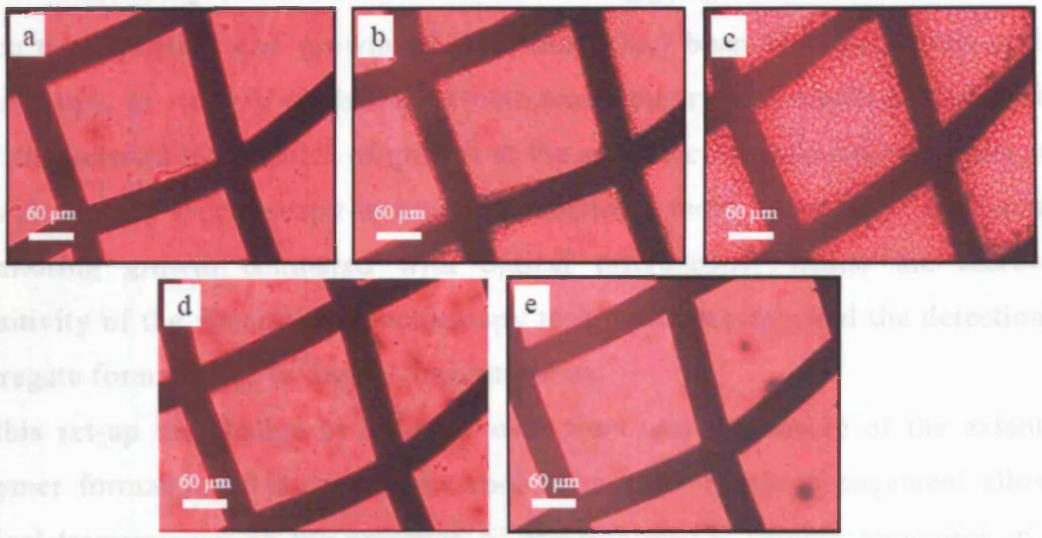

Figure 4.2: Optical microscope images showing HbS aggregate growth and the control HbA at the Au micromesh WE. Experiment conditions: HbS concentration 300 mg cm^{-3}; 1.5 M pH 7.0 phosphate buffer; 0.5 M NaCl; E = -0.55 V *vs.* Ag/AgCl for 4500 s. (**a**) HbS at 0 s; (**b**) HbS at 1458 s; (**c**) HbS at 3327 s; (**d**) HbA at 0 s; (**e**) HbA at 4500 s

Optical transparency was achieved by using an optically transparent mesh as the WE whilst a thin layer was obtained by housing the electrodes in a 1 mm pathlength cuvette. The micromesh geometry allowed a more efficient electrochemical reduction of O_2 than a coil. Thiol modifications of the Au surface allowed surface properties to be changed easily thus enabling the effect of surface properties on nucleation and growth of HbS aggregates to be investigated (Chapter **6.6.2**). Au surface has the advantage of undergoing fast and simple protein desorption and rapid thiol cleavage. Complete deoxygenation at the micromesh electrode was confirmed electrochemically by comparing the minimum charge needed to remove all O_2 from a cell of total volume 50 µl air-saturated Hb solution, calculated to be 1.93×10^{-3} C, with the experimentally obtained value of 1.00×10^{-2} C passed over a period of 4500 s. CV of the solution, performed after chronoamperometry, also showed the absence of the O_2 present in the HbS solution at the start of the experiment, as illustrated in Figure **2.2**. Furthermore, figure **2.3** shows that the conversion of oxyHbS to deoxyHbS at the mesh electrode occurred within 200 s.

4.4 Turbidity Measurements of HbS Aggregated Structures

Once the induction and growth of HbS fibres had been visualised with optical microscopy, *in situ* UV-visible spectroelectrochemistry was employed to monitor and characterise the kinetics of growth at the same electrochemical thin layer cell. The absorption spectroscopy technique permitted a more quantitative approach to monitoring growth compared with optical microscopy, whilst the increased sensitivity of the absorption spectroscopy technique also allowed the detection of aggregate formation at far lower concentrations.

In this set-up the change in turbidity over time was a measure of the extent of polymer formation at the mesh electrode. The micro-mesh arrangement allowed optical transparency so the presence of any aggregated protein structures in the apertures, formed due to electrochemical reduction of O_2 *in situ*, could be detected as a result of wavelength independent light scattering caused by the polymers. Turbidity values were determined from the absorbance according to the relation $A = \log(I_o/I)$, where turbidity = (I_o/I). The intensity of scattered light by a particle is proportional to the mass squared, so a few large fibrils will scatter the same amount of light as many smaller fibrils. However, care was taken over the experimental conditions and the starting sample to ensure the solution was composed of only protein monomers meant that the results obtained were accurate and reproducible.

At a protein concentration of 300 mg cm^{-3} (the same as used in the optical microscopy experiments) large time dependent increases in turbidity were seen over the wavelength range 600 to 1100 nm, figure **4.3**. This wavelength-independent turbidity was directly due to light scattering caused by the formation of HbS aggregated structures. The blank in this experiment was the HbS solution before the potential was applied, so the spectra shown in figure **4.3** shows the change in turbidity relative to the starting solution.

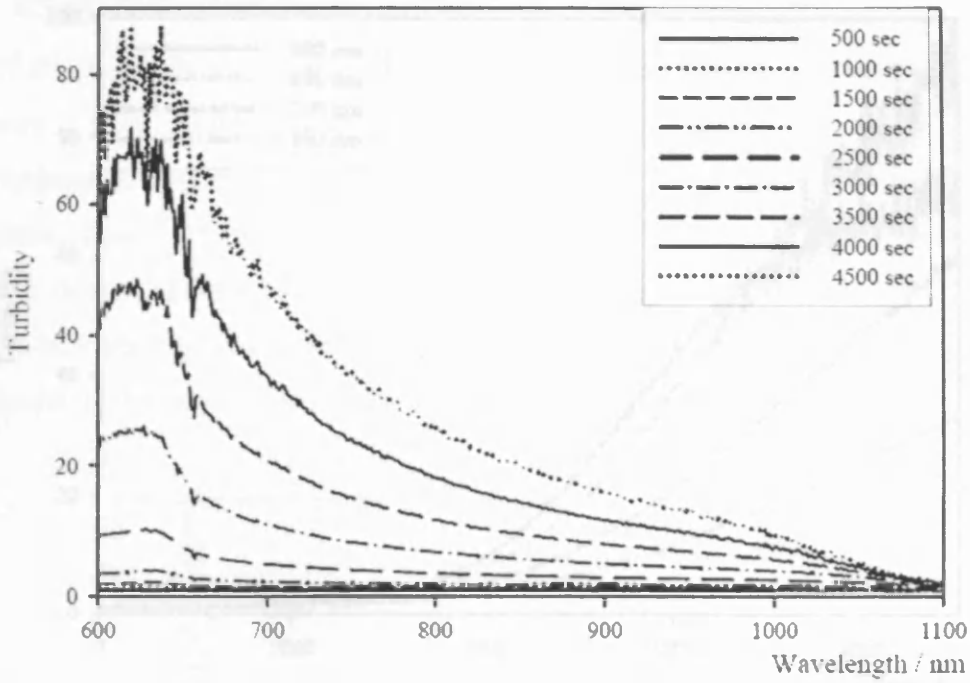

Figure 4.3: Wavelength independent light scattering due to formation of HbS fibres by electrochemical reduction of O_2 at Au micromesh electrode. Experimental conditions: HbS concentration 300 mg cm^{-3} in 1.5 M phosphate buffer (pH 7.0); 0.5 M NaCl; E = -0.55V *vs.* Ag/AgCl for 4500 s.

The rate of turbidity change at four specific wavelengths, 600 nm, 650 nm, 700nm and 800 nm were monitored to investigate the kinetics of nucleation and growth, both at the early and latter stages of the polymerisation process. These four wavelengths were thought to represent the best points at which these processes could be observed. Wavelengths below 600 nm are associated with the macromolecular structure of the protein, in particular the effects of Soret bands upon interaction with photons and thus were not included in these results.

Figure **4.4** shows time traces for changes in absorbance at the aforementioned wavelengths. The time traces in figure **4.4** are from the same results as that of figure **4.3**. The results showed that the rate of change in turbidity at each wavelength followed a sigmoidal pattern with an initial lag period up to 1000 s where little increase in absorbance was apparent (turbidity less than 2.00). This was followed by a large exponential increase from 1000 s to 4500 s where the turbidity increased forty fold to 85.36.

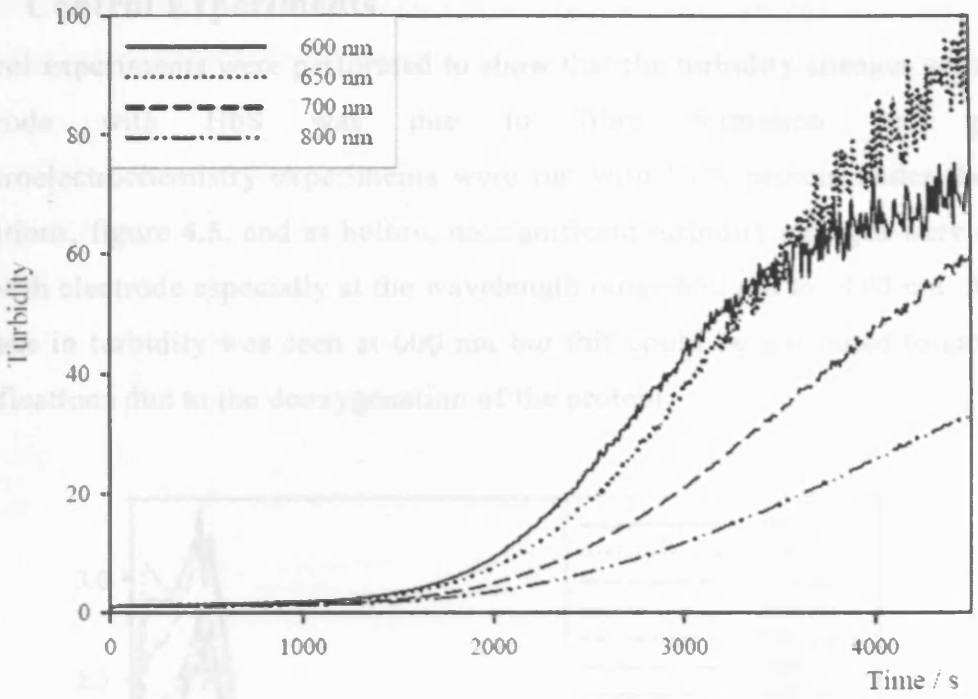

Figure 4.4: UV-visible spectroelectrochemistry time traces for HbS showing changes in turbidity at Au micromesh electrode. Experimental conditions: HbS concentration 300 mg cm^{-3} in pH 7.0, 1.5 M phosphate buffer; 0.5 M NaCl; E = - 0.55 V vs Ag/AgCl for 4500 s.

The initial period up to 1000 s incorporates the nucleation step as well as limited growth on the electrode surface and hence light scattering due to HbS aggregation is minimal. After 1000 s, elongation and further nucleation on existing fibres gives rise to extended growth and branching on the electrode surface and into the bulk solution thereby causing intensive light scattering. Consequently, a large increase in absorbance is obtained. The Au micromesh cell data did not provide further evidence to the hypothesis that nucleation and growth at a conducting electrode surface follows a three stage process (nucleation, early stage growth and late stage growth). This data was fitted to a kinetic scheme model which is explained in detail in section 4.6.

4.5 Control Experiments

Control experiments were performed to show that the turbidity changes seen at the electrode with HbS was due to fibre formation and growth. Spectroelectrochemistry experiments were run with HbA protein under the same conditions, figure **4.5**, and as before, no significant turbidity changes were seen at the mesh electrode especially at the wavelength range 650 nm to 1100 nm. A slight increase in turbidity was seen at 600 nm but this could be attributed to structural modifications due to the deoxygenation of the protein.

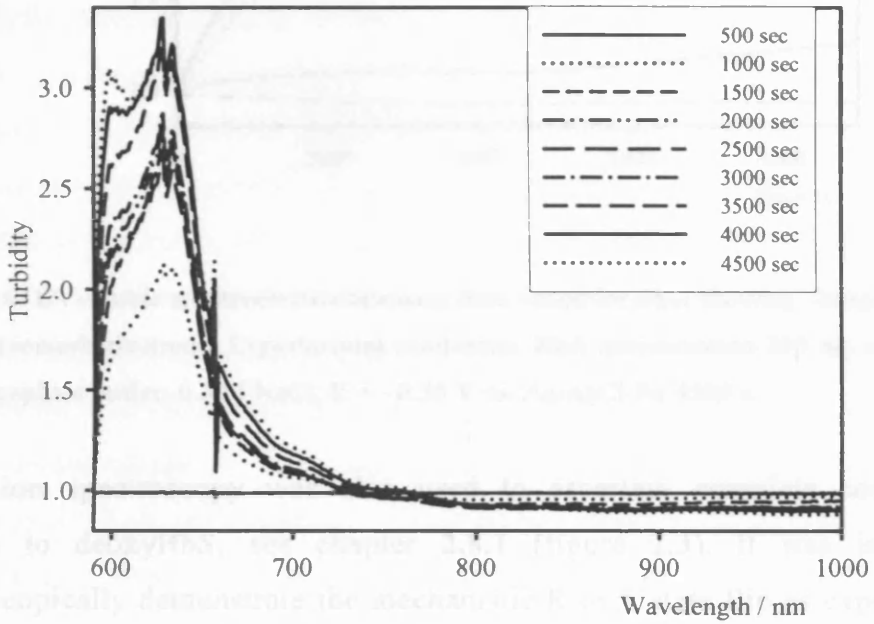

Figure 4.5: Wavelength independent light scattering of HbA at Au micromesh electrode as a result of electrochemical reduction of O_2. Experimental conditions: HbA concentration 300 mg cm^{-3} in pH 7, 1.5 M phosphate buffer; 0.5 M NaCl; E = - 0.55 V *vs.* Ag/AgCl for 4500 s.

Moreover, absorbance changes monitored at the four specific wavelengths (600 nm, 650 nm, 700 nm and 800 nm) from the same HbA experiment as figure **4.5** showed no significant increases in turbidity especially at 700 nm and 800 nm and there was no characteristic sigmoidal relationship, figure **4.6**. The change in turbidity at 700nm for HbA (1.26 at 4500 s) was approximately forty six times lower than the turbidity measured for the same experiment with HbS in the same cell (59.37 at 4500 s). The HbA controls data provided strong evidence that any

changes in turbidity with HbS were due to HbS aggregation and growth, induced through electrochemical deoxygenation.

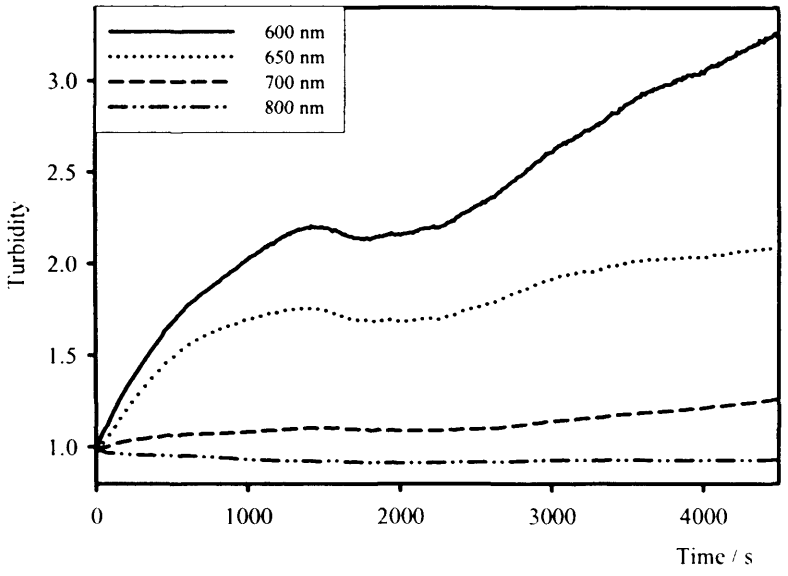

Figure 4.6: UV-visible spectroelectrochemistry time traces for HbA showing changes in turbidity at Au micromesh electrode. Experimental conditions: HbA concentration 300 mg cm^{-3} in pH 7.0 1.5 M phosphate buffer; 0.5 M NaCl; E = - 0.55 V *vs.* Ag/AgCl for 4500 s.

Absorption spectroscopy was also used to ascertain complete conversion of oxyHbS to deoxyHbS, see chapter **2.8.1** (figure **2.3**). It was important to spectroscopically demonstrate the mechanistic R to T state flip as exposure of the hydrophobic pocket by which HbS molecules aggregate only occurs in the T state.

4.6 Kinetics of Protein Aggregating Systems

One of the typical kinetic characteristics in protein fibre formation is a nucleation-dependent polymerisation mechanism, used to analyse a mechanism composed of an initial nucleation phase and an elongation phase. Examples of such protein aggregating systems include HbS polymerisation [90], β-amyloid fibrillogenesis [91] and silk fibroin [92]. In β-amyloid fibrillogenesis, unstructured monomers in solution nucleate and form a critical nucleus which in turn forms intermediate peptides termed protofibrils. These intermediaries subsequently act as precursors by associating end to end and laterally and thereby elongating the protofibrils to form fibrils. Furthermore, a reservoir of micelle monomer associates is formed once the concentration exceeds a certain level called the critical micelle concentration (CMC), which allows an autocatalytic reaction for the aggregation of β-amyloid [91, 93]. The assembly process of silk fibres occurs in a similar manner. The defining characteristic in all of the above mentioned protein aggregating systems is the formation of an ordered nucleus. Nucleus formation is a thermodynamically unfavourable interaction because the entropic cost encountered upon loss of molecular movement does not outweigh the resultant intermolecular polymer lattice formation. Upon nucleation, further monomers contact the growing polymer at multiple sites leading to rapid polymerisation and growth. Sabate *et al.* [93] have used a modification of the mathematical model developed by Kamihira *et al.* [94] to propose a simple two step autocatalytic reaction mechanism for β-amyloid fibril formation, thereby permitting quantitative monitoring of the kinetics of fibrillogenesis and enabling the nucleation rate and elongation rate to be determined. Knowledge of these rate constants is key to understanding the underlying molecular factors which govern fibril nucleation and growth.

4.6.1 Kinetics of HbS Polymerisation

For HbS polymerisation, many studies have been devoted to investigate the kinetics using a large variety of techniques [53-56, 59-62] and the results from all of these techniques have shown the same basic kinetic features of polymerisation, a sigmoidal time course for polymerisation of an initially polymer-free solution, see figure **1.8** for a typical progress curve for HbS polymerisation. A marked delay in the initial part of the progress curve, during which no signal is observed, corresponds to the nucleation time or the time taken to form the critical nucleus. The energetic gain needed to form critical nuclei is dependent on the initial concentration of HbS. The nucleation time is also found to be related to the solubility of HbS, and thus dependent on the variables which alter the solubility of HbS. The effect of variables which alter the solubility of HbS on the nucleation and growth of polymerisation has been investigated at a Pt matrix electrochemical cell in chapter **5**. Nucleation is followed by a comparatively fast and highly autocatalytic formation of polymer.

The kinetic scheme developed for the fibrillation mechanism of human calcitonin by Kamihira *et al.* [94] and subsequently modified for β-amyloid fibrillogenesis by Sabaté *et al.* [93] was be fitted to our HbS polymerisation data. To analyse the kinetic properties of a system where non-aggregated Aβ becomes aggregated fibrillar Aβ the nucleation process can be expressed as:

$$n M \xrightarrow{k_1} P_n \qquad \textbf{(4.1)}$$

and the elongation process can be described as:

$$M + P_n \xrightarrow{k_2} P_{n+1} \qquad \textbf{(4.2)}$$

with M representing monomeric HbS, n the number of HbS molecules and P_n the fibre nucleus. The kinetics of the process is controlled by two key parameters, the nucleation rate constant k_1, and the elongation described by the rate constant k_2. The overall kinetic equation for the nucleation and growth of the fibres can be expressed as in:

$$\left(\frac{df}{dt}\right) = k_1(1-f) + k_2 af(1-f) \qquad \textbf{(4.3)}$$

where f is the fraction of fibres in the system and a is the initial concentration of HbS in the solution. Equation **4.3** can be integrated under the boundary condition of $t = 0, f = 0$, to give:

$$f = \frac{\rho\{\exp[(1+\rho)kt] - 1\}}{\{1 + \rho\exp[(1+\rho)kt]\}} \qquad \textbf{(4.4)}$$

where $k = k_2 a$ and $\rho = k_1/k$. Least square fitting of equation **4.4**, to the turbidity data at 800 nm for two HbS concentrations was used to obtain values of k_1 and k_2. As shown in figure **4.7** the fit of equation **4.4** to the normalised turbidity data (normalised using a turbidity of 75, which was the maximum turbidity at 800 nm) was good for the high protein concentration data (300 mg cm^{-3}, r^2 = 0.998) but only reasonable for the lower protein concentration (50 mg cm^{-3}, r^2 = 0.968). The fit to the low protein concentration data was affected by solution evaporation from the cell which ultimately limited the length of the experiment to 4500 s.

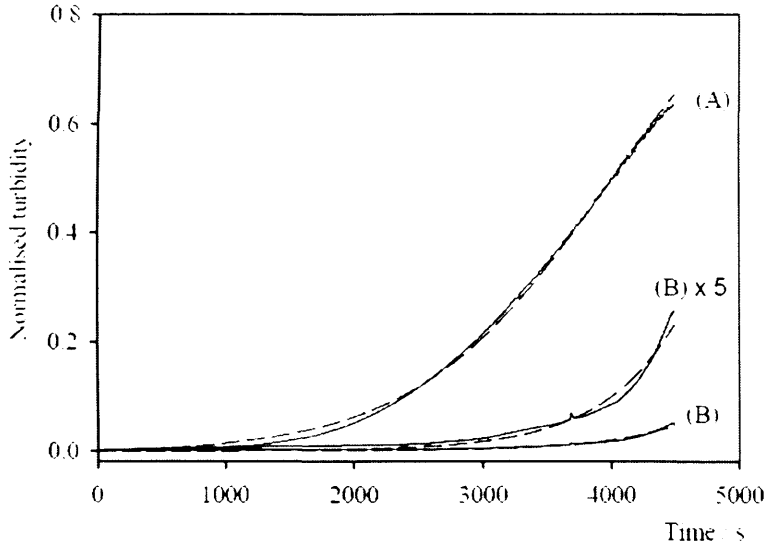

Figure 4.7: Solid lines showing the experimental values of normalised turbidity, using a max turbidity of 75 corresponding to maximum absorbance of fibres at 800 nm, versus time for **(A)** 50 mg cm^{-3} HbS and **(B)** 300 mg cm^{-3} HbS. The dashed lines are the best-fit lines to equation 4.4.

The rate constants obtained from these fits are summarised in Table **4.1**. The effective growth rate constant, ak_2, did not show significant correlation with HbS

concentration under these conditions. However, the values for k_1 are several orders of magnitude smaller than k_2 for both 50 and 300 mg cm^{-3} of Hb, indicating that the nucleation process was far slower than the elongation process. There was a clear concentration dependence on the nucleation rate constant. This was expected, as in this case nucleation was expected to take place on the electrode surface where it is more thermodynamically favourable than homogenous nucleation free in solution.

HbS Concentration	k_1 / s^{-1}	k_2 / M^{-1} s^{-1}	ak_2 / s^{-1}
50 mg cm^{-3} (7.752 x 10^{-4} M)	2.99 (± 0.4) x 10^{-8}	1.39 (± 0.6)	1.08 (± 0.2) x 10^{-3}
300 mg cm^{-3} (4.65 x 10^{-3} M)	9.45 (± 0.08) x 10^{-6}	0.26 (± 0.01)	1.22 (± 0.03) x 10^{-3}

Table 4.1: Nucleation rate constants k_1 and growth rate constants k_2 to describe the HbS aggregation formation for 50 mg cm^{-3} and 300 mg cm^{-3} protein concentration at a Au micromesh electrode surface. Experiment conditions: HbS concentrations 50 mg cm^{-3} and 300 mg cm^{-3}; 1.5 M pH 7.0 phosphate buffer; 0.5 M NaCl; temperature 25°C; E = - 0.55 V *vs.* Ag/AgCl for 4500 s.

4.7 2,3-DPG

2,3-DPG acts by stabilising the deoxy or T-state of Hb by binding in the cavity between the β chains of the deoxygenated state of Hb, making electrostatic interactions with positively charged groups surrounding this opening. However, even though the effect of 2,3-DPG in normal adult Hb is quite well established, the role of 2,3-DPG in the pathophysiology of sickle cell disease has been a point of long-standing dispute. Some studies have claimed that 2,3-DPG promotes the intracellular polymerisation of deoxy-HbS [51, 53, 95], whereas others assert that it has no such effect [54, 55].

The effect of 2,3-DPG in promoting HbS polymerisation in the Au micromesh thin-layer electrochemical system was investigated by the addition of different concentrations of this anionic organic phosphate to a solution of HbS protein and measuring the changes in turbidity. Three concentrations 3 mM, 5 mM, and 100 mM of 2,3-DPG were used and the results are shown in figure **4.8**.

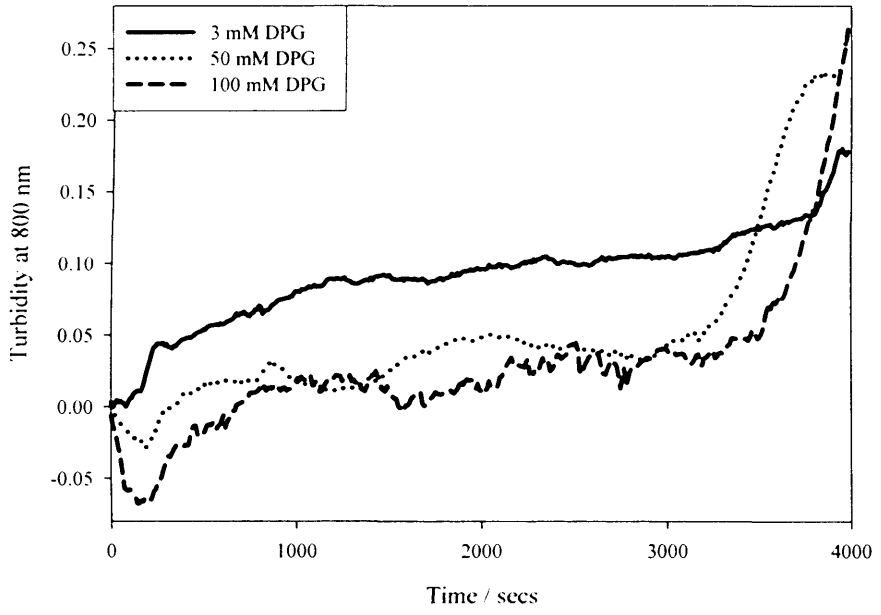

Figure 4.8: UV-visible spectroelectrochemistry time traces of HbS solution containing different concentrations of 2,3-DPG showing changes in turbidity at a bare Au micromesh electrode. Experimental conditions: HbS concentration 50 mg cm^{-3} (0.78 mM) in pH 7, 1.5 M phosphate buffer; 2,3-DPG concentrations 3 mM, 50 mM, 100 mM; 0.5 M NaCl; E = - 0.55 V *vs.* Ag/AgCl for 4500 s.

The results showed that all three 2,3-DPG concentrations had an enormous effect on the aggregation of HbS, as 3 mM 2,3-DPG showed the same turbidity levels as

100 mM 2,3-DPG. *In vivo* Hb concentration per red blood cell (MCHC) is 320 mg cm^{-3} (4.96 mM) to 360 mg cm^{-3} (5.58 mM) and 2,3-DPG is present in human RBCs at about the same molar ratio of Hb [96]. In our experiments, 2,3-DPG concentrations far greater than the experimental Hb concentration of 50 mg cm^{-3} (0.78 mM) was employed, therefore the use of even 3 mM 2,3-DPG would have ensured Hb binding site saturation. Subsequent increases to 50 mM and 100 mM 2,3-DPG therefore did not exhibit any additional effect. Further experiments need to be performed at concentrations far below saturation levels to investigate the effect of 2,3-DPG on HbS polymerisation in more detail.

4.8 Conclusions

UV-visible spectroscopy was successfully employed to monitor changes in the nucleation and growth of HbS aggregates and polymers at the surface of a conducting electrode. It was shown that incorporating a Au micromesh WE demonstrated significant growth of HbS protein aggregates at the electrode. Rapid growth of these structures was primarily achieved as a result of the micromesh geometry of the WE which provided an efficient arrangement for O_2 depletion within the thin layer electrochemical cell. The extent of polymerisation at the optically transparent electrode was monitored using turbidity measurements which were a measure of the extent of polymer formation at the electrode. The results showed that the rate of change in turbidity followed a sigmoidal pattern with an initial lag period where little increase in turbidity was apparent before large increases, of up to forty fold, were observed in the turbidity. The change in turbidity was shown to be dependent on HbS polymerisation and not protein precipitation, as shown by important control experiments replacing HbS for normal non-polymerising HbA.

It was found that the turbidity versus time traces fit the kinetic model for fibre formation well. Kinetic constants were determined for two concentrations of HbS protein which showed that the nucleation rate was far slower than the growth. A clear concentration dependence was seen with the nucleation rate constant but the effective growth rate did not show significant correlation with HbS concentration at the Au micromesh cell. Moreover, the effect of DPG was also investigated to optimise conditions for maximal growth of HbS aggregates at a thin layer electrochemical cell and the results showed that high concentrations of this allosteric effector had a significant effect on the turbidity levels. However, further experiments need to be performed at concentrations of DPG which do not cause saturation to investigate the effect of DPG as a therapeutic agent. This method may not only be used to gain an understanding of the pathophysiology of SCD but also as a screening method for drugs that might lead to novel therapeutic strategies for disrupting nucleation and/or growth in patients with sickle cell crisis. This will be achieved by investigating the effect of new potential compounds, whose mode of action is specific to the disruption of fibre formation, in the electrochemical thin-layer cell.

Chapter 5: HbS Aggregation in Pt Matrix Cell

5.1 Introduction

In the previous chapter a novel technique was developed which monitored HbS polymerisation as a change in turbidity by reducing a small volume of HbS within a custom built thin layer electrochemical cell. A similar technique has been used in this chapter to define the effect of four parameters, HbS concentration, temperature, solution pH and ionic strength, on the kinetics and thermodynamics of HbS gelation in a Pt matrix electrochemical cell. This cell was the last in the series of electrochemical cells built to modulate electrochemical reduction at the electrode. Theoretical modeling of the depletion of O_2 concentration at the matrix electrode, accurately recreated using reference diagrams, is described. Kinetic nucleation and elongation rate constants and the activation energies for deoxyHbS gelation at the Pt surface are presented and the relevance of the double nucleation mechanism at a conducting surface in our electrochemical system is discussed. Although free solution studies of factors affecting HbS polymerisation have been performed, this is the first known study which has combined electrochemical deoxygenation and protein polymerisation to investigate the effect of different variables on the kinetics of HbS aggregation at an artificial surface.

5.2 Experimental

5.2.1 Materials, Instrumentation and Procedures

The following conditions were employed when investigating each parameter: for HbS concentration, 10 mg cm^{-3}, 20 mg cm^{-3}, 30 mg cm^{-3}, 40 mg cm^{-3}, 50 mg cm^{-3}, 75 mg cm^{-3} and 100 mg cm^{-3} HbS were used at a temperature of 38 °C; for investigating temperature dependence, HbS concentrations of 30 mg cm^{-3} and 75 mg cm^{-3} were each tested at 25 °C, 30 °C, 34 °C, 38 °C and 42 °C; for pH, phosphate buffer of pH 6.8, 7.0, 7.2, 7.4 and 7.62 at 30 mg cm^{-3} and 75 mg cm^{-3} HbS at 38 °C were used; whilst for the ionic strength experiments, 0.1 M, 0.25 M, 0.50 M, 0.75 M and 1.00 M NaCl were used as the supporting electrolyte for HbS concentrations of 30 mg cm^{-3} and 75 mg cm^{-3} at 38 °C. HbS solutions were made up by dissolving each specific HbS protein in air-saturated phosphate buffer solution with the addition of NaCl. The UV-visible spectroelectrochemistry experiments were performed according to experimental procedure **6**. HbA was used for the control experiments. Pt sheet (thickness 500 μm, size 25 mm x 25 mm, temper as rolled, 99.99 % purity), Pt wire (diameter 100 μm, hard temper, 99.99 % purity) and Ag wire (grade 1, diameter 50 μm) were used as electrodes. All experiments were performed at room temperature unless stated otherwise. Analysis of the results was performed using Sigmaplot, whilst modeling analysis was performed with Comsol® software. The general experimental and all apparatus for the above techniques are described in chapter **2**.

5.2.2 Construction of the Pt Matrix Thin Layer Electrochemical Cell

A spectroelectrochemical thin layer cell similar to that described previously was constructed. However, in this case a different WE was used, figure **5.1** shows a schematic representation of this cell. The WE in this cell consisted of a Pt sheet (3 mm x 4 mm x 0.25 mm) in which regular holes of 350 μm diameter were drilled in a matrix style array. The distance between each hole was also 350 μm. A Pt coil (diameter 100 μm) served as the auxiliary electrode whilst all potentials were given versus the quasi-reference electrode (Ag/AgCl). The three electrodes were connected to copper electrical wires, placed into a 1 mm pathlength quartz cuvette which had been cut in half and fixed with epoxy resin. The cuvette was cut not only to minimise solution volume but also to have an open ended cell, thus allowing electrodes to be positioned from one end and the solution to be introduced from the other. The cell had a typical total volume of 100 μl ± 10 μl. The entire cuvette, except for a small window on the Pt matrix WE (1.0 mm by 1.5 mm), was blanked for the light beam.

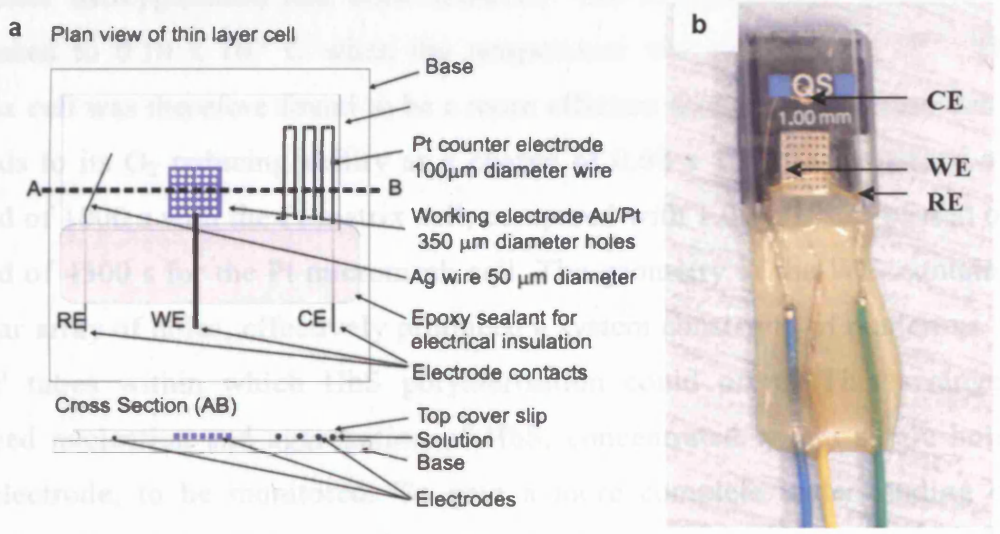

Figure 5.1: Figure showing (**a**) Schematic plan view and (**b**) actual image of the Pt matrix thin layer electrochemical cell incorporating a three electrode system with a Pt sheet in which a regular array of holes of 350 μm diameter have been drilled as the WE, a 100 μm coil shaped Pt wire CE and a 50 μm Ag wire RE. The CE coil was composed of ten turns and the Ag wire was anodised with AgCl prior to use. The cuvette was attached to a coverslip to form the base for the wires and epoxy sealant. Black tape was fixed to the back of the cell to blank the entire light beam except a small area. Not to scale.

5.3 Optimisation of the Pt Matrix Electrochemical Cell

A Pt matrix thin layer electrochemical cell was fabricated to monitor and provide additional information on the kinetics and thermodynamics of HbS polymerisation at the Pt surface. Coil and micromesh electrode geometries had been used previously but in this cell a 250 μm thick Pt sheet was employed as the WE. Optical transparency was achieved by drilling holes of 350 μm diameter in a matrix style array into the Pt sheet, whilst a thin layer was obtained by housing the electrodes in a 1 mm pathlength cuvette which had been cut in half to minimise the solution volume, figure **5.1**. The modified cuvette also allowed easy access to the electrodes for cleaning purposes and removal of any air bubbles trapped beneath the WE.

Complete deoxygenation of the solution was confirmed electrochemically by comparing the minimum charge needed to remove all O_2 from the Pt matrix cell with the actual experimentally obtained value. The minimum charge required for removal of O_2 from a cell of total volume 100 μl air-saturated Hb solution was calculated to be 4.63×10^{-4} C, which, compared with the experimentally obtained value of 0.60×10^{-2} C passed over a period of 1000 s at 25 °C showed that complete deoxygenation had been achieved. The experimentally obtained value increased to 0.10×10^{-1} C when the temperature was raised to 38 °C. The Pt matrix cell was therefore found to be a more efficient than the micromesh cell with regards to its O_2 reducing ability as a charge of 0.60×10^{-2} C was passed over a period of 1000 s with the Pt matrix cell, compared with 1.00×10^{-2} C passed over a period of 4500 s for the Pt micromesh cell. The geometry of the WE, containing a regular array of holes, effectively produced a system consisting of numerous 'stand alone' tubes within which HbS polymerisation could occur. This arrangement allowed nucleation and aggregation of HbS, concentrated within single holes on the electrode, to be monitored. To gain a more complete understanding of O_2 depletion in the Pt matrix cell finite element modeling using Comsol® was performed, chapter **5.4**.

5.4 Modeling of O_2 Depletion in the Pt Matrix Thin Layer Cell

The modeling was performed by Matthew Li (UCL). O_2 depletion that occurred at the Pt matrix thin layer electrochemical cell during the experiment was explored by theoretical modeling using Comsol® which is based on finite element methods. The thin layer electrochemical cell was accurately recreated in Comsol® to scale, using reference diagrams and photographs of the electrochemical cell. The model was prepared such that each section of the cell could be explored in detail as shown in Figure **5.2 (a)** and **(b)**, and was described by nonlinear-diffusion equation:

Area	**Equation**
Bulk of the liquid	$\frac{\partial c_O}{\partial t} = \nabla.(D(x)\nabla c_O)$
Insulated areas and liquid boundaries	$D(x)\nabla c_O.n = 0$
Electrode boundaries	$D(x)\nabla c_O.n = N_O$

Table 5.1: The bulk and boundary equations used in the model where c_O, N_O and $D(x)$ represent the concentration, outward flux of O_2 and the function of diffusion as a function of x respectively [97, 98].

In the case of the electrode boundaries, the flux was approximated by using the Butler-Volmer equation [99, 100] to derive a current, and when the charge of O_2 was given, could be used to deduce the depletion of O_2. As O_2 was the reactant of interest (and was being depleted), the area of the electrode was managed by Comsol® and the change transfer coefficient, α, was taken as 1, the flux equation was simplified to the following equation:

$$N_o = \frac{-c_o \exp\left[\frac{4F}{RT}\left(E - E^{0'}\right)\right]}{4F} \qquad (5.1)$$

The following values were applied to the bulk liquid of the model to simulate the conditions experienced by O_2 dissolved in water experimentally:

Property	Value
Diffusion of O_2	2.42×10^{-9} m s^{-1}
O_2 Electrode Potential	1.23 $E^{\emptyset}$ V
Initial O_2 Concentration	0.3 M
Temperature	298 K
Voltage applied	2

Table 5.2: Values used to approximate experimental conditions that were applied to the bulk liquid in the model [101].

Although the model was solved for a range of times, the actual time of interest in the experiments performed with the Pt matrix cell was 0 s to 1000 s (at 1 s intervals) and so the results for these are presented. Beyond a 1000 s there was little change in the results.

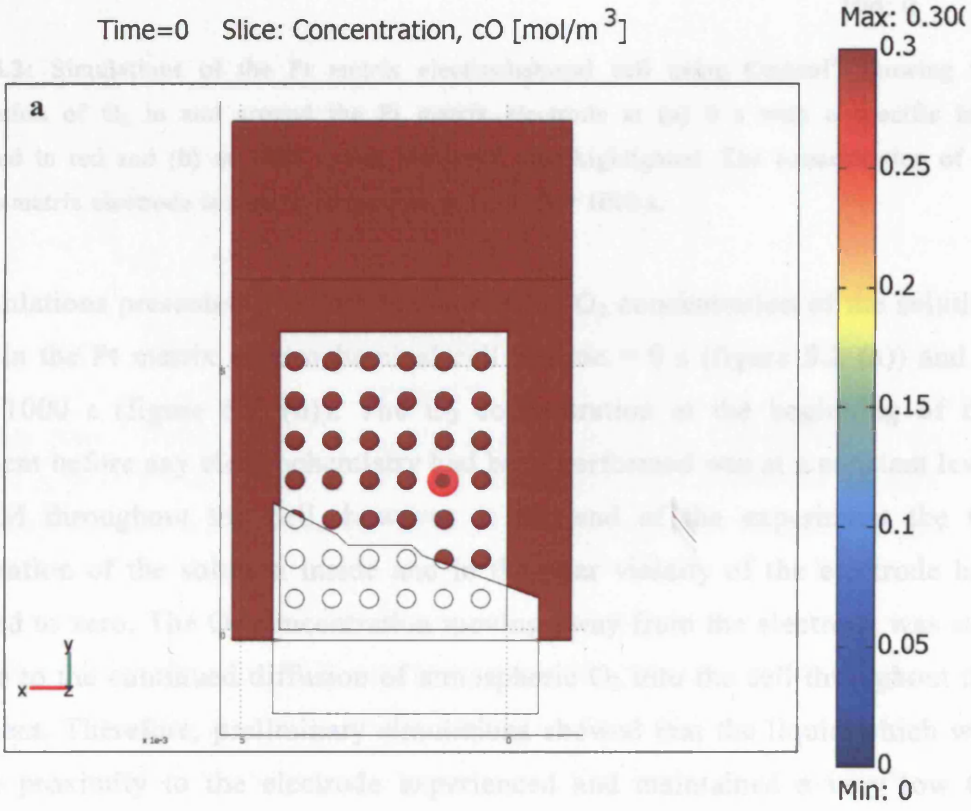

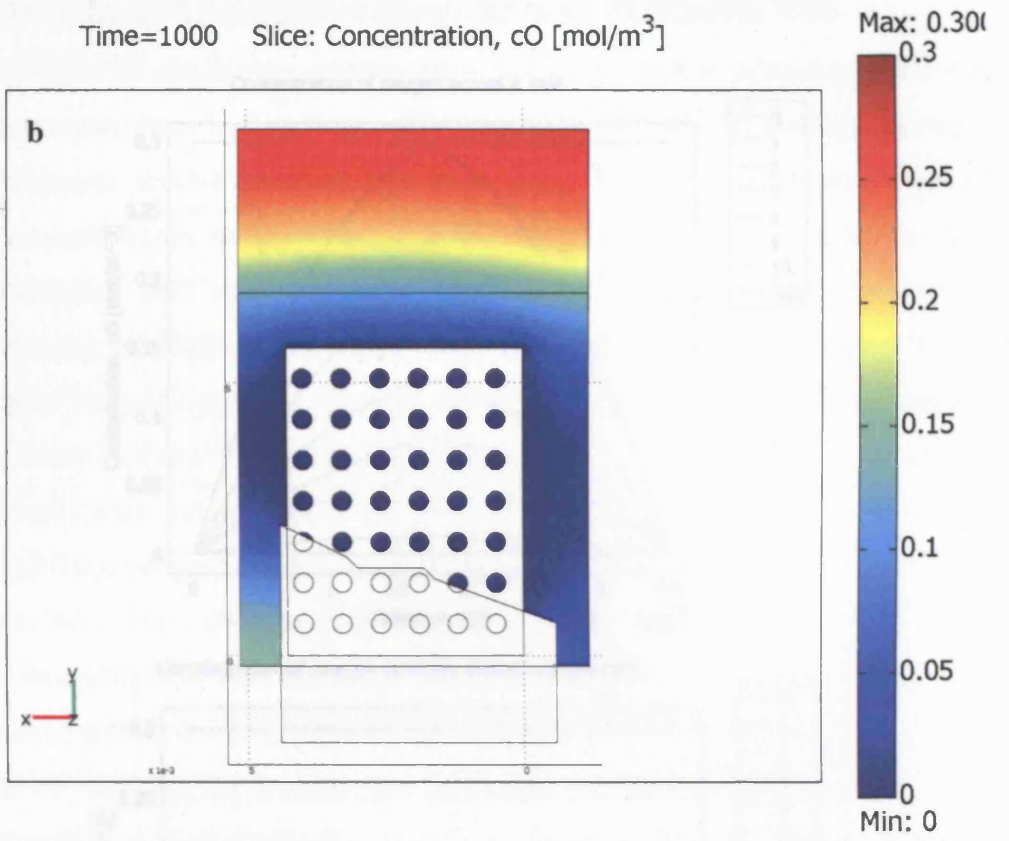

Figure 5.2: Simulations of the Pt matrix electrochemical cell using Comsol® showing the concentration of O_2 in and around the Pt matrix electrode at **(a)** 0 s with a specific hole highlighted in red and **(b)** at 1000 s with sectioned area highlighted. The concentration of O_2 inside the matrix electrode is seen to be reduced to zero after 1000 s.

The simulations presented in figure **5.2** shows the O_2 concentration of the solution present in the Pt matrix electrochemical cell at time = 0 s (figure **5.2 (a)**) and at time = 1000 s (figure **5.2 (b)**). The O_2 concentration at the beginning of the experiment before any electrochemistry had been performed was at a constant level of 0.3 M throughout the cell, however at the end of the experiment the O_2 concentration of the solution inside and in the near vicinity of the electrode had decreased to zero. The O_2 concentration moving away from the electrode was still high due to the continued diffusion of atmospheric O_2 into the cell throughout the experiment. Therefore, preliminary simulations showed that the liquid which was in close proximity to the electrode experienced and maintained a very low O_2 concentration when compared to areas that were not in close contact with the electrode.

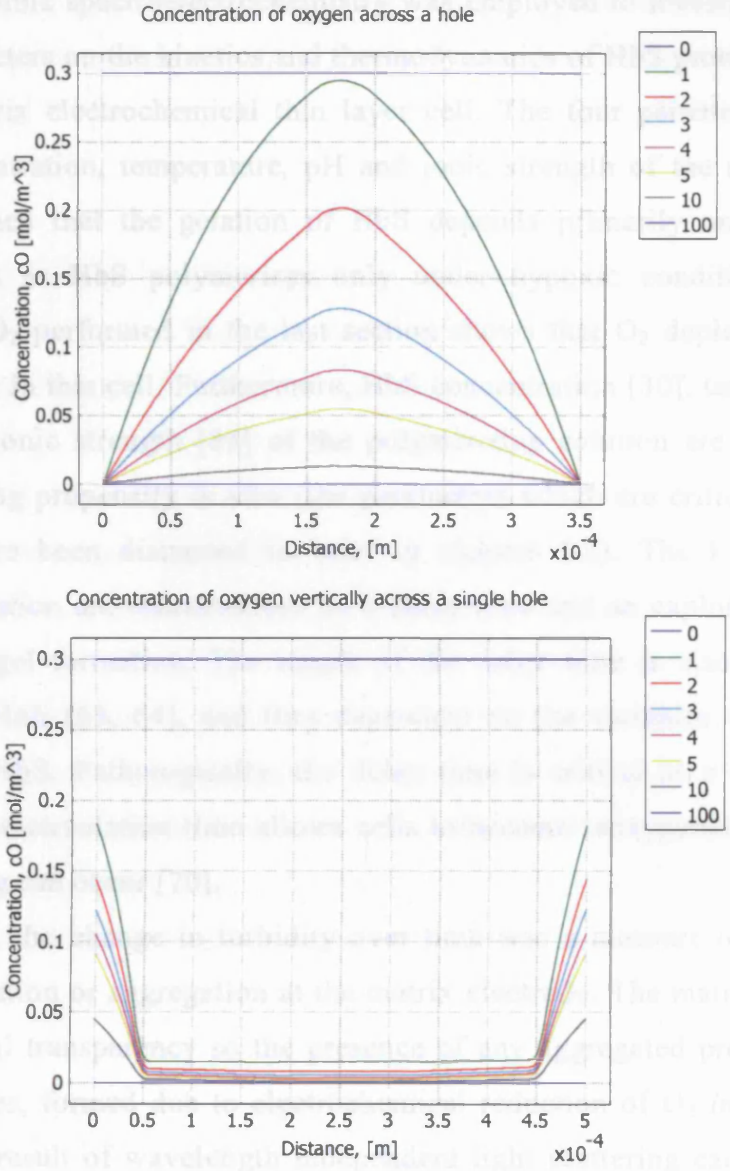

Figure 5.3: Plots showing **(a)** the change in O_2 concentration horizontally across the hole highlighted in figure **5.2 (a)** for various times; **(b)** the change in O_2 concentration vertically 5µm away from the electrode and 5µm into the bulk at either end of the hole highlighted in figure **5.2 (a)** at various times

Figures **5.3 (a)** and **(b)** show O_2 depletion occurring rapidly within 10 s and full depletion occurring before 100 s within a single hole in the matrix electrode. This is consistent with experimental evidence discussed later, that given the right conditions HbS nucleation can occur within 20 s. From modeling O_2 depletion in Comsol® it has been shown the presence of O_2 in the experiment is not a limiting factor in fibre formation due to rapid depletion within the cell.

5.5 Growth of Aggregated Structures at Pt Matrix Cell

In situ UV-visible spectroelectrochemistry was employed to investigate the effect of four parameters on the kinetics and thermodynamics of HbS protein aggregation in the Pt matrix electrochemical thin layer cell. The four parameters were HbS protein concentration, temperature, pH and ionic strength of the solution. It has been established that the gelation of HbS depends primarily on the extent of deoxygenation as HbS polymerises only under hypoxic conditions [26]. The modeling of O_2 performed in the last section shows that O_2 depletion was not a limiting factor in this cell. Furthermore, HbS concentration [30], temperature [35], pH [28] and ionic strength [85] of the polymerising solution are also known to alter the gelling propensity *in vivo* (the parameters which are critical for polymer formation have been discussed in brief in chapter **1.2**). The kinetics of HbS polymer formation are characterised by a delay time and an explosive and highly autocatalytic gel formation. The length of the delay time is also related to the solubility of HbS [63, 64], and thus dependent on the variables which alter the solubility of HbS. Pathologically, the delay time is critical as a delay which is longer than the circulation time allows cells to become reoxygenated at the lungs before sickling can occur [70].

In this set-up, the change in turbidity over time was a measure of the extent of polymer formation or aggregation at the matrix electrode. The matrix arrangement allowed optical transparency so the presence of any aggregated protein structures in the apertures, formed due to electrochemical reduction of O_2 *in situ*, could be detected as a result of wavelength independent light scattering caused by protein aggregation. The rate of turbidity change at 600 nm, 650 nm, 700nm and 800 nm were monitored as a function of time to investigate the kinetics of HbS aggregation. Turbidity values were determined from the absorbance according to the relation $A = \log (I_0/I)$, where turbidity = (I_0/I). Control experiments with HbA at the same conditions showed no significant turbidity change at the Pt matrix WE especially at the wavelength range 650 nm to 1100 nm proving conclusively that any changes in turbidity were due to HbS protein aggregation (this data is not shown). The blank in these experiments was the HbS solution before the potential was applied, so the spectra shown in the following figures shows the change in turbidity relative to the starting solution.

5.5.1 Analysis of Growth Rates

Two methods were employed to analyse the turbidity profile of each condition and obtain kinetic and thermodynamic values for the nucleation and growth phases of HbS aggregation.

Kinetic Scheme:

The modified Sabaté *et al.* [93] kinetic scheme model used in Chapter **4.6** was fitted to the Pt matrix cell data and least squares fitting of equation **4.4** to the turbidity data at 700 nm was used to obtain k_1 and k_2 values for each parameter. However, although a satisfactory to good fitting was obtained for most turbidity profiles (figure **5.4 (a)** shows the fitting of the turbidity profile at 40 mg cm^{-3} HbS concentration), some profiles exhibited a poor fit to the kinetic model especially in the early part of the curve due to the lag period for the nucleation phase not being present, figure **5.4 (b)** shows the poor fit obtained for 100 mg cm^{-3} HbS concentration. Therefore, in these cases a linear regression method was employed to obtain nucleation and growth rates. The linear regression method was also used for those profiles which exhibited a decrease in the turbidity during the experiment (termed as Phase II, figure **5.5**) as the kinetic model could not recognise a decrease in turbidity values further contributing to a poor fitting.

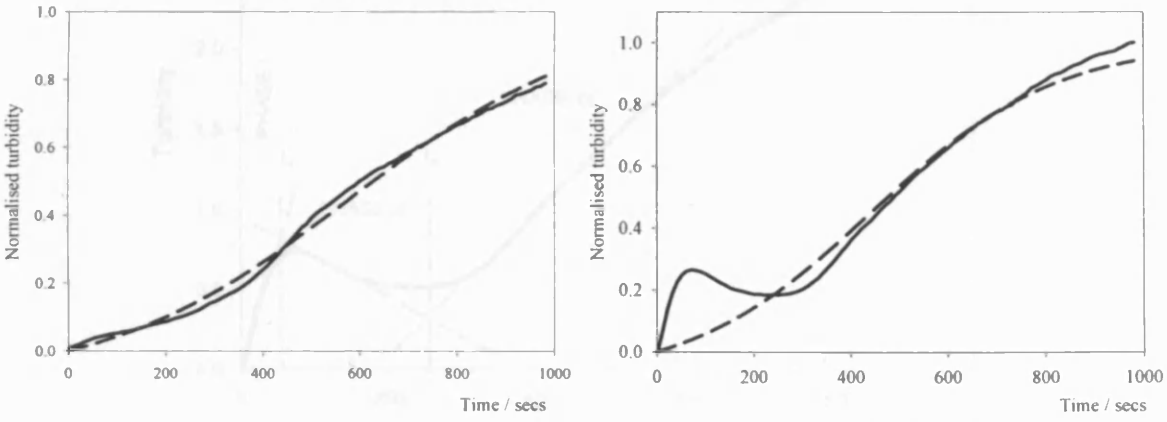

Figure 5.4: Solid lines showing the experimental values of normalised turbidity versus time for **(a)** 40 mg cm^{-3}, and **(b)** 100 mg cm^{-3}. The dashed lines are the best-fit lines to equation **4.4**. A good fitting to the kinetic model is obtained for 40 mg cm^{-3} (R^2 = 0.999), however, a poor fit is seen for 100 mg cm^{-3} (R^2 = 0.935) mainly due to the absence of the time delay and a large decrease in turbidity after 150 s.

Linear Regression:

The linear regression method of analysis was employed to obtain growth rates, specifically for those turbidity profiles which did not satisfactorily fit the two step kinetic scheme model. Figure **5.5** shows a turbidity profile exhibiting the three phases seen experimentally: Phase I is the nucleation phase, Phase II is the intermediary phase and Phase III is the growth or elongation phase. The gradient of best fit was calculated for all phases using a linear regression fit in Sigmaplot, and these values were compared with other matrix cell rate values as well as free solution data. The value of t_1 and t_2 indicated the time at which the nucleation phase stopped and the time at which the growth phase commenced respectively, whilst the intercept on the time axis related to the delay time or the time taken for nucleation to start. This analysis was also employed for those turbidity profiles which did not possess the intermediary Phase II. In these cases, only data for Phase I and Phase III were calculated. Unlike the kinetic scheme analysis, this method cannot be used to obtain kinetic rate constants but only nucleation and growth rates.

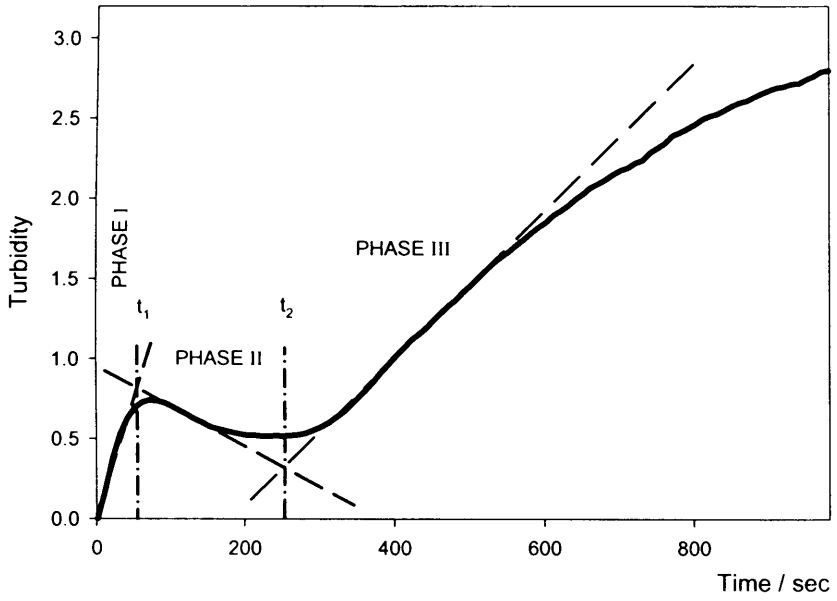

Figure 5.5: Turbidity profile exhibiting the three phases seen experimentally: Phase I is the nucleation phase; Phase II is the intermediary phase; Phase III is the growth phase. The gradient of best fit was calculated using a linear regression fit in Sigmaplot. t_1 and t_2 are the times at which the nucleation phase stopped and the time at which the growth phase commenced respectively, whilst the intercept on the time axis relates to the delay time or the time taken for nucleation to start.

5.5.2 Effect of Changing HbS Concentration

The effect of increasing HbS protein concentration on turbidity, and therefore polymer formation, at a Pt surface was investigated by performing experiments at protein concentrations of 10 mg cm^{-3}, 20 mg cm^{-3}, 30 mg cm^{-3}, 40 mg cm^{-3}, 50 mg cm^{-3}, 75 mg cm^{-3} and 100 mg cm^{-3} at 38 °C. Figure **5.6** shows the effect of protein concentration on the rate of turbidity change at a wavelength of 700 nm (results at wavelength of 700 nm only are shown, however, all other wavelengths showed a similar trend. A wavelength of 800 nm was not used as the turbidity at 700 nm was more pronounced than 800 nm).

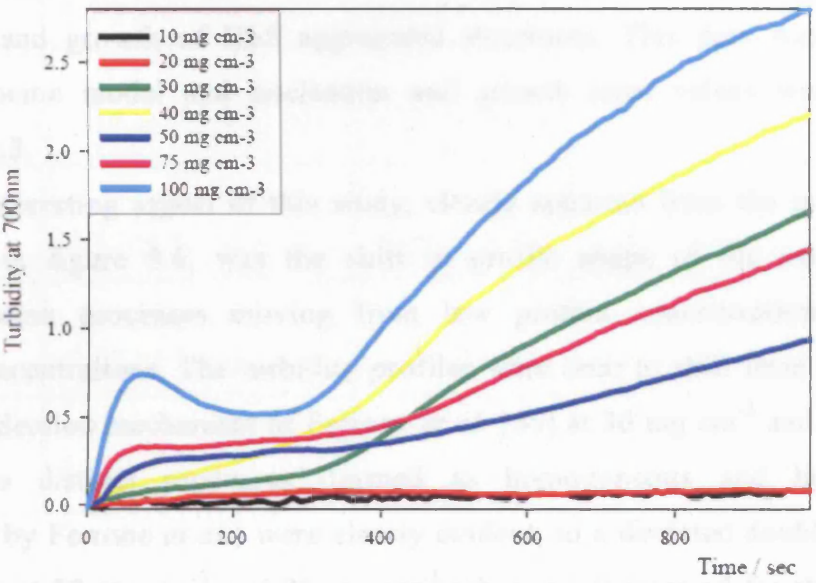

Figure 5.6: UV-visible spectroelectrochemistry time traces showing the changes seen in turbidity levels at 700 nm at a Pt matrix electrode with increasing HbS concentrations. Experimental conditions: HbS range 10 mg cm^{-3} to 100 mg cm^{-3}; 1.5 M (pH 7.0) phosphate buffer; 0.5 M NaCl; T = 38.0 C; E = - 0.55 V *vs.* Ag/AgCl; run time 1000 s.

The results showed a clear concentration dependence on the extent of aggregate formation at the Pt matrix cell. DeoxyHbS aggregation occurred with a clear demonstration of a delay time (the time taken before significant growth was seen) and the results showed that the delay time was prolonged upon dilution of HbS. For instance, the delay time decreased from 250 s with a protein concentration of 30 mg cm^{-3} to 230 s with a slightly higher concentration of 40 mg cm^{-3}, whilst, further increases in protein concentration to 50 mg cm^{-3} decreased the time delay to only 20 s. At even higher protein concentrations of 75 mg cm^{-3} and 100 mg cm^{-3}

the total disappearance of the time delay was apparent, being instead replaced with a large increase in turbidity as soon as the experiment had begun. Consequently, the kinetics of nucleation at these higher concentrations (75 mg cm^{-3} and 100 mg cm^{-3}) was considered to be too fast to be detected by the spectrophotometer.

The results in figure **5.6** also demonstrated significant HbS aggregation with increasing protein concentration. Low protein concentration of 10 mg cm^{-3} showed little increase in turbidity with a value of only 0.09 being recorded after 1000 s, whilst at a higher concentration of 50 mg cm^{-3} a turbidity value of 0.94 (an increase of over ten fold) was apparent at the end of the experiment, and a thirty one fold increase (to a value of 2.80) was seen for a protein concentration of 100 mg cm^{-3}. This was due to an increase in light scattering caused by extensive formation and growth of HbS aggregated structures. This data was fitted to a kinetic scheme model and nucleation and growth rates values were obtained, section **5.5.3**.

Another interesting aspect of this study, clearly apparent from the graphical data presented in figure **5.6**, was the shift in profile shape of the nucleation and polymerisation processes moving from low protein concentrations to higher protein concentrations. The turbidity profiles were seen to shift from the classical double nucleation mechanism of Ferrone *et al.* [66] at 30 mg cm^{-3} and 40 mg cm^{-3}, where two distinct processes (termed as homogeneous and heterogeneous nucleation by Ferrone *et al.*) were clearly evident, to a deviated double nucleation mechanism at 50 mg cm^{-3} and 75 mg cm^{-3} where no lag period for the nucleation phase was seen but an initial increase in turbidity was followed by growth. However it was the profile at 100 mg cm^{-3} which was of real interest as an intermediary process (termed as Phase II, figure **5.5**), consisting of a decrease in turbidity (from time 100 s to 300 s), was apparent. This was the first time such a process had been seen to the best of our knowledge with regards to monitoring the polymerisation of HbS at a surface. This was a real life process as shown by the presence of this intermediary phase in repeat experiments and its absence in control experiments at 100 mg cm^{-3}. Reasons for the occurrence of this phase are further alluded to in section **5.6**.

5.5.3 HbS Concentration Analysis

Kinetic Scheme Analysis:

The rate constants for each specific concentration are listed in table **5.3**. Rate constants for 10 mg cm^{-3} and 20 mg cm^{-3} HbS were not calculated due to nominal changes in turbidity levels being seen with these two concentrations.

HbS conc. / mg cm^{-3}	k_1 / s^{-1}	k_2 / M^{-1} s^{-1}	ak_2 / s^{-1}	R^2
30	0.28 (± 0.09) x 10^{-3}	6.37 (± 1.22)	2.96 (± 0.1) x 10^{-3}	0.988
40	0.37 (± 0.02) x 10^{-3}	5.71 (± 0.16)	3.54 (± 0.1) x 10^{-3}	0.999
50	0.36 (± 0.47) x 10^{-3}	0.25 (± 0.25)	0.19 (± 0.2) x 10^{-3}	0.926
75	0.40 (± 0.01) x 10^{-3}	1.11(± 0.17)	1.29 (± 0.2) x 10^{-3}	0.942
100	0.14 (± 0.03) x 10^{-3}	0.58 (± 0.05)	4.82 (± 0.4) x 10^{-3}	0.935

Table 5.3: Nucleation rate constants k_1 and elongation rate constants k_2 to describe the aggregation formation for HbS concentration in the range 30 mg cm^{-3} to 100 mg cm^{-3} at a Pt matrix electrode. Experiment conditions: HbS concentrations 30 mg cm^{-3} to 100 mg cm^{-3}; 1.5 M pH 7.0 phosphate buffer; 0.5 M NaCl; temperature 38 °C; E = - 0.55 V *vs.* Ag/AgCl for 1000 s.

The fit of equation **4.4** to the normalised turbidity data (normalised with the maximum turbidity value of 2.52 seen with 100 mg cm^{-3} at 1000 s) was shown to be extremely good for low protein concentrations such as 30 mg cm^{-3} (R^2 = 0.988) and 40 mg cm^{-3} (R^2 = 0.999) but extremely poor for the higher protein concentrations, 50 mg cm^{-3} (R^2 = 0.926), 75 mg cm^{-3} (R^2 = 0.942) and 100 mg cm^{-3} (R^2 = 0.935).

The rate constants for 30 mg cm^{-3} and 40 mg cm^{-3}, the two concentrations which did fit the kinetic model well, showed a clear concentration dependence on the

effective growth rate, ak_2. The nucleation rate constant k_1 also showed concentration dependence, however the elongation rate constant k_2 did not show significant correlation with concentration. This was due to nucleation at a surface being more thermodynamically favourable than growth free in solution. Once again, k_1 was several orders of magnitude smaller than k_2 showing that the nucleation process was slower than the growth process and thus the rate limiting step.

The results seen with 30 mg cm^{-3} and 40 mg cm^{-3} at the matrix cell were significantly different to those seen with the Au micromesh cell, table **4.1**. The k_1 value for 30 mg cm^{-3} (2.37 (± 0.92) x 10^{-4} s^{-1}) at the matrix electrode was several orders of magnitude greater than even 300 mg cm^{-3} (9.45 (± 0.08) x 10^{-6} s^{-1}) of Hb at the micromesh cell, whilst a large difference was also seen in the k_2 values between the two cells. These results indicated that the polymerisation process was far slower in the micromesh cell as compared with the matrix cell. As the modeling of O_2 concentration at the matrix electrode has shown total O_2 depletion was achieved within 100 s of the start of the experiment compared to the 200 s seen for the micromesh cell (figure **2.3**)

Linear Regression Analysis:

Table **5.4** shows linear regression gradient rate data of Phase I, Phase II and Phase III for protein concentrations in the range 30 mg cm^{-3} to 100 mg cm^{-3}. Again, 10 mg cm^{-3} and 20 mg cm^{-3} were not analysed due to the small changes in turbidity seen at these two concentrations.

HbS conc. / mg cm^{-3}	Rate of Phase I / s^{-1}	Rate of Phase II / s^{-1}	Rate of Phase III / s^{-1}
30	0.74 (± 0.03) x 10^{-3}		2.72 (± 0.04) x 10^{-3}
40	1.69 (± 0.06) x 10^{-3}		4.25 (± 0.05) x 10^{-3}
50	5.65 (± 0.41) x 10^{-3}		1.01 (± 0.01) x 10^{-3}
75	11.8 (± 0.10) x 10^{-3}	-0.12 (± 0.04) x 10^{-3}	1.86 (± 0.01) x 10^{-3}
100	17.8 (± 0.74) x 10^{-3}	-2.48 (± 0.03) x 10^{-3}	5.11 (± 0.06) x 10^{-3}

Table 5.4: Rate values for Phase I, Phase II and Phase III calculated using linear regression analysis for protein concentration in the range 30 mg cm^{-3} to 100 mg cm^{-3} at a Pt matrix electrode surface. Experiment conditions: HbS concentrations 30 mg cm^{-3} to 100 mg cm^{-3}; 1.5 M pH 7.0 phosphate buffer; 0.5 M NaCl; temperature 38 °C; E = - 0.55 V *vs.* Ag/AgCl for 1000 s.

The results showed a clear concentration dependence on the nucleation phase with the rate values of Phase I becoming steadily faster with increasing concentrations. However, the growth phase or Phase III did not vary considerably with concentration due to the initial nucleation at the surface being more favourable than the growth process. The intermediary Phase II process which consisted of a negative turbidity gradient was only present at two concentrations. The linear regression analysis provided a closer reflection of the experimental data seen in figure **5.6** than the kinetic scheme analysis as a result of the poor fitting obtained for certain concentrations.

5.5.4 Effect of Changing Temperature

In this section the dependence of HbS fibrillogenesis on temperature at a conducting surface is reported. The effect of a range of HbS solution temperatures (25 °C, 30 °C, 34 °C, 38 °C and 42 °C) on the rate of protein aggregation at two HbS concentrations, 30 mg cm^{-3} and 75 mg cm^{-3}, were investigated using the Pt matrix electrochemical cell, figure **5.7**.

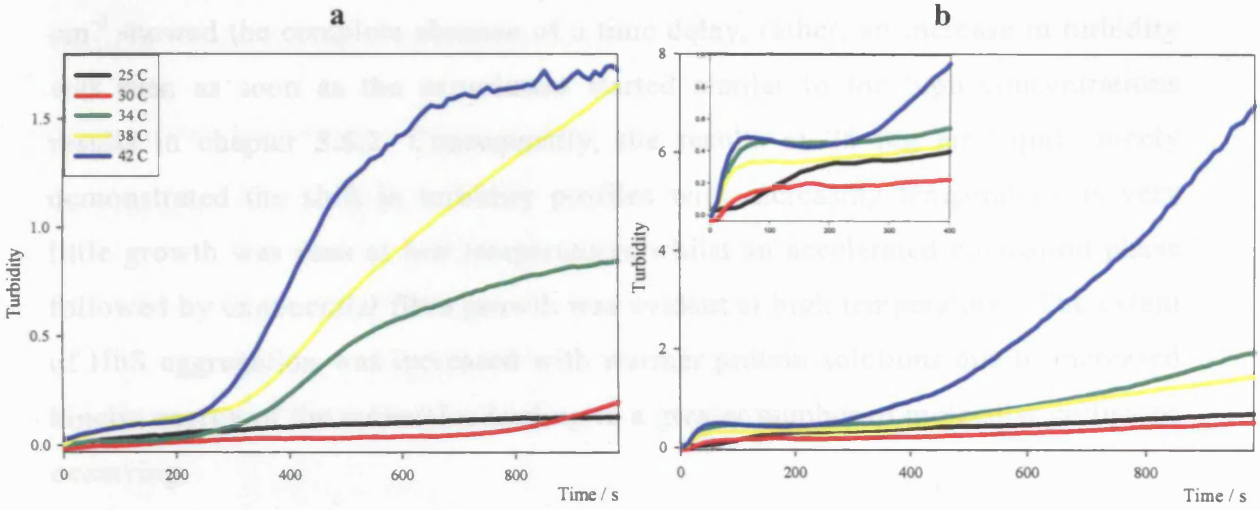

Figure 5.7: UV-visible spectroelectrochemistry time traces showing the changes seen in the turbidity at 700 nm at the Pt matrix electrode with increasing solution temperature for two HbS concentrations **(a)** 30 mg cm^{-3} and **(b)** 75 mg cm^{-3}. Experimental conditions: solution temperature range 25 °C to 42 °C; 1.5 M (pH 7.0) phosphate buffer; 0.5 M NaCl; 38.0 °C; E = -0.55 V *vs.* Ag/AgCl; run time 1000 s.

For 30 mg cm^{-3} HbS concentration (figure **5.7 (a)**), a clear temperature dependence on the extent of aggregate formation was demonstrated as increasing the temperature from 25 °C to above physiological temperature caused a reduction in the time delay and an increase in the turbidity amplitude. For instance, a solution incubated at 30 °C exhibited a delay of 575 s whilst at 34 °C a delay of 290 s was seen. Further increases in temperature to 42 °C led to the nucleation lag period occurring even faster with a delay of only 232 s being seen before the growth period. On the other hand, an increase in solution temperature by 12 °C (from 30 °C to 42 °C) gave rise to an eight-fold increase in the final turbidity value seen at the end of the experiment.

The results obtained for a HbS concentration of 75 mg cm^{-3} (figure **5.7 (b)**) did not mirror those seen with 30 mg cm^{-3}. The growth of HbS aggregates was found to be

largely dependent on the temperature with a substantial increase in turbidity seen with all temperatures. Increasing solution temperature by 12 °C from 30 °C to 42 °C gave rise to a thirteen-fold increase in turbidity from 0.52 to 6.96 respectively, compared to the eight fold increase seen with 30 mg cm^{-3}.

However, the major difference between the two concentrations was the nucleation phase. Whereas a considerable time delay was observed for all temperatures at 30 mg cm^{-3}, the experiments performed at temperatures of 38 °C and 42 °C at 75 mg cm^{-3} showed the complete absence of a time delay, rather, an increase in turbidity was seen as soon as the experiment started similar to the high concentrations results in chapter **5.5.2**. Consequently, the results at 75 mg cm^{-3} quite nicely demonstrated the shift in turbidity profiles with increasing temperature as very little growth was seen at low temperatures whilst an accelerated nucleation phase followed by exponential fibre growth was evident at high temperatures. The extent of HbS aggregation was increased with warmer protein solutions due to increased kinetic energy of the molecules leading to a greater number of molecular collisions occurring.

Furthermore, the presence of an intermediary phase, seen previously at 100 mg cm^{-3} in chapter **5.5.2** (figure **5.6**), was apparent once again for the 75 mg cm^{-3} experiment performed at 42 °C. This intermediary process was seen to occur at conditions which were favourable to rapid and accelerated HbS polymerisation such as at high temperatures and concentrations, or in other words at conditions which were conducive to fast kinetics, see chapter **5.6** for a discussion concerning the nature of the intermediary phase. The largest increase in polymer aggregation was seen at 42 °C for both experimental concentrations. This value is in contrast to the free solution literature reported data of 35 °C where the solubility of HbS was reported to decrease to a minimum and then increase again at higher temperatures [36]. The difference between the free solution experiment and the conducting surface experiments could be due to differences in the mechanism of protein aggregation at a liquid-liquid interface as compared to liquid-solid interfaces. Further work in the future will be focussed upon investigating the mechanism of action of protein aggregation at various interfaces.

5.5.5 Temperature Analysis

Kinetic Scheme Analysis:

The rate constants obtained from the turbidity experiments performed with 30 mg cm^{-3} protein in the temperature range 25 °C to 42 °C are listed in table **5.5**. In this set of data, the fit of equation **4.4** with the normalized turbidity data (normalized with a maximum turbidity value of 1.75 at 42 °C) was extremely good for the higher temperatures such as 38 °C (R^2 = 0.996) and 42 °C (R^2 = 0.996), but extremely poor for lower temperatures such as 25 °C (R^2 = 0.811).

Temperature / °C	k_1 / s^{-1}	k_2 / M^{-1} s^{-1}	ak_2 / s^{-1}	R^2
25	0.10 (± 1.29) x 10^{-3}	0.04 (± 4.10)	0.02 (± 0.2) x 10^{-3}	0.811
30	0.01 (± 0.002) x 10^{-3}	8.21 (± 0.43)	3.82 (± 0.2) x 10^{-3}	0.934
34	0.29 (± 0.05) x 10^{-3}	4.90 (± 0.43)	2.28 (± 0.2) x 10^{-3}	0.952
38	0.19 (± 0.01) x 10^{-3}	12.33 (± 0.22)	5.73 (± 0.1) x 10^{-3}	0.996
42	0.13 (± 0.01) x 10^{-3}	21.35 (± 0.01)	9.93 (± 0.2) x 10^{-3}	0.996

Table 5.5: Nucleation rate constants k_1 and elongation rate constants k_2 to describe the HbS aggregation formation for temperatures in the range 25 °C to 42 °C for 30 mg cm^{-3} HbS at a Pt matrix electrode. Experiment conditions: HbS concentration 30 mg cm^{-3}; temperature range 25 °C to 42 °C; 1.5 M pH 7.0 phosphate buffer; 0.5 M NaCl; E = - 0.55 V *vs.* Ag/AgCl for 1000 s.

The results seen with those conditions which had a reasonable to good fit (i.e. 34 °C, 38 °C and 42 °C) showed a significant temperature dependence on the effective growth rate. However, in contrast to the results seen in table **5.3**, k_1 was shown to decrease with increasing temperature (k_1 at 34 °C = 2.88 (± 0.5) x 10^{-4} s^{-1}; k_1 at 42 °C = 1.28 (± 0.1) x 10^{-4} s^{-1}), whilst an 8 °C increase in temperature from

34 °C to 42 °C caused a four fold increase in k_2. This showed that varying temperature had a significant effect on the growth process, more so than just varying the concentration. This was because equilibration of the protein solution with the required temperature before the start of the experiment had probably caused initiation of the polymerisation process even before electrochemical depletion of O_2. Experiments performed with 75 mg cm^{-3} HbS showed an extremely poor fit of equation **4.4** to the normalised turbidity data (normalised with a value of 6.96) for all temperatures and so no kinetic rate constants were calculated.

Linear Regression Analysis:

Table **5.6** shows the linear regression gradient data for protein concentration of 30 mg cm^{-3} at temperatures of 30 °C, 34 °C, 38 °C and 42 °C. No data was obtained for 25 °C as very little changes in turbidity were seen at this condition. Furthermore, only the rate of Phase I and Phase III were calculated as no intermediary Phase II was present at any of these conditions.

Temperature / °C	Rate of Phase I / s^{-1}	Rate of Phase II / s^{-1}	Rate of Phase III / s^{-1}
30	0.24 (± 0.005) x 10^{-3}		0.60 (± 0.01) x 10^{-3}
34	0.06 (± 0.004) x 10^{-3}		2.23 (± 0.01) x 10^{-3}
38	1.52 (± 0.007) x 10^{-3}		3.01 (± 0.02) x 10^{-3}
42	0.79 (± 0.02) x 10^{-3}		5.29 (± 0.05) x 10^{-3}

Table 5.6: Rate values for Phase I and Phase III, calculated using linear regression analysis, for temperatures in the range 30 °C to 42 °C for 30 mg cm^{-3} HbS concentration at a Pt matrix electrode. Experiment conditions: HbS concentration 30 mg cm^{-3}; temperature range 30 °C to 42 °C; 1.5 M pH 7.0 phosphate buffer; 0.5 M NaCl; E = - 0.55 V *vs.* Ag/AgCl for 1000 s.

The results did not show a clear temperature dependence on the nucleation Phase I, however there seemed to be a slight correlation between the elongation Phase III and temperature. This correlation between the growth phase and temperature was also evident in the results obtained from the kinetic model fitting, where an increase in k_2 was seen with increasing temperature.

Temperature / °C	Rate of Phase I / s^{-1}	Rate of Phase II / s^{-1}	Rate of Phase III / s^{-1}
30	4.74 (± 0.07) x 10^{-3}		0.44 (± 0.003) x 10^{-3}
34	11.90 (± 0.01) x 10^{-3}		1.96 (± 0.02) x 10^{-3}
38	8.21 (± 0.001) x 10^{-3}	- 0.04 (± 0.03) x 10^{-3}	1.84 (± 0.01) x 10^{-3}
42	13.20 (± 1.12) x 10^{-3}	- 0.77 (± 0.02) x 10^{-3}	10.0 (± 0.06) x 10^{-3}

Table 5.7: Rate values for Phase I, Phase II and Phase III, calculated using linear regression analysis, for temperature in the range 30 °C to 42 °C for 75 mg cm^{-3} HbS concentration at a Pt matrix electrode. Experiment conditions: HbS concentration 75 mg cm^{-3}; temperature range 30 °C to 42 °C; 1.5 M pH 7.0 phosphate buffer; 0.5 M NaCl; E = - 0.55 V *vs.* Ag/AgCl for 1000 s.

The linear regression gradient data for a protein concentration of 75 mg cm^{-3} is listed in Table **5.7**. The rate of Phase III showed significant correlation with temperature as the highest rate was seen at 42 °C, far more so than the rate of the nucleation Phase I which was seen to be similar, possibly again due to polymerisation starting in the water bath even before the start of the experiment.

5.5.6 Thermodynamic Calculations

The k_1 and k_2 values for only three temperatures, 34 °C, 38 °C and 42 °C at 30 mg cm^{-3} were used for the thermodynamic calculations as the fitting of the kinetic model to these profiles was good. All other temperature data points showed a poor fitting to the kinetic model and with large error values and so the rate constants obtained from these fittings would not have provided accurate thermodynamic values. Therefore, rate constants for 25 °C, 30 °C at 30 mg cm^{-3} and all temperatures at 75 mg cm^{-3} were not used in the thermodynamic calculations.

Activation Energies:

The rate constants were used to calculate activation energies for the nucleation and elongation process using the Arrhenius equation [102]. The Arrhenius equation is an expression that shows the dependence of the rate constant, k, of a known chemical reaction on the temperature T (in kelvins) and activation energy E_a:

$$k = Ae^{-E_a / RT} \tag{5.2}$$

where A is the pre-exponential factor or frequency factor and R is the gas constant. By taking the natural logarithms, the equation yields:

$$\ln k = \left(\frac{-E_a}{R}\right)\left(\frac{1}{T}\right) + \ln A \tag{5.3}$$

Therefore, a plot of ln k vs 1/T gives a gradient of $-E_a/R$ and the slope of the straight line determines the activation energy. From figure **5.8**, which shows a plot of the nucleation rate constant as a function of reciprocal temperature, the nucleation activation energy, E_1, was calculated to be 81.59 (± 1.22) KJ mol^{-1}. The nucleation activation energy can be defined as the energy required for the sequential addition of monomers to form the critical nuclei, or in other words to make the reaction thermodynamically favourable.

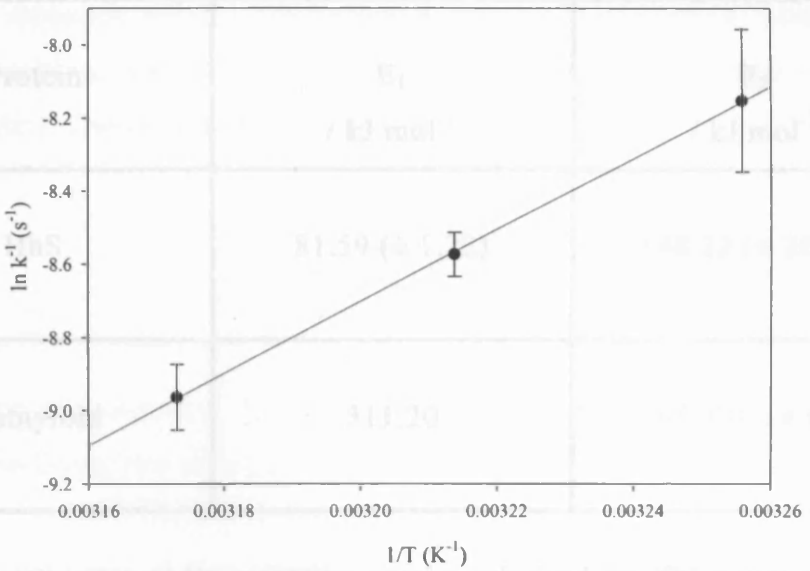

Figure 5.8: A plot of the log of nucleation rate constant, k_1, as a function of reciprocal temperature in kelvin. The gradient of the best fit line which equals $-E_a/R$ was 9813.0 (± 147.2) s^{-1} K and the intercept was – 4.01 (± 0.47) s^{-1}. Only three temperature data points (34 °C, 38 °C and 42 °C for 30 mg cm^{-3} protein concentration) were used as these showed a good fit to the kinetic model. All other temperature values showed a very poor fit to the model and so gave rate constants which had large errors and were not a true reflection of the actual experimentally obtained results.

The elongation activation energy, E_2, was calculated in a similar manner. A plot of the elongation rate constant as a function of the reciprocal temperature yielded a gradient of 17827.1 (± 2479) s^{-1} K, from which E_2 was calculated to be 148.22 (± 20.61) KJ mol^{-1}. Consequently, the elongation activation energy, defined as the energy required for the initiation of the elongation phase, was calculated as requiring nearly twice as much energy as the nucleation phase. It was expected that the nucleation phase would require a larger amount of energy as this process involves the thermodynamically unfavourable sequential addition of free monomers. However, in our system nucleation occurred at a surface rather than free in solution which is more thermodynamically favourable. A comparison of the activation energies calculated for HbS polymerisation at an electrode surface and the activation energy of ß-amyloid fibrils is shown in table **5.8**.

Protein	E_1 / kJ mol^{-1}	E_2 / kJ mol^{-1}
HbS	81.59 (± 1.22)	148.22 (± 20.61)
ß-amyloid	311.20	95.30 (± 4.60)

Table 5.8: A comparison of the activation energies calculated for HbS polymerisation at an electrode surface with the activation energy of ß-amyloid fibrils. The nucleation activation energy, E_1 for ß-amyloid fibrils was obtained from a study performed by Sabate *et al* [103]. No error values were provided in their calculations. Experimental conditions: 1 mg ß-amyloid protein was dissolved in 500 µl HFIP, incubated at room temperature for 10 minutes and then Tris-HCl buffer (10 mM, pH 7.4) was added; temperatures assayed from 28.5 °C to 44.5 °C at intervals of 4 °C. The elongation activation energy, E_2 for ß-amyloid fibrils was obtained from a study performed by Kusumoto *et al* [104]. Experimental conditions: 250 µm ß-amyloid protein was dissolved in 0.1 M HCl pH 1 at 4 °C and the sample was incubated for 4 hrs at 25 C; fibrillogenesis was monitored at temperatures of 4 °C, 15 °C, 25 °C and 35 °C. The HbS polymerisation E_1 and E_2 values were obtained by experiments performed at a Pt matrix electrode. Experimental conditions: HbS concentration 30 mg cm^{-3}; temperature range 34 °C to 42 °C; 1.5 M pH 7.0 phosphate buffer; 0.5 M NaCl; E = - 0.55 V *vs.* Ag/AgCl for 1000 s.

Table **5.8** shows that the ß-amyloid fibril nucleation activation energy was calculated to be nearly three times larger than the value obtained for HbS. The differences in energy values can be explained by the different experimental conditions of protein concentration and pH used. Moreover, several authors [105-108] have also indicated that prior to nucleation the ß-amyloid monomer is activated, through a slow conformational transition from the soluble peptide to the amyloid peptide. Therefore, a larger energy barrier needs to be overcome in this case. This is the first time activation energies of the HbS nucleation and aggregation processes have been calculated at a solid interface. Use of agents which increase the activation energies of these processes could be a good therapeutic strategy for achieving a major reduction in the polymerisation process.

Eyring Transition State Model:

The Eyring equation relates the reaction rate to temperature, similar to the Arrhenius equation, and follows on from the transition state theory (activated complex model). The general form of the Eyring equation is:

$$k = \frac{k_B T}{h} e^{-\Delta G^{*}/RT} \tag{5.4}$$

where k is the rate constant, k_B is the Boltzmann constant, h is Plancks constant and ΔG^{*} is the Gibbs free energy of activation. It can be rewritten as:

$$k = \left(\frac{k_B T}{h}\right)\exp\left(\frac{\Delta S^{\mp}}{R}\right)\exp\left(\frac{-\Delta H^{\mp}}{RT}\right) \tag{5.5}$$

where ΔS is the entropy of activation and ΔH is the enthalpy of activation. By taking the natural logarithms the equation becomes:

$$\ln\left(\frac{k}{T}\right) = \frac{-\Delta H^{\mp}}{R}.\frac{1}{T} + \ln\left(\frac{k_B}{h}\right) + \frac{\Delta S^{\mp}}{R} \tag{5.6}$$

A plot of ln (k/T) as a function of reciprocal temperature gives a straight line with gradient – $\Delta H/R$ from which the enthalpy of activation can be derived, and intercept ln (k_B/h) + ΔS/R from which the entropy of activation can be extrapolated. For the nucleation rate constant, the slope of the straight line was 10124.44 (± 146.0) and the intercept was -46.85 (± 0.47), figure **5.9**. Consequently, the enthalpy of activation for the nucleation process ΔH_1 was calculated to be -84.18 (± 1.21) kJ mol^{-1}, whilst the entropy of activation for the nucleation process ΔS_1 was derived to be – 0.59 (± 0.01) kJ mol^{-1} K^{-1}.

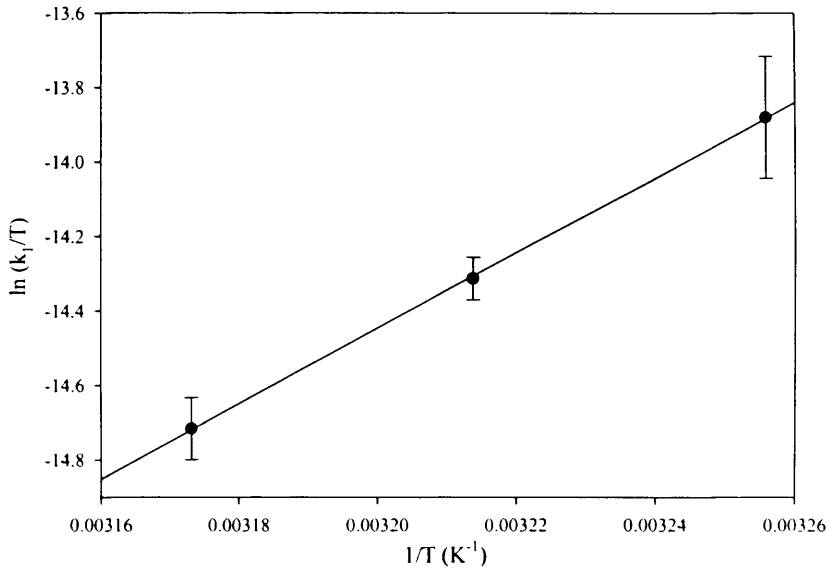

Figure 5.9: A plot of the nucleation rate constant over temperature as a function of reciprocal temperature. The gradient of the best fit line which is equal to – $\Delta H/R$ was 10124.4 (± 146.0) and the intercept ln (k_B/h) + $\Delta S/R$ was – 46.85 (± 0.47). Only three temperature data points (34 °C, 38 °C and 42 °C for 30 mg cm^{-3} protein concentration) were used as these showed a good fit to the kinetic model. All other temperature values showed a very poor fit to the model and so gave rate constants which had large errors and were not a true reflection of the actual experimentally obtained results.

The enthalpy of activation, ΔH_2, and the entropy of activation, ΔS_2, for the elongation phase were graphically derived in the same way using k_2. Thus, ΔH_2 was calculated to be + 145.64 (± 20.62) kJ mol^{-1} whilst the ΔS_2 was calculated as + 0.24 (± 0.04) kJ mol^{-1} K^{-1}. Furthermore, the Gibbs free energy of activation, ΔG can also be obtained from the following relationship:

$$\Delta G = \Delta H - T\Delta S \qquad (5.7)$$

At physiological temperature of 310 K, ΔG_1 was calculated as + 97.79 kJ mol^{-1} for the nucleation phase, and + 70.31 kJ mol^{-1} for the elongation phase. The experimentally obtained thermodynamic parameters of deoxyHbS polymerisation are summarised in table **5.9** along with the values for ß-amyloid fibrillation.

Thermodynamic Parameters	HbS Nucleation	HbS Elongation	ß-amyloid
E_1 /kJ mol^{-1}	81.59 (± 1.22)		311.20
E_2 /kJ mol^{-1}		148.22 (± 20.61)	95.30 (± 4.60)
ΔH /kJ mol^{-1}	- 84.18 (± 1.21)	+ 145.64 (± 20.62)	+ 308.60
ΔS /kJ mol^{-1} K^{-1}	- 0.59 (± 0.01)	+ 0.24 (± 0.04)	+ 0.641
ΔG /kJ mol^{-1}	+ 97.79 (± 1.21)	+ 70.31(± 20.62)	+ 109.8

Table 5.9: A comparison of the thermodynamic parameters for HbS polymerisation and ß-amyloid fibrillation. HbS polymerisation experimental condition: HbS concentration 30 mg cm^{-3}; temperatures 34 C, 38 C and 42 C; 1.5 M pH 7.0 phosphate buffer; 0.5 M NaCl; E = - 0.55 V *vs.* Ag/AgCl for 1000 s. ß-amyloid fibrillation data obtained from study performed by Sabate *et al.* [103], see table **5.8** for experimental conditions.

The summation of the thermodynamic parameters in table **5.9** shows that the enthalpy of activation (ΔH_1 and ΔH_2) is approximately equal to the activation energy (E_1 and E_2 respectively), the conversion of one to the other depends on the molecularity. ΔG represents the driving power for a reaction and the sign of ΔG determines if the reaction is spontaneous or not. The ΔG value was relatively constant for both processes. The positive sign for the ΔG values shows that the nucleation and elongation processes at the surface were not spontaneous, whilst the negative enthalpy value for nucleation indicated that the reactants, in this case, the formation of the nuclei was more stable than the reactants, the HbS monomers. The

opposite was seen for the enthalpy of elongation. In comparison, table **5.10** [60] gives a summary of the thermodynamic data obtained for deoxyHbS gelation from scanning calorimetric measurements in the temperature range 15 °C to 45 °C. It shows that the Gibbs free energy change is relatively constant as the temperature is increased from 15 °C to 45 °C, whilst in contrast there is a large decrease in enthalpy and entropy as a result of the large change in heat capacity accompanying polymerisation.

Temp (°C)	C_{sat} (mg cm^{-3})	K^b (M^{-1})	ΔG (kJ mol^{-1})	ΔH^a (kJ mol^{-1})	$T\Delta S$ (kJ mol^{-1})
15	2140	220	-13.0	31.0	43.9
25	1760	315	-14.2	16.7	30.9
35	1620	368	-14.7	2.5	17.2
45	1740	323	-15.5	-12.1	3.3

Table 5.10: Thermodynamic parameters for deoxy-HbS polymerisation obtained from scanning calorimetric measurements. Experimental conditions: 0.15 M potassium phosphate, 0.05 M sodium dithionite, pH 7.15. [a]from van't Hoff analysis of solubility data [60].

Positive enthalpy and entropy changes and the negative heat capacity for polymer formation are characteristic of protein aggregation driven by hydrophobic interactions. These results predict that the intermolecular contacts in the polymer are composed of van der Waals interactions rather than hydrogen bonds or ion-pair bonds. The difference in values between the calorimetric measurements and those obtained from electrochemical modulated growth can be assigned to the different techniques and conditions used [30, 60].

5.5.7 Effect of Changing pH

The effect of changing pH on turbidity was investigated by performing experiments in pH of 6.80, 7.00, 7.20, 7.40 and 7.62 at HbS protein concentrations of 30 mg cm^{-3} (Figure **5.10 (a)**) and 75 mg cm^{-3} (Figure **5.10 (b)**). 0.5 M NaCl was used as an additive and the experiments was performed at a temperature of 38 °C.

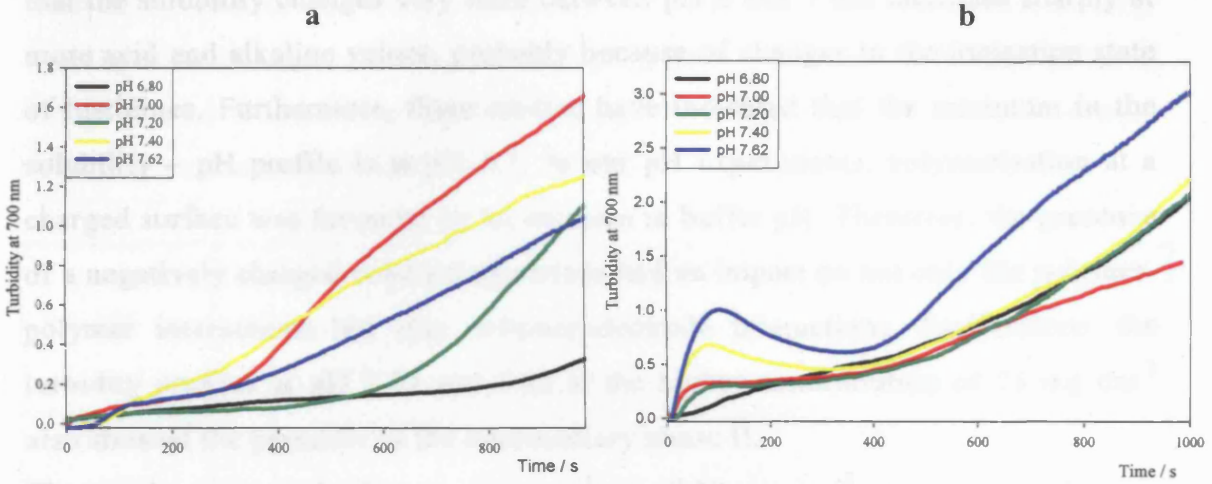

Figure 5.10: UV-visible spectroelectrochemistry time traces showing changes in turbidity at 700 nm at a Pt matrix electrode with increasing buffer pH at two HbS concentrations **(a)** 30 mg cm^{-3}; **(b):** 75 mg cm^{-3}; pH range 6.80 to 7.62; 1.5 M phosphate buffer; 0.5 M NaCl; 38.0 C; E = -0.55 V vs Ag/AgCl; run time 1000 s.

The aggregation of HbS was shown to be markedly dependent on the pH as the results obtained at the higher concentration of 75 mg cm^{-3} (figure **5.10 (b)**) showed protein aggregation was favoured by a slightly alkaline pH with the extent of polymer nucleation and growth being greatest at pH levels of 7.62 and 7.40. The results seen at both of these slightly basic pHs showed nucleation occurring immediately with no visible time delay. Furthermore, growth of HbS fibres at pH 7.62 reached a turbidity level of 3.00 at the end of the experiment, nearly a third more than that seen at pH 7.40. Acidic pH of 6.80 was the only data which showed a clear time delay for nucleation at 75 mg cm^{-3}. At a pH of 7.40 and 7.62 monomeric HbS carries approximately 1 negative charge as the isoelectric point of molecular HbA is 6.80 [109], however, the overall net charge of the polymeric protein is not known as the effect of a structural change into an ordered gel-like system of HbS polymers on the pI value has not been established. Therefore, the high level of turbidity seen at pH 7.62, as compared to other pHs, could possibly

have been due to the stabilisation of HbS aggregates through a decrease in the net electrostatic repulsion between the polymers. Alternatively, a more basic pH could have provided greater hydrophobic specific interactions between HbS monomers leading to enhanced polymerisation of HbS fibres.

Previous free solution studies [28, 29, 110, 111] have shown that aggregation of HbS is markedly dependent on the pH (chapter **1.2.2**). These studies have shown that the solubility changes very little between pH 6 and 7 but increases sharply at more acid and alkaline values, probably because of changes in the ionisation state of histidines. Furthermore, these studies have indicated that the minimum in the solubility – pH profile is at pH 6.5. In our pH experiments, polymerisation at a charged surface was favoured by an increase in buffer pH. Therefore, the presence of a negatively charged conducting surface had an impact on not only the polymer-polymer interactions but also polymer-electrode interactions. Furthermore, the turbidity profiles at pH 7.40 and 7.62 at the higher concentration of 75 mg cm^{-3} also showed the presence of the intermediary phase II.

The results seen at the lower concentration of 30 mg cm^{-3} were not as clear as those for 75 mg cm^{-3}. All data contained a time delay for nucleation before growth was seen whilst a neutral pH of 7.00, rather than 7.62, exhibited the largest increase in turbidity. Acidic pH of 6.80 once again showed no considerable change in turbidity levels compared to the other results.

5.5.8 pH Analysis

Kinetic Scheme Analysis:

The fit of equation **4.4** to the pH turbidity profiles obtained for 30 mg cm^{-3} was extremely good for all pH's (R^2 > 0.990) except for pH 6.80, table **5.11**. The results showed that alkaline pH of 7.40 and 7.62 exhibited the largest k_1 value whilst pH 7 and 7.2 had the largest k_2 value as shown by the turbidity time profiles seen in figure **5.10 (a)**. Furthermore, small changes in the pH gave rise to large variations in the rate constants, for example, a 0.2 unit increase in pH from 7.2 to 7.4 gave a 2.5 fold decrease in the k_1 value. The effective growth rate did not show significant correlation with pH.

pH	k_1 / s^{-1}	k_2 / M^{-1} s^{-1}	ak_2 / s^{-1}	R^2
6.80	0.16 (± 0.15) x 10^{-3}	0.31 (± 0.22)	0.14 (± 0.10) x 10^{-3}	0.906
7.00	0.17 (± 0.01) x 10^{-3}	13.32 (± 0.22)	6.19 (± 0.10) x 10^{-3}	0.995
7.20	0.02 (± 0.001) x 10^{-3}	14.51 (± 0.22)	6.75 (± 0.10) x 10^{-3}	0.991
7.40	0.48 (± 0.02) x 10^{-3}	5.80 (± 0.03)	2.70 (± 0.10) x 10^{-3}	0.997
7.62	0.25 (± 0.003) x 10^{-3}	6.27 (± 0.03)	2.92 (± 0.01) x 10^{-3}	0.998

Table 5.11: Nucleation rate constants k_1 and elongation rate constants k_2 to describe the HbS aggregation formation for pH in the range 6.8 to 7.62 at 30 mg cm^{-3} at the Pt matrix electrode. Experiment conditions: HbS 30 mg cm^{-3}; pH 6.8 to 7.62; 1.5 M pH 7 phosphate buffer; 0.5 M NaCl; 38 °C; E = - 0.55 V *vs.* Ag/AgCl for 1000 s.

The fit of equation **4.4** to the turbidity profiles obtained from experiments performed at 75 mg cm^{-3} was extremely poor for all pH values and so rate constants were not calculated. This was due to a rapid increase in turbidity seen at the start of the experiment coupled with the decrease in turbidity seen during phase II.

Linear Regression Analysis:

Table **5.12** shows the Phase I and Phase III linear regression data for pHs 6.8, 7, 7.2, 7.4 and 7.62 obtained for a protein concentration of 30 mg cm^{-3}. It was seen that pH 7.62 showed the fastest phase I rate with a value more than twice that seen for other pHs. The rate of phase I for pHs 7.00, 7.30 and 7.40 were similar whilst pH 6.80 exhibited the slowest rate. The rates of Phase III however did not follow this pattern; the rate values for pH 7 and 7.2 were seen to be far greater than pH 7.62 whilst acidic pH of 6.8 once again exhibited the slowest rate. No general trend was seen for either Phase I or Phase III with 30 mg cm^{-3} protein.

Solution pH	Rate of Phase I / s^{-1}	Rate of Phase II / s^{-1}	Rate of Phase III / s^{-1}
6.8	0.30 (± 0.008) x 10^{-3}		0.77 (± 0.007) x 10^{-3}
7.0	0.73 (± 0.04) x 10^{-3}		2.90 (± 0.03) x 10^{-3}
7.2	0.61 (± 0.02) x 10^{-3}		2.85 (± 0.005) x 10^{-3}
7.4	0.49 (± 0.03) x 10^{-3}		1.70 (± 0.009) x 10^{-3}
7.62	1.75 (± 0.02) x 10^{-3}		1.29 (± 0.002) x 10^{-3}

Table 5.12: Rate values for Phase I and Phase III, calculated using linear regression analysis, for pH in the range 6.8 to 7.62 for 30 mg cm^{-3} HbS concentration at a Pt matrix electrode. Experiment conditions: HbS concentration 30 mg cm^{-3}; pH range 6.8 to 7.62; 1.5 M pH 7.0 phosphate buffer; 0.5 M NaCl; temperature 38 °C; E = - 0.55 V *vs.* Ag/AgCl for 1000 s.

The pH linear regression data for 75 mg cm^{-3} is listed in table **5.13**. Both Phase I and Phase III rate values were seen to increase with an increase in pH. The fastest Phase I rates were seen with the slightly alkaline pH of 7.4 (22.4 (± 0.25) x 10^{-3} s^{-1}) and 7.62 (22.2 (± 0.02) x 10^{-3} s^{-1}) whilst the slowest was pH 6.8 (1.18 (± 0.01) x 10^{-3} s^{-1}); Phase I rate for pH 6.8 was shown to be ten times smaller than the rate

value for pH 7 whilst eighteen times smaller than the rate value for pH 7.62. However, although a general trend of an increase in rate was seen with increasing pH for Phase III, only a small difference was seen as the rate of pH 7.62 was only two and a half fold greater than the rate of pH 6.8. The rates of Phase II, only calculated for pH 7.4 and 7.62, showed a 0.6 (± 0.01) ms^{-1} decrease with a 0.22 increase in pH unit.

Solution pH	Rate of Phase I / s^{-1}	Rate of Phase II / s^{-1}	Rate of Phase III / s^{-1}
6.8	1.18 (± 0.01) x 10^{-3}		1.90 (± 0.01) x 10^{-3}
7.0	12.00 (± 0.01) x 10^{-3}		1.92 (± 0.01) x 10^{-3}
7.2	8.01 (± 0.14) x 10^{-3}		2.69 (± 0.02) x 10^{-3}
7.4	22.4 (± 0.25) x 10^{-3}	-1.84 (± 0.04) x 10^{-3}	2.00 (± 0.01) x 10^{-3}
7.62	22.20 (± 0.02) x 10^{-3}	-2.43 (± 0.13) x 10^{-3}	4.59 (± 0.01) x 10^{-3}

Table 5.13: Rate values for Phase I, Phase II and Phase III, calculated using linear regression analysis, for pH in the range 6.8 to 7.62 for 75 mg cm^{-3} HbS concentration at a Pt matrix electrode surface. Experiment conditions: HbS concentration 75 mg cm^{-3}; pH range 6.8 to 7.62; 1.5 M pH 7.0 phosphate buffer; 0.5 M NaCl; temperature 38 C; E = - 0.55 V *vs.* Ag/AgCl for 1000 s.

5.5.9 Effect of Changing Salt Concentration

The effect of changing salt concentration or ionic strength on HbS gelation was investigated by performing experiments at varying NaCl concentrations (0.10 M, 0.25 M, 0.50 M, 0.75 M and 1.0 M) at HbS concentrations of 30 mg cm^{-3} (figure **5.11 (a)**) and 75 mg cm^{-3} (figure **5.11 (b)**). Turbidity changes at the Pt matrix were monitored at a temperature of 38 °C.

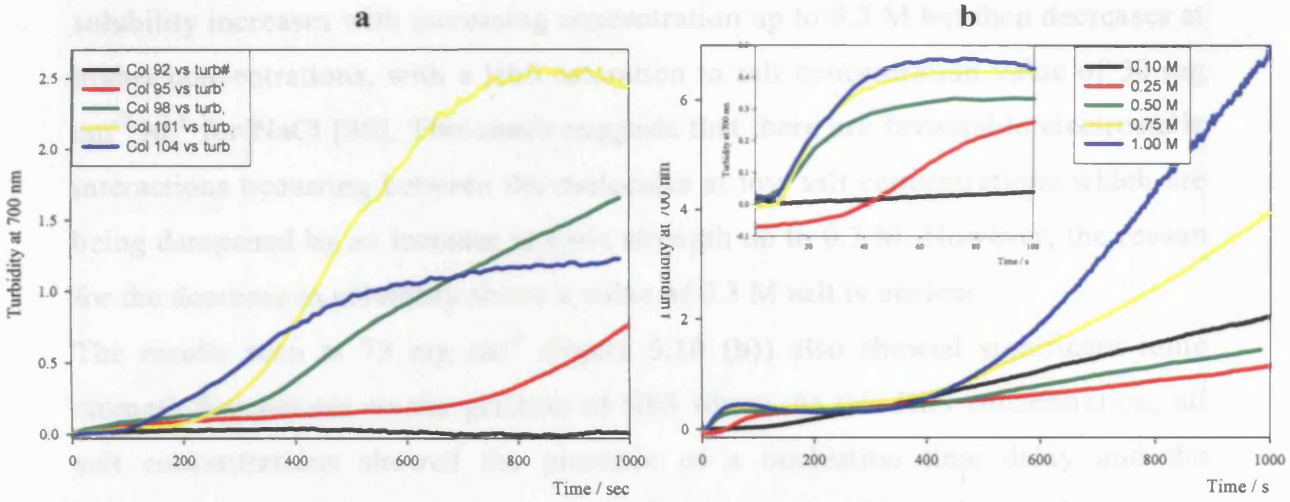

Figure 5.11: UV-visible spectroelectrochemistry time traces showing changes in turbidity at 700 nm in a Pt matrix cell with increasing NaCl concentration at two HbS concentrations **(a)** 30 mg cm^{-3}; **(b)** 75 mg cm^{-3}; NaCl range 0.10 M to 1.00 M; 1.5 M (pH 7.0) phosphate buffer; 38.0 C; E = -0.55 V vs. Ag/AgCl; run time 1000 s.

The results seen at 30 mg cm^{-3} showed that NaCl salt concentration had a marked effect on HbS fibre formation. Increasing salt concentration in the range 0.25 M to 1.00 M decreased the time delay from nearly 620 s at 0.25 M to 90 s at 1.00 M. Furthermore, the turbidity amplitude also increased as the salt concentration was increased up to 0.75 M. A further increment to 1.00 M, however, slightly inhibited gelation. Although the shortest time delay was apparent with 1.00 M NaCl, the largest turbidity at the end of the experiment was seen with a concentration of 0.75 M, meaning that different factors were influencing the two distinct nucleation and growth pathways. A salting-in effect occurs at low salt concentrations where the solubility of protein is increased slightly due to the Hb protein being screened by the salt counter ions (ions of opposite net charge). This results in decreased electrostatic free energy of the protein and increased activity of the solvent, thus leading to increased solubility. At higher salt concentrations, a salting-out effect,

where the solvating power of the salt ions is decreased due to the abundance of the salt ions, leads to the solubility of the proteins being decreased also. Consequently, a significant increase in polymer growth was seen at the higher salt concentrations as compared to the lower concentrations.

Literature studies of salt effects have shown that the effect of ionic strength on the aggregation and growth of HbS depends on the particular salt and concentration of salt used [85, 111]. For the sodium and potassium salts of monovalent anions, the solubility increases with increasing concentration up to 0.3 M but then decreases at higher concentrations, with a HbS saturation to salt concentration value of 50 mg cm^{-3} M^{-1} for NaCl [30]. This result suggests that there are favourable electrostatic interactions occurring between the molecules at low salt concentrations which are being dampened by an increase in ionic strength up to 0.3 M. However, the reason for the decrease in solubility above a value of 0.3 M salt is unclear.

The results seen at 75 mg cm^{-3} (figure **5.10 (b)**) also showed significant ionic strength dependence on the gelation of HbS fibres. At this HbS concentration, all salt concentrations showed the presence of a nucleation time delay and the turbidity amplitude at 1.0 M was significantly larger than other molarities, in contrast to the results seen at 30 mg cm^{-3}. Moreover, the presence of the intermediary phase was also observed with 1.0 M salt concentration. This phenomenon, seen previously with other parameters at conditions conducive to fast polymerisation kinetics such as at high HbS concentrations (figure 5.**6**) and temperatures (figure 5.7), only occurred when the combined salt and buffer ionic strength was maximal, i.e. at a salt concentration of 1.00 M in 1.50 M phosphate buffer.

5.5.10 Salt Concentration Analysis

Kinetic Scheme Analysis:

Table **5.14** shows the rate constants derived from NaCl salt concentration experiments performed at 30 mg cm^{-3}. In this data set only salt concentrations of 0.50 M and 0.75 M showed a good fit. k_1 was seen to decrease by increasing the salt molarity from 0.50 M to 0.75 M whilst k_2 increased three fold at the same salt range. Consequently, it was seen that the effective growth rate was dependent on salt molarity.

Salt conc.	k_1 / s^{-1}	k_2 / M^{-1} s^{-1}	ak_2 / s^{-1}	R^2
0.25	0.04 (± 0.003) x 10^{-3}	7.50 (± 0.22)	3.49 (± 0.1) x 10^{-3}	0.935
0.50	0.24 (± 0.02) x 10^{-3}	6.90 (± 0.22)	3.21 (± 0.1) x 10^{-3}	0.989
0.75	0.007 (± 0.002) x 10^{-3}	22.30 (± 0.23)	10.4 (± 0.1) x 10^{-3}	0.999
1.00	0.74 (± 1.85) x 10^{-3}	0.25 (± 0.50)	0.01 (± 0.2) x 10^{-3}	0.947

Table 5.14: Nucleation rate constants k_1 and growth rate constants k_2 to describe the HbS aggregation formation for NaCl salt concentration in the range 0.25 M to 1.00 M at HbS concentration of 30 mg cm^{-3}at a Pt matrix electrode. Experiment conditions: HbS concentration 30 mg cm^{-3}; NaCl salt concentration range 0.25 M to 1.00 M; 1.5 M pH 7.0 phosphate buffer; temperature 38 °C; E = - 0.55 V *vs.* Ag/AgCl for 1000 s.

On the other hand, all turbidity profiles at 75 mg cm^{-3} showed a good fit with the predicted values obtained from the kinetic model. The rate constants and R^2 values for 75 mg cm^{-3} are tabulated in table **5.15**. The k_1 values were generally seen to decrease with increasing salt concentrations. A ten fold increase in NaCl molarity from 0.1 M to 1.0 M saw a six fold decrease in the polymerisation k_1 value, whilst, k_2 values were generally seen to be linearly dependent on the salt concentration.

The effective growth rate was shown to have significant correlation with salt concentration.

Salt conc. / M	k_1 / s^{-1}	k_2 / M^{-1} s^{-1}	ak_2 / s^{-1}	R^2
0.1	0.16 (± 0.004) x 10^{-3}	1.39 (± 0.009)	1.61 (± 0.01) x 10^{-3}	0.994
0.25	0.17 (± 0.09) x 10^{-3}	0.07 (± 0.007)	0.08 (± 0.01) x 10^{-3}	0.955
0.50	0.17 (± 0.05) x 10^{-3}	0.56 (± 0.09)	0.65 (± 0.10) x 10^{-3}	0.945
0.75	0.013 (± 0.001) x 10^{-3}	2.94 (± 0.01)	3.41 (± 0.01) x 10^{-3}	0.986
1.0	0.028 (± 0.002) x 10^{-3}	6.69 (± 0.09)	7.76 (± 0.10) x 10^{-3}	0.991

Table 5.15: Nucleation rate constants k_1 and growth rate constants k_2 to describe the HbS aggregation formation for NaCl salt concentration in the range 0.25 M to 1.00 M at HbS concentration of 75 mg cm^{-3}at a Pt matrix electrode surface. Experiment conditions: HbS concentration 75 mg cm^{-3}; NaCl salt concentration range 0.25 M to 1.00 M; 1.5 M pH 7.0 phosphate buffer; temperature 38 °C; E = - 0.55 V *vs.* Ag/AgCl for 1000 s.

Linear Regression Analysis:

Table **5.16** lists the linear regression gradient data of Phase I and Phase III for 30 mg cm^{-3} HbS. 0.1 M data is not shown due to very little growth being seen. No correlation was seen for either Phase I or Phase II with salt concentration. On the other hand Table **5.17** which lists the Phase I, Phase II and Phase III data for 75 mg cm^{-3} shows a significant correlation with salt concentration. The rates of Phase I and Phase III were both seen to increase significantly with increasing salt concentration. Furthermore, it can also be noticed that the rate of nucleation Phase I tended to be greater than the respective rate of growth Phase III. The initial nucleation step is usually the rate limiting step and is slower than the growth step of polymerisation but this was not seen in table **5.17**.

Salt Concentration / M	Rate of Phase I / s^{-1}	Rate of Phase II / s^{-1}	Rate of Phase III / s^{-1}
0.25	0.37 (± 0.01) x 10^{-3}		1.85 (± 0.01) x 10^{-3}
0.50	0.49 (± 0.02) x 10^{-3}		3.01 (± 0.02) x 10^{-3}
0.75	0.43 (± 0.01) x 10^{-3}		6.87 (± 0.02) x 10^{-3}
1.00	0.33 (± 0.02) x 10^{-3}		3.20 (± 0.02) x 10^{-3}

Table 5.16: Rate values for Phase I and Phase III, calculated using linear regression analysis, for NaCl salt in the range 0.1 M to 1.0 M for 30 mg cm^{-3} HbS concentration at a Pt matrix electrode. Experiment conditions: HbS concentration 30 mg cm^{-3}; NaCl salt range 0.1 M to 1.0 M; 1.5 M pH 7.0 phosphate buffer; 0.5 M NaCl; temperature 38 C; E = - 0.55 V *vs.* Ag/AgCl for 1000 s. Salt concentration of 0.1 M showed minimal growth and so was not analysed. Turbidity profiles showed no Phase II for these results.

Salt Concentration / M	Rate of Phase I / s^{-1}	Rate of Phase II / s^{-1}	Rate of Phase III / s^{-1}
0.10	0.40 (± 0.01) x 10^{-3}		2.50 (± 0.01) x 10^{-3}
0.25	5.94 (± 0.08) x 10^{-3}		0.97 (± 0.01) x 10^{-3}
0.50	8.18 (± 2.00) x 10^{-3}		1.76 (± 0.01) x 10^{-3}
0.75	17.6 (± 0.34) x 10^{-3}		4.78 (± 0.01) x 10^{-3}
1.00	15.4 (± 0.32) x 10^{-3}	-1.80 (± 0.04) x 10^{-3}	12.0 (± 0.09) x 10^{-3}

Table 5.17: Rate values for Phase I, Phase II and Phase III, calculated using linear regression analysis, for NaCl salt in the range 0.1 M to 1.0 M for 75 mg cm^{-3} HbS concentration at a Pt matrix electrode surface. Experiment conditions: HbS concentration 75 mg cm^{-3}; NaCl salt range 0.1 M to 1.0 M; 1.5 M pH 7.0 phosphate buffer; 0.5 M NaCl; temperature 38 C; E = - 0.55 V *vs.* Ag/AgCl for 1000 s.

5.6 The Double Nucleation Mechanism at Surfaces

Traditionally, the nucleation controlled polymerisation mechanism of HbS, generally referred to as the double nucleation mechanism, has been shown to consist of two types of kinetic processes in equilibrium; the rate limiting critical nuclei formation or homogeneous nucleation and autocatalytic explosive growth termed as heterogeneous nucleation. However, the absorption spectra of certain light scattering experiments conducted in this chapter showed the presence of an intermediary process (Phase II, figure **5.5**), consisting of a large decrease in turbidity, after the initial nucleation step.

Figure **5.12** shows a schematic representation of the shift in turbidity profiles from low to high concentrations whilst figure **5.12 (c)** specifically shows a representation of this unknown intermediary Phase II seen at a protein concentration of 100 mg cm^{-3}. This phenomenon was also seen at experiments performed at high temperatures, such as 42 °C, as well as at high pH levels and salt concentrations. To the best of our knowledge, this was the first time such a process had been seen with regards to the polymerisation of HbS at a conducting surface.

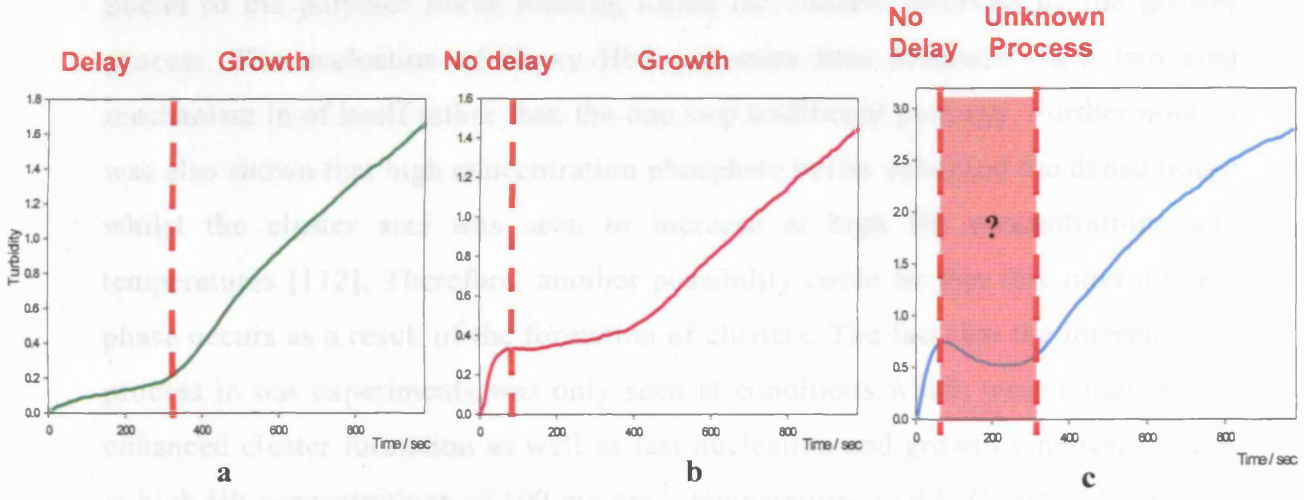

Figure 5.12: A schematic representation of the shift in turbidity profiles from low to high protein concentrations. **(a)** turbidity profile of HbS concentration of 30 mg cm^{-3} showing the classical two phase polymerisation process consisting of a nucleation time delay followed by growth. **(b)** turbidity profile of 75 mg cm^{-3} HbS showing an unorthodox two phase polymerisation process with no time delay followed by steady protein growth. **(c)** turbidity profile of 100 mg cm^{-3} HbS showing deviation from the two step mechanism, instead a three step mechanism was seen with no initial time delay followed by an unknown process, characterised by a decrease in turbidity (highlighted in red), and completed by protein growth. Not to scale.

The large decrease in turbidity, seen in the red shaded section in figure **5.12 (c)**, occurred as a result of changes to the structure of the aggregates at the electrode leading to changes in their absorbance properties. This subsequently caused light to be scattered in a different way to before. Changes in polymer structure which might have caused this decrease in turbidity could have been due to the depletion of the polymer structure from the light path, such as the hair like polymer structures seen in figure **3.3 (b)** dissolving in the solution or breaking away from within the holes, or, due to some sort of reorganisation or realignment of the fibres during the transition between the hair-like hair strands (seen in figure **3.3 (b)**) and the globular phase (seen in figure **3.5 (b)**). Furthermore, this phenomenon was cell-specific as this phase was only seen with experiments conducted with the Pt matrix cell. No such results were seen with the Au micro-mesh cell. Consequently, the multiple hole geometry of the Pt matrix WE aided the observation of this process.

Recent studies by Pan *et al.* [112, 113] have shown that metastable clusters of dense liquid, several hundred nanometres in size, can form in solutions of HbS within a few seconds and participate in the nucleation mechanism. The polymerisation process in this case proceeds via a three step mechanism with the nuclei of the polymer fibres forming inside the clusters followed by the growth process. The nucleation of deoxy HbS polymers thus proceeds via a two step mechanism in of itself rather than the one step traditional pathway. Furthermore, it was also shown that high concentration phosphate buffer enhanced the dense liquid whilst the cluster size was seen to increase at high Hb concentrations and temperatures [112]. Therefore, another possibility could be that this intermediary phase occurs as a result of the formation of clusters. The fact that the intermediary process in our experiments was only seen at conditions which were conducive to enhanced cluster formation as well as fast nucleation and growth kinetics, such as at high Hb concentrations of 100 mg cm^{-3}, temperatures of 42 °C, pHs 7.62 of 7.40 and salt concentrations of 1.0 M, suggested that at these conditions a stronger driving force for cluster formation was provided within which nucleation of the polymer fibres could occur. Other nucleation dependent polymerisation mechanisms, such as ß-amyloid fibrillogenesis are also seen to occur with the presence of intermediate peptides termed protofibrils. These form after the nucleation stage and associate end to end and laterally to form amyloid fibrils. Amyloid monomers also form micelles, once the concentration exceeds a certain

level called the critical micellar concentration, which act as a reservoir of monomers and form nuclei through the monomers [93].

Although it has been established that the aggregation of HbS free in solution consists of two phases, no study thus far has focussed on the polymerisation of HbS at a conducting surface. Consequently, it is believed that this phenomenon was 'surface facilitated' and only detected by the light scattering experiments at conditions where kinetics tended to be fast. The presence of a surface could have acted as an anchor for the formation of intermediate structures allowing three phases to be present at any one time in equilibrium, a monomer-containing solution phase, a polymer phase and the intermediate phase. However, further work is required to ascertain the exact nature of the structures involved in our study and whether this process was an intermediary phase due to the presence of intermediate hair-like aggregate structures or the formation of intermediate dense protein clusters. The lack of studies performed in the presence of a surface, which possibly facilitates this intermediary phase II, explains why this has not been reported by other investigators previously. This finding could have a significant impact on the understanding of the fundamental mechanism of HbS polymerisation and thus not only the pathophysiology of the disease but also strategies to combat this condition. Although not concrete, there is information which suggests that variations to the double nucleation mechanism could exist.

5.7 Conclusions

In this chapter, a Pt matrix thin layer electrochemical cell was fabricated to investigate the effect of four parameters on the gelation of HbS at a conducting surface. It was shown that the design of this particular cell was better than those used previously as this arrangement effectively allowed HbS nucleation and aggregation to be monitored in the vicinity of individual holes. Theoretical modeling of O_2 depletion in the Pt matrix cell was performed with Comsol® and showed that O_2 was reduced within 20 s of the start of the experiment, compared to the spectroscopy obtained 200 s seen with the Pt micromesh cell. Experiments performed with varying protein concentration showed a large concentration dependence on the kinetics of HbS fibre aggregation. A clear exhibition of a delay period was seen which was prolonged with dilution of HbS solutions, whilst protein elongation was also directly related to HbS concentration. This was because as solutions became more concentrated, HbS molecular collisions increased and thus there was more chance of a hydrophobic interaction occurring between the mutated valine residue of one HbS and the ß subunit of another, leading to a decrease in nucleation time and an increase in polymer growth. It was also shown that aggregation of HbS at a conducting Pt matrix surface was linearly dependent on the temperature in the range 25 °C to 42 °C and that polymer growth at a conducting surface was favoured by elevated temperatures with the largest increase in fibre growth being seen at 42 °C. This value was in contrast to the reported data of 35 °C at which temperature the solubility-minimum of HbS was seen, possibly due to differences in the mechanism of protein aggregation at a liquid-liquid interface as opposed to liquid-solid interfaces. Moreover, the investigations revealed that protein aggregation was favoured by a slightly alkaline pH with the extent of polymer nucleation and elongation being greatest at pH levels of 7.62 and 7.40 whilst significant ionic strength dependence on the gelation of HbS fibres was also shown.

Experiments performed at protein concentrations of 100 mg cm^{-3}, temperatures of 42 °C, as well as alkaline pH levels and high salt concentrations showed the presence of an intermediary Phase II process in the turbidity profile, consisting of a large decrease in turbidity after the initial nucleation step. Comparisons with control proteins showed that this was a real process and it was postulated that this

process could have been as a result of intermediary aggregates causing a decrease in the extent of light scattering.

Kinetic parameters were calculated using two methods of analysis. It was shown that the highest effective growth rate, calculated using the kinetic scheme model, was obtained for a temperature of 42 °C at a HbS concentration of 30 mg cm^{-3} (9.93 (± 0.2) x 10^{-3} s^{-1}) whilst the lowest value was obtained for a salt concentration of 0.1 M at 75 mg cm^{-3} HbS (1.61 (± 0.01) x 10^{-3} s^{-1}). k_1 was seen to be several orders of magnitude smaller than k_2 showing that the nucleation process was slower than the growth process and thus the rate limiting step. Comparison of the linear regression rate values showed that the highest nucleation Phase I value was obtained for a pH of 7.62 at 75 mg cm^{-3} HbS (22.20 (± 0.02) x 10^{-3} s^{-1}) whilst the highest Phase III value was for 1.0 M salt concentration at 75 mg cm^{-3} (12.0 (± 0.09) x 10^{-3} s^{-1}) HbS. The linear regression analysis provided a closer reflection of the experimental data than the kinetic scheme as a number of conditions showed a poor fitting to the model. Thermodynamic parameters were also derived from the temperature rate constants. Activation energies for the nucleation and elongation stages of HbS polymerisation were calculated to be 81.59 (± 1.22) kJ mol^{-1} and 148.22 (± 20.61) kJ mol^{-1} respectively whilst the Gibbs free energy was calculated to be 97.79 (± 20.62) kJ mol^{-1} and 70.31 (± 1.21) kJ mol^{-1} respectively. A larger elongation activation energy value indicated that nucleation at the surface was more favourable than elongation.

This is the first known study which has been performed at a solid conducting metal surface, combining electrochemical deoxygenation and HbS, to investigate the effect of different variables on the kinetics of HbS polymerisation. This study has shown the possibility of using this advanced electrochemical matrix cell as a screening device even when there is limited availability of protein, whilst also showing the great importance of coupling concentration with temperature to achieve an accelerated fibre growth rate for future use as a screening device. A screening device could be used to test a variety of compounds which disrupt the polymer formation as a route to a therapeutic strategy for this disease. Knowledge of how these parameters affect the kinetics and dynamics of nucleation and growth of HbS polymerisation at a surface will provide a better understanding of the pathophysiology of sickle cell disease *in vivo* in order to improve therapeutic strategies for this common, and frequently disabling, genetic disorder.

Chapter 6: Anti-Sickling Strategies

6.1 Introduction

In this chapter, therapeutic strategies which affect the anti-sickling properties of HbS polymers were investigated. Two strategies which could be investigated easily using our electrochemical system were firstly testing compounds whose mechanism of action was specific to disrupting fibre formation of HbS polymers. As such, the effect of two anti-sickling biological agents, vanillin and 5-HMF, on the extent of polymerisation and kinetics of growth was investigated at the Pt matrix WE. Secondly, the effect of changing electrode surface properties was investigated by thiolation of the conducting surface. This was performed to define properties which minimise protein growth and therefore reduce the damage which occurs to the plasma membrane *in vivo* during the polymerisation process. The damage encountered by the membrane during the polymerisation process forms an integral part of the pathophysiology of SCD and thus can be a targeted as a therapeutic strategy.

6.2 Experimental

6.2.1 Materials and Procedures

The experiments were performed according to experimental procedure **6**. HbS protein was dissolved in air-saturated 1.5 M (pH 7) phosphate buffer solution and 0.5 M NaCl and UV-visible spectroelectrochemistry was employed. The Pt matrix and Au micromesh thin layer electrochemical cells were used. Vanillin and 5HMF were used as supplied and added to the protein solution in concentrations ranging from 0.29 mM to 11.6 mM. The thiol compounds used were 3-mercapto-1-propenesulfonic acid, 2-mercaptoethanol, 1-butanethiol and cystamine dihydrochloride in concentrations of 2 mM. HbA protein was used for the control experiments and the mixtures were prepared in the same way. All experiments were performed at room temperature unless otherwise stated. The general experimental and all apparatus for the above techniques are described in chapter **2**.

6.2.2 Forming a Thiol Monolayer on Au

Forming a thiol self assembled monolayer on the Au surface, be it the Au micromesh or the Au matrix cell, was performed in the same manner. A 1.6 mM solution of dilute H_2SO_4 was placed in a beaker and 2 mM of the thiol compound was added. The electrode surface was thoroughly cleaned electrochemically and the thiol solution was pippetted inside the coverslip and left to incubate for 2 hrs. After 2 hrs the cell was rinsed with copious amounts of water and stored in water to prevent any oxidation of the thiols occurring until used. HbS solution was placed inside the cell and CVs were performed on the thiolated Au surface to ascertain the potential window for the adsorption and desorption of thiols so that the O_2 reduction process did not cause reduction of thiols. This set of experiments was performed for each thiol separately. Figure **6.1** shows a CV performed at a 3-mercapto-1-propenesulfonic acid thiolated surface and the presence of two shoulders can be seen. The first shoulder was due to the presence of O_2 (-0.4 V to -0.8 V) and the second, in the range -0.8 V to – 1.0 V was attributable to the reduction of the thiol.

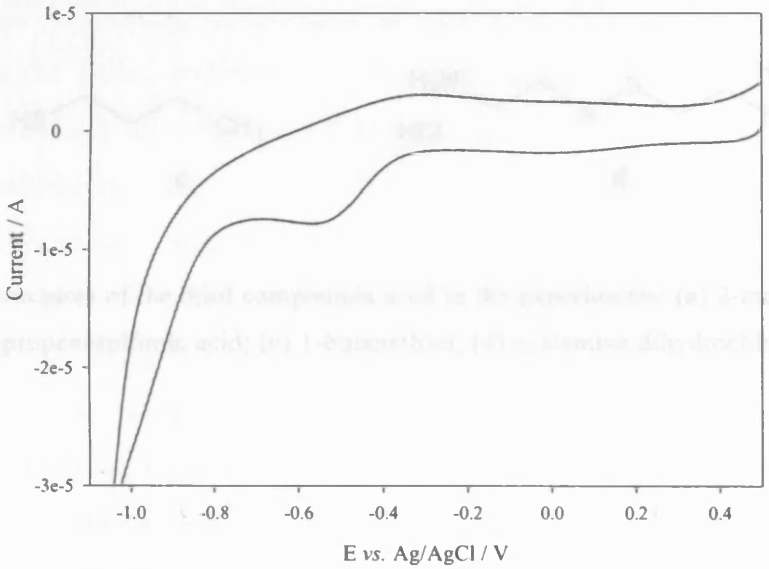

Figure 6.1: CV of 3-mercapto-1-propenesulfonic acid thiolated Au surface performed at a scan rate of 100 mV s^{-1} to ascertain the potential window for the reduction of the thiol. The first shoulder between -0.4 V to -0.8 V was attributable to O_2 reduction whilst the thiol reduction shoulder was seen from -0.8 V to around -1.0 V.

Once the HbS experiment had finished, the removal of thiols was achieved by rinsing the cell with copious amounts of water to remove the excess protein underneath the coverslip (i.e. protein which might be stuck to the electrodes or the glass surface) and placing it in an equimolar mixture of ethanol/H_2O for 5 mins. Subsequently, the thiols were stripped by electrochemical cycling of dilute H_2SO_4 (two sets of 30 cycles were performed), a larger potential window than normal (+ 1.35 V to – 0.90 V) was used as the reduction of thiols occurs at more negative potentials. The cell was again rinsed thoroughly to remove recycled acid along with any stripped thiols and a new solution of H_2SO_4 was used to electrochemically clean the electrodes, but this time at the normal potential window used earlier to clean the bare Au electrode (+ 1.35 V to – 0.50 V). A final rinse was performed to remove traces of any contaminations. Figure **6.2** shows the structures of the thiol compounds used in the thiol experiments

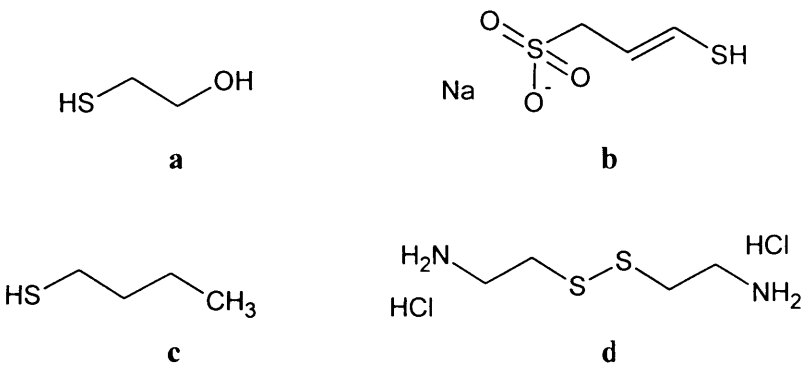

Figure 6.2: Structures of the thiol compounds used in the experiments: **(a)** 2-mercaptoethanol; **(b)** 3-mercapto-1-propenesulfonic acid; **(c)** 1-butanethiol; **(d)** cystamine dihydrochloride

6.3 Pathophysiology of SCD

The polymerisation of HbS is the primary process in the pathophysiology of the disease. Normal bi-concave shaped RBCs, approximately 8 μm in diameter, are elastic and therefore easily pass through smaller blood vessels of 3 μm diameter [114]. However, repeated episodes of sickling cause a permanent change in the shape of the cell and loss of cell elasticity even when O_2 concentration increases. Consequently, rigidified sickled cells lead to occlusion of capillaries and small vessels, triggering an avalanche of haemolysis and vaso-occlusive events including local inflammation, oxidant damage, deregulated homeostasis of nitric oxide (NO) and endothelial-cell injury. This subsequently leads to a number of complications including painful episodes, chronic haemolytic anaemia and possible end organ damage and premature mortality [114, 115].

HbS polymerisation, in addition to deforming the cell into a sickle shape, also causes injury to the erythrocyte by damaging the plasma membrane cytoskeleton, thus reducing cation and water content and altering the distribution of membrane proteins and lipids, such as the extracellular exposure of protein epitopes and glycolipids that are normally found inside the cell [116]. Cellular damage and the disruption of the plasma membranes in particular, increase adhesive interactions between sickle cells, endothelial cells and leukocytes; multiple studies have implicated virtually all major adhesion pathways in the interactions between sickle cells and endothelial cells [116 - 118]. Thus, sickle adhesion to the endothelium plays a significant role in sickle cell vaso-occlusion, figure **6.3**.

Furthermore, plasma membrane injury and chronic haemolysis impairs cation homeostasis and triggers local inflammation [115]. Sickle cells have a reduced Mg^{2+} content due to the net loss of Mg^{2+} during sickling, possibly due to an increased activity of the Na^+ - Mg^{2+} exchanger, whilst the K^+ - Cl^- co-transport, which mediates sickle cell dehydration, is significantly higher in patients with SCD [119]. On the other hand, dehydrated dense sickle cells expose negatively charged glycolipids on the outer layer of the plasma membrane, which subsequently activate the coagulation cascade, leading to the generation of tissue factor and thrombin, and thus promoting an inflammatory response [116, 120].

Figure 6.3: Sickle cell vasoocclusion. Adhesion of sickle RBC to endothelial cells induces the expression of inflammatory and coagulation mediators leading to the activation of the vascular endothelium. Stimulated endothelial cells recruit rolling leukocytes which capture sickle RBC leading to transient episodes of vascular occlusions that are initiated in the venules [116].

Moreover, haemolytic anaemia or the premature destruction of RBCs causes Hb to be liberated into the plasma. This plasma Hb converts NO to bio-inactive nitrate whilst the substrate for the production of NO, *L*-arginine, is also destroyed. Reduced endothelial bioavailablity of NO impairs important functions such as inhibition of platelet activation and repression of cell-adhesion molecule and also enhances vasoconstriction, which again increases the likelihood of sickle cell vaso-occlusion and induces endothelial damage [115, 121]. Consequently, HbS polymerisation not only causes rigid and sharp sickled cells leading to occlusion of capillaries and small vessels, but also leads to a heterogeneous population of sickle cells with damaged membrane cytoskeletons (figure **6.4**), triggering a cascade of events resulting in ischaemia amd tissue and organ damage.

Figure 6.4: Membrane cytoskeleton and plasma membrane damage due to HbS polymerisation. HbS polymers disrupt the RBC cytoskeletion and form protusions which results in exposure of the transmembrane protein epitopes and lipid exchanges, notably of phosphatidylserine (PS) between the inside and outside of the cell [116]

Although the pathophysiology of the disease is manifested and modulated through various types of factors, including genetic, cellular and environmental, two interrelated events, vaso-occlusion and haemolytic anaemia, essentially cause clinical disease. These events are driven by the degree of sickle erythrocyte adhesion to the vascular endothelium and the extent of plasma membrane damage. The presence of such diverse mechanisms and factors driving these processes need to be carefully considered before physiologically relevant therapeutic agents can be delineated.

6.4 Current Therapies for SCA

Even though major strides are being made in developing pharmacologically efficacious agents, currently, no clinically useful anti-sickling agents exist even though numerous have been studied and reported. At the moment, there are four potential pathophysiological based therapeutic approaches to SCD and these mechanisms can be listed as follows:

1. inhibition of HbS polymerisation
2. prevention of RBC dehydration
3. prevention of RBC adhesion to vascular endothelium
4. gene therapy

Inhibition of HbS Polymerisation

The therapeutic strategy of specifically inhibiting the polymerisation of deoxygenated HbS to combat SCD can be broken down into two further approaches: pharmacological induction of HbF and chemical modification of HbS polymerisation.

HbF induction:

Pharmacological induction of HbF can be considered as the most successful approach to date. An increase in HbF levels causes hybrid Hb tetramers to form which are not incorporated into the polymer phase, thus causing the solubility of HbS to be increased as a result of a variable intracellular Hb composition. The mechanism of HbF induction is thought to occur either through gene hypomethylation or by cytotoxicity which offers a selective advantage for HbF-producing erythroid progenitors [114, 122, 123].

Hydroxyurea, a potent inducer of HbF, was first demonstrated to be biologically active in 1928 [124] and a clinical study conducted in 1995 showed that hydroxyurea reduced the frequency of episodes of pain, acute chest syndrome, hospitalisation and the need for blood transfusion [125]. Hydroxyurea prevents RBC sickling by increasing the synthesis of HbF. Recent studies have indicated that the effects of hydroxyurea are not only caused by an increase in HbF concentration but may also be dependent on a number of additional mechanisms,

including an increase in soluble guanylyl cyclase, which in turn, leads to increased cyclic guanosine monophosphate, a facilitator of γ-globin gene induction [126]. It has also been implicated in the stimulation of a potent vasodilator NO [127] and been shown to decrease the adhesion of sickle cells to endothelium [115]. However, even though currently hydroxyurea remains the only approved therapeutic agent for SCD therapy, a lack of efficacy and numerous adverse effects ensure that the long term benefits and toxicities of hydroxyurea are controversial [114] and are still being investigated.

Chemical Modification of HbS Polymerisation:

Chemical modification of HbS by an agent, which interacts directly with HbS causing an inhibition of the polymerisation process, is an attractive therapeutic approach to combat this disease. Disruption at this stage of the disease life cycle would mean the cascade of adverse events associated with the secondary processes in the pathophysiology of SCD would not be manifested. Consequently, investigations in this chapter focussed on using the thin layer electrochemical cell as a novel assay system to investigate the efficacy of potential anti-sickling agents which may disrupt the polymerisation of HbS.

Although many compounds have been tested, the lack of success in developing a clinically useful anti-sickling agent to date has been due to the excessive amount of drug required to interact stereospecifically with the large quantity of Hb present in humans. Covalent modification of the HbS protein would require at least an equimolar concentration of the drug to increase anti-gelling activity and therefore a substance with little or no toxicity would be needed.

A number of naturally occurring and synthetic aldehydes were investigated by Zaugg *et al.* [128] and found that aromatic aldehydes, particularly vanillin (2,4-dihydroxybenzaldehyde) and 5-hydroxymethyl-2-furfural (5HMF) markedly increased the O_2 affinity of HbA and HbS under hypoxic conditions by forming Schiff base (imine) linkages with the N-terminal αVal1 nitrogens of Hb [129]. In Schiff-base formation, equilibrium of the following type is established:

$$Hb - NH_2 + R - CHO \leftrightarrow Hb - N = CH - R + H_2O$$

Vanillin (figure **6.5 (a)**) decreases HbS polymerisation by allosterically modulating the HbS molecule to the high affinity state, and concurrently inhibiting the T state HbS polymerisation. Furthermore, vanillin is an extremely good candidate as an anti-sickling agent as it is a food additive on the GRAS (generally regarded as safe) list and has little adverse effects at high dosages [130]. However, vanillin has low oral bioavaiability due to rapid decomposition in the digestive tract, and thus a pro-drug of vanillin has been developed. The pro-drug, MX-1520, has been investigated in rodents and shown to be bioavailable after oral administration in rats and still retain its efficacy [131]. 5HMF (figure **6.5 (b)**), another naturally occurring compound, has been reported to inhibit sickling by up to four times more than vanillin [132]. 5-HMF also allosterically shifts O_2 equilibrium curves towards the left and was found to be rapidly absorbed into the bloodstream, binding and modifying HbS molecules at levels as high as 90% without being destroyed in the gastrointestinal tract [132].

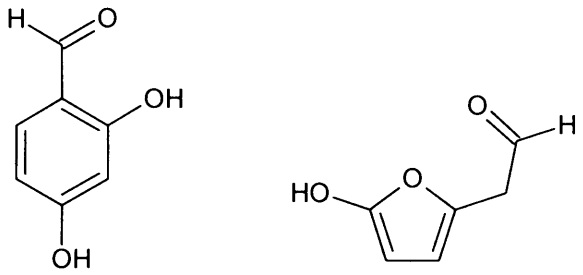

a **b**

Figure 6.5: The structures of **(a)** vanillin and **(b)** 5HMF

Prevention of RBC Dehydration

The formation of dense and dehydrated sickle RBCs play a key role in the initiation of vaso-occlusion as HbS concentration directly impacts on HbS polymerisation. Therefore, hydration of erythrocytes by way of transport pathways that mediate red cell dehydration have led to the development of specific therapies to reduce cell density and HbS polymerisation. Studies have shown that decreasing the MCHC increases the delay time of sickling, providing enough time for cells to return to the lungs and be reoxygenated [114].

Currently, magnesium (Mg) pidolate [133], which increases erythrocyte Mg levels and decreases K^+-Cl^- co-transport activity and cell dehydration, as well as ICA-

17043 [134], which is a potent inhibitor of the Gardos channel thereby preventing Ca^{2+} dependent dehydration of sickle cells, have shown huge promise. Both of these drugs are currently in Phase III clinical trials.

Prevention of RBC Adhesion

Cell injury as a direct result of HbS polymerisation leads to enhanced interaction of sickled cells with the vascular endothelium as well as to other cells such as activated neutrophils. Enhanced RBC adhesion leads to augmentation of vaso-occlusive events and therefore agents which might prevent these adhesive interactions in SCD are being investigated for possible therapeutic use. One such agent is Flocor [135], a complex non-ionic surfactant block copolymer, which decreases RBC aggregation and friction between RBCs and vessel walls by blocking cell-cell or cell-protein interactions.

Gene Therapy

Gene therapy represents a vital hope for SCD cure in the long term and recent improvements in vector design have fuelled interest in gene therapy approaches to the treatment of SCD. However, this type of therapeutic strategy falls outside the remit of this thesis and therefore will not be discussed in further detail. For a concise review on this topic the reader is directed to a publication by Abdulmalik *et al.* [114].

6.5 Use of Compounds which Modify HbS Protein Structure or Composition

The thin layer Pt matrix electrochemical cell was used to test compounds which acted through covalent modification of HbS protein. Two compounds, vanillin and 5HMF, were investigated to show that our system could be used to test for compounds which specifically disrupt the aggregation process. Whereas in the literature the effect of these compounds on the O_2 affinity of the protein, through a reduction in the P_{50} value, was used to measure the efficacy, our system used a light scattering method where growth in protein was reflected by an increase in turbidity. Furthermore, the effect of different proportions of HbS was investigated using the Pt matrix cell by modifying the composition of HbS to HbA in the solution mixture. The experiments performed in this chapter were only preliminary investigations and not a detailed study of any particular therapeutic strategy due to the time constraints.

6.5.1 Vanillin

Vanillin was added to a polymerising solution mixture composed of 75 mg cm^{-3} (1.16 mM) HbS protein and 0.5 M NaCl dissolved in 1.5 M, pH 7 phosphate buffer and the experiments were performed at 38 °C. Vanillin was incubated in the protein solution prior to the start of the experiment for 5 minutes to allow chemical modification of the protein structure to occur. Figure **6.6** presents the turbidity profiles of HbS solutions containing different concentrations of vanillin as well as control experiments performed with HbA and free vanillin.

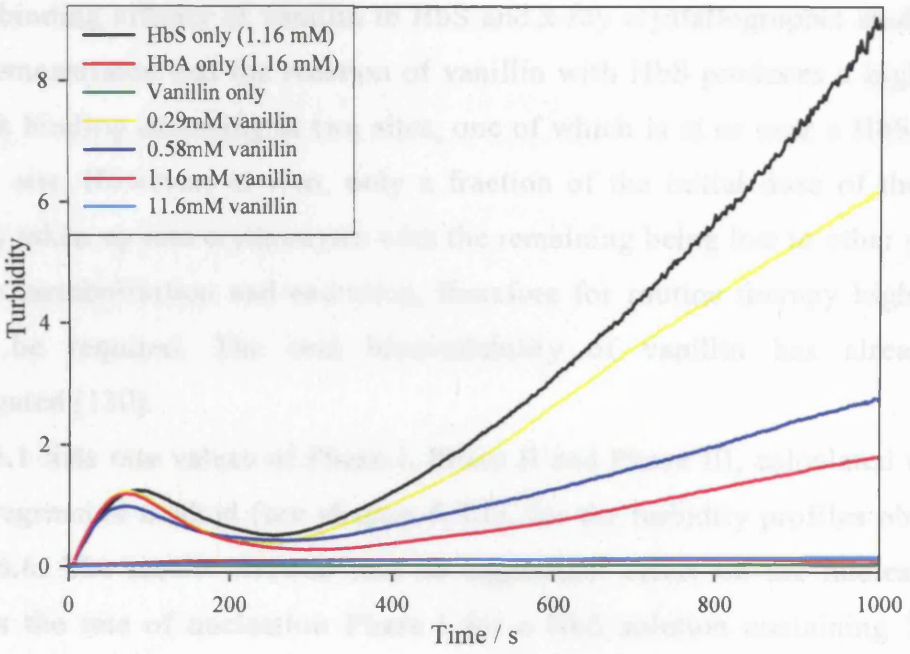

Figure 6.6: UV-visible spectroelectrochemistry time traces showing changes in turbidity at 700 nm at the Pt matrix electrode for different concentrations of vanillin. Experiment conditions: HbS concentration 75 mg cm^{-3} (1.16 mM); various concentrations of vanillin (see figure legend); 1.5 M pH 7.0 phosphate buffer; 0.5 M NaCl; T = 38 °C; E = - 0.55V *vs.* Ag/AgCl. HbA concentration of 75 mg cm^{-3} (1.16 mM) was used for control experiments.

An increase in vanillin concentration was seen to cause a decrease in the nucleation and growth turbidity levels. No delay time was noticeable for any of the turbidity profiles, with vanillin concentrations up to 1.16 mM showing a rapid increase in turbidity as soon as the experiment started. However, significant differences were seen in the growth levels. The maximum turbidity level (turbidity at 1000 s) for a solution containing HbS only (i.e. no vanillin) decreased one and a

half fold when 0.29 mM concentration of vanillin was added, whilst a five fold decrease in turbidity was seen when an equimolar vanillin concentration of 1.16 mM was added. Furthermore, increasing the concentration of vanillin by a factor of ten to 11.6 mM saw a sixty nine fold decrease in the turbidity. Moreover, the presence of the intermediary phase II was seen with the turbidity profiles at low concentrations of vanillin and at vanillin concentrations of 5.80 mM and 8.70 mM (data not shown), suggesting that although a decrease in protein growth was seen, even at these high concentrations a significant nucleation phase was present. A total disappearance of the nucleation and growth phases was seen once vanillin concentration had been increased to 11.60 mM. Therapeutic efficacy would depend on the binding affinity of vanillin to HbS and x-ray crystallographic studies [130] have demonstrated that the reaction of vanillin with HbS produces a high affinity Hb with binding occurring at two sites, one of which is at or near a HbS polymer contact site. However, *in vivo*, only a fraction of the initial dose of the drug is actively taken up into erythrocytes with the remaining being lost to other processes such as metabolisation and excretion, therefore for routine therapy high dosages would be required. The oral bioavailability of vanillin has already been investigated [130].

Table **6.1** lists rate values of Phase I, Phase II and Phase III, calculated using the linear regression method (see chapter **5.5.1**), for the turbidity profiles obtained in figure **6.6**. The results showed that no significant effect on the nucleation was seen, as the rate of nucleation Phase I for a HbS solution containing 1.16 mM concentration of vanillin was 31 ms^{-1}, whilst for a HbS solution containing no vanillin it was 26 ms^{-1}. Furthermore, decreasing the vanillin concentration to a quarter of the concentration of HbS (0.29 mM) showed a similar rate for the nucleation phase. The decrease in the turbidity level with increasing vanillin concentration was reflected more clearly by the Phase III growth rate values, as the growth rate for a HbS only experiment was 11.7 ms^{-1} whilst for 1.16 mM vanillin it decreased to 2.94 ms^{-1}.

Vanillin concentration / mM	Rate of Phase I / s^{-1}	Rate of Phase II / s^{-1}	Rate of Phase III / s^{-1}
0 (HbS only)	26.1 (± 0.51) x 10^{-3}	-5.83 (± 0.12) x 10^{-3}	11.7 (± 0.08) x 10^{-3}
0.29	30.0 (± 0.40) x 10^{-3}	-8.74 (± 0.09) x 10^{-3}	9.63 (± 0.06) x 10^{-3}
0.58	32.0 (± 1.08) x 10^{-3}	-5.40 (± 0.16) x 10^{-3}	2.94 (± 0.01) x 10^{-3}
1.16	31.3 (± 0.54) x 10^{-3}	-8.43 (± 0.12) x 10^{-3}	2.67 (± 0.02) x 10^{-3}

Table 6.1: Rate values for Phase I, Phase II and Phase III calculated using linear regression analysis for vanillin concentration in the range 0.29 mM and 1.16 mM at a Pt matrix electrode surface. HbS concentration 75 mg cm^{-3} (1.16 mM); various concentrations of vanillin; 1.5 M pH 7.0 phosphate buffer; 0.5 M NaCl; T = 38 °C; E = - 0.55V *vs.* Ag/AgCl.

Another study was performed with vanillin to investigate the effect of adding vanillin (of concentration 11.60 mM) to an already polymerising HbS solution at different points in the lifecycle of HbS aggregation. Consequently, vanillin was injected into the electrochemical cell at four stages: the early nucleation stage (before 70 s); at the cusp of the intermediary Phase II (between 75 s to 85 s); at the bottom of the trough seen in the turbidity profile before the beginning of Phase III (at 250 s); and in the middle of the elongation Phase III (after 300 s). The results seen in figure **6.7** showed that the injection of vanillin at all four points in the experiments all led to a sudden decrease in the turbidity levels. Although, a small decrease in turbidity was predicted straight after the injection of the solution due to disruption of the polymers decreasing light scattering, it was thought that an increase in turbidity would follow soon after with the polymers reassembling. However, this was not seen, and all experiments showed a dramatic loss in protein growth no matter at which point the vanillin was added. This could not have been due to a diluting factor as the same amount of vanillin solution, to what was already present in the cell, was added. These set of experiments were performed to

ascertain if covalent modification by Schiff base linkage affected all stages in the polymerisation life cycle, or whether certain points in the polymerisation process showed irreversibility. It is hoped that these preliminary experiments will form the basis for future studies which will help to identify those who would be best suited to this type of therapy.

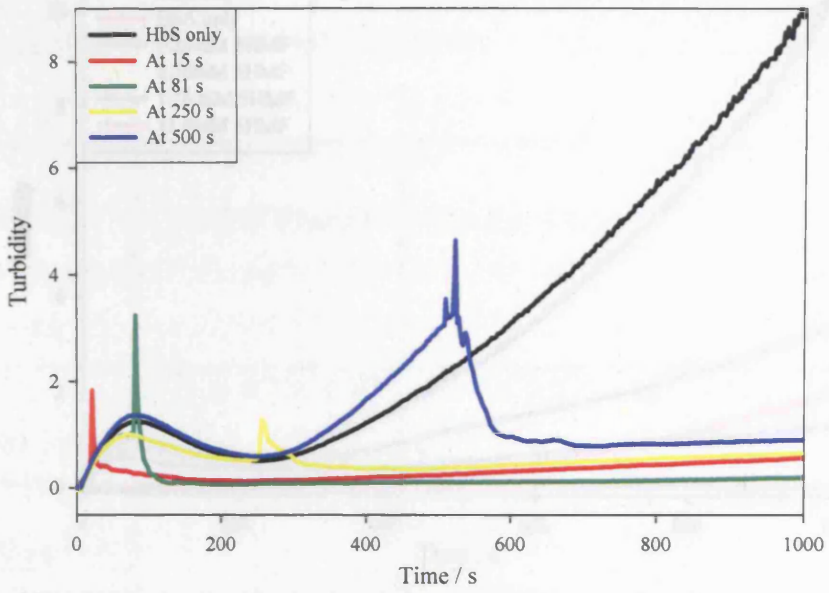

Figure 6.7: UV-visible spectroelectrochemistry time traces showing changes in turbidity at 700 nm at Pt matrix electrode when vanillin was added at different points in the aggregating system. Experiment conditions: HbS concentration 75 mg cm^{-3} (1.16 mM); 1.5 M pH 7.0 phosphate buffer solution (100µl); 0.5 M NaCl; T = 38 °C; E = - 0.55V *vs.* Ag/AgCl. Vanillin concentration 11.6 mM in 1.5 M pH 7.0 phosphate buffer solution (100µl) added at 15 s, 81 s, 250 s and 500 s.

6.5.2 5HMF

The same set of experiments performed previously with vanillin was performed with another naturally occurring carbonyl compound, 5HMF, which has shown to be far more efficacious than vanillin in literature [132].

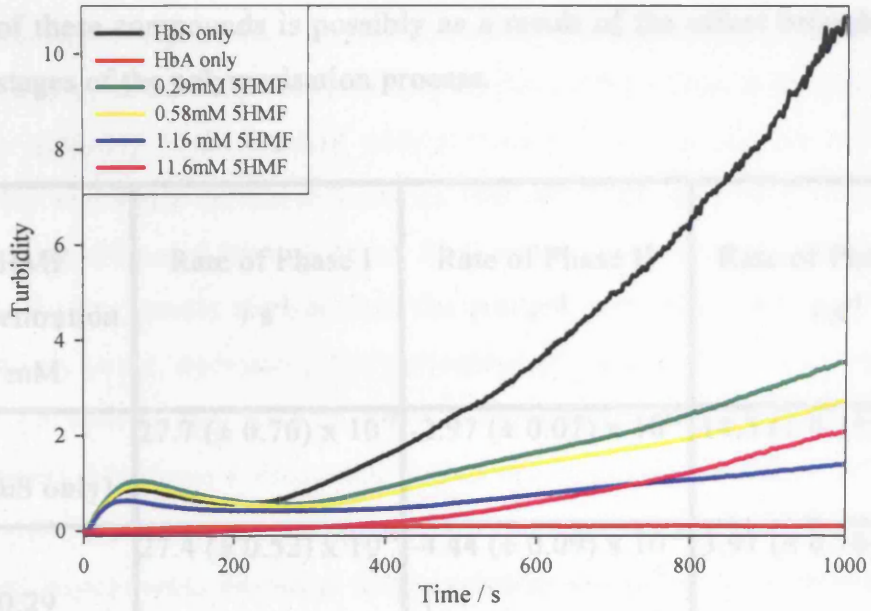

Figure 6.8: UV-visible spectroelectrochemistry time traces showing changes in turbidity at 700 nm at Pt matrix electrode for different concentrations of 5HMF. Experiment conditions: HbS concentration 75 mg cm^{-3} (1.16 mM); various concentrations of 5HMF; 1.5 M pH 7.0 phosphate buffer; 0.5 M NaCl; T = 38 °C; E = - 0.55V *vs.* Ag/AgCl. HbA concentration of 75 mg cm^{-3} (1.16 mM) was used for control experiments.

Figure **6.8** shows the changes in the turbidity profiles of HbS protein when different concentrations of 5HMF were added. Increasing the concentration of 5HMF caused a significant decrease in the growth phase of HbS protein aggregation. This was exemplified by the eight fold decrease in maximum turbidity seen with the addition of an equimolar concentration of 1.16 mM 5HMF compared with a HbS only solution. Furthermore, a quick comparison shows that only a five fold decrease in the maximum turbidity was seen with the same concentration of vanillin (i.e. 1.16 mM) compared with the eight fold decrease seen with 5HMF. This however was not true for all concentrations as the turbidity decreased by sixty nine times for 11.6 mM of vanillin but only a mere five fold reduction was seen for 5HMF at the same concentration.

The nucleation phase, as shown by the rate calculations shown in table **6.2**, did not show much variation for low concentrations of 5HMF. However, whereas most of the turbidity profiles showed a large increase in turbidity followed by the intermediary Phase II process, the profile for 11.6 mM 5HMF exhibited a clear time delay of 177 s. Moreover, the nucleation Phase I rates seen for 5HMF in table **6.2** are very similar to the Phase I rates seen for vanillin showing that the differing efficacy of these compounds is possibly as a result of the effect brought about in the later stages of the polymerisation process.

5HMF Concentration / mM	Rate of Phase I / s^{-1}	Rate of Phase II / $^{-1}$	Rate of Phase III / s^{-1}
0 (HbS only)	27.7 (± 0.76) x 10^{-3}	-2.97 (± 0.07) x 10^{-3}	14.3 (± 0.15) x 10^{-3}
0.29	27.4 (± 0.52) x 10^{-3}	-4.44 (± 0.09) x 10^{-3}	3.91 (± 0.16) x 10^{-3}
0.58	24.3 (± 0.34) x 10^{-3}	-4.00 (± 0.08) x 10^{-3}	3.64 (± 0.02) x 10^{-3}
1.16	23.7 (± 0.66) x 10^{-3}	-1.91 (± 0.05) x 10^{-3}	1.63 (± 0.01) x 10^{-3}
11.60			2.75 (± 0.02) x 10^{-3}

Table 6.2: Rate values for Phase I, Phase II and Phase III calculated using linear regression analysis for 5HMF concentration in the range 0.29 mM and 11.6 mM at a Pt matrix electrode surface. HbS concentration 75 mg cm^{-3} (1.16 mM); various concentrations of 5HMF; 1.5 M pH 7.0 phosphate buffer; 0.5 M NaCl; T = 38 °C; E = - 0.55V *vs.* Ag/AgCl.

6.5.3 Different Proportions of HbS

Another strategy which was investigated using the thin layer Pt matrix electrochemical cell was measuring the protein growth obtained from solutions composed of different ratios of HbS and HbA. Consequently, five solutions consisting of 0% HbS (or 100% HbA), 25% HbS, 50% HbS, 75% HbS and 100% HbS (or 0% HbA) were tested and the results are shown in figure **6.9**. As studies [34] have shown, the presence of other Hb variants in mixtures with HbS generally has the effect of increasing the solubility of deoxyHbS. This is because the HbS molecular crowding is diminished with a variable intracellular Hb composition, and thus the molecular collisions between HbS particles are fewer. Consequently, increased proportions of HbA, HbF or HbC results in decreased clinical severity (section **6.4**). The results showed that the greatest protein growth was seen with 100% HbS. However, decreasing the percentage of HbS by 25%, or in other words having a 75% HbS to 25% HbA ratio saw the maximum turbidity level decrease by nearly thirteen fold from a value near 1.0 to one below 0.1. Further reductions in the ratio of HbS only caused small decreases in the turbidity. These were preliminary experiments designed to test whether any effect was present. Further work will be required to ascertain the mechanisms as well as detailed contributions of the presence of other Hb mixtures.

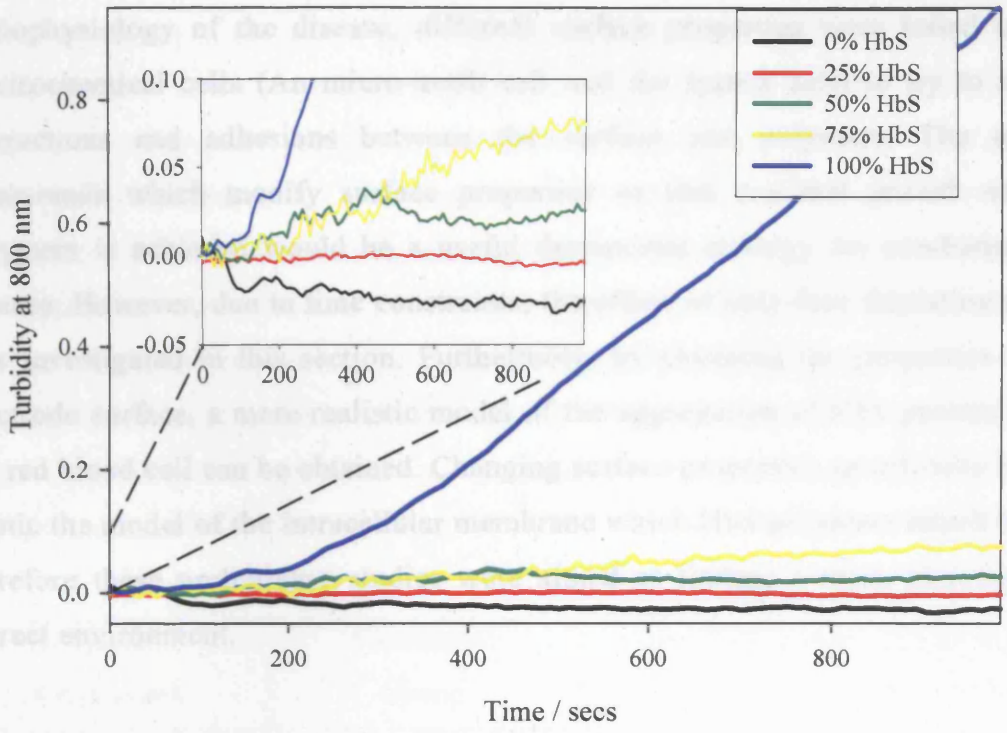

Figure 6.9: UV-visible spectroelectrochemistry time traces showing changes in turbidity at Pt matrix electrode for different proportions of HbS. Experiment conditions: total protein concentration 60 mg cm^{-3}; 1.5 M pH 7.0 phosphate buffer; 0.5 M NaCl; T = 38 °C; E = - 0.55V *vs.* Ag/AgCl; proportions of HbS: HbA = 0%;100% (60 mg cm^{-3} HbA); 25%:75% (15 mg cm^{-3} HbS: 45 mg cm^{-3} HbA); 50%:50% (30 mg cm^{-3} HbS: 30 mg cm^{-3} HbA); 75%:25% (45 mg cm^{-3} HbS: 15 mg cm^{-3} HbA); 100%:0% (60 mg cm^{-3} HbA).

6.6 Use of Compounds which Modify Surface Properties

As the damage of the plasma membrane *in vivo* has a big impact on the pathophysiology of the disease, different surface properties were tested in two electrochemical cells (Au micro-mesh cell and Au matrix cell) to try to reduce interactions and adhesions between the surface and polymers. The use of compounds which modify surface properties so that minimal growth of HbS polymers is achieved would be a useful therapeutic strategy for combating this disease. However, due to time constraints, the effect of only four thiolating agents was investigated in this section. Furthermore, by changing the properties of the electrode surface, a more realistic model of the aggregation of HbS protein inside the red blood cell can be obtained. Changing surface properties specifically tries to mimic the model of the intracellular membrane which HbS polymers attach to, and therefore these preliminary studies were aimed at finding a more physiological correct environment.

6.6.1 Effect of changing surface properties on the Growth of HbS Aggregates in Au matrix cell

An investigation of the effect of surface modification on HbS protein aggregation was performed at an Au matrix cell by thiolating the Au surface with different thiol-based compounds. The compounds used were 3-mercapto-1-propenesulfonic acid, 2-mercaptoethanol, 1-butanethiol and cystamine dihydrochloride (the structures of these compounds are shown in figure **6.2**). Each specific thiol compound provided a varied surface such that the effect of a range of different surfaces on HbS polymerisation could be investigated. Thus, thiolating with 3-mercapto-1-propenesulfonic acid provided a SO_3^- end group giving the surface a negatively charged functionality, see table **6.3** for a description of each thiol group and its functionality.

Thiol Compound	Functional Group	Functional group at pH 7	Functionality at pH 7
3-mercapto-1-propenesulfonic acid	$-CH_2-CH_2=C-SO_3^-$	$-CH_2=CH_2-C-\mathbf{SO_3^-}$	Negatively charged
2-mercaptoethanol	$-CH_2-CH_2-OH$	$-CH_2-CH_2-\mathbf{OH_2^+}$	Hydrophilic
1-butanethiol	$-CH_2-CH_2-CH_2-CH_3$	$-CH_2-CH_2-CH_2-\mathbf{CH_3}$	Hydrophobic
Cystamine dihydrochloride	$-CH_2-CH_2-NH_2$	$-CH_2-CH_2-\mathbf{NH_3^+}$	Positively charged

Table 6.3: Structure and functionality of the thiol-based compounds used to alter the surface properties of the gold surfaces

In this section the experiments were performed with a Au matrix cell rather than the Pt matrix cell. The matrix cell provided a system in which reduction of O_2 was more efficient than the micromesh cell and thus closer to the physiological reducing power. The Au matrix cell was fabricated specifically for this investigation as the Au surface allowed the surface properties to be easily modified through thiolation of the surface. The Au matrix cell was manufactured in exactly the same way as its Pt counterpart, using an Au sheet of the same dimensions with holes of 350 μm in diameter.

The effect of changing surface properties on the turbidity was investigated at two HbS protein concentrations, 30 mg cm^{-3} and 75 mg cm^{-3}, see figure **6.10**. The Au electrode was incubated in a solution of the thiolating agent and HbS protein dissolved in 1.5 M pH 7.0 phosphate buffer was added to the cell to study the variance in polymer growth and aggregation.

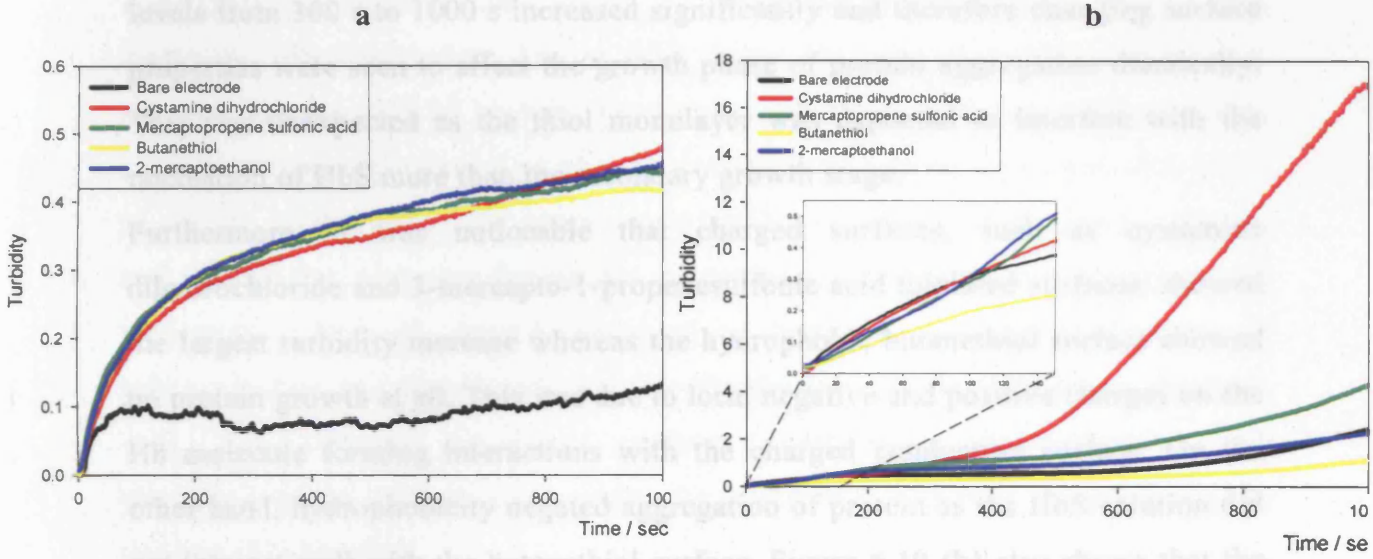

Figure 6.10: UV-visible spectroelectrochemistry time traces showing the effect of different surface properties on changes in turbidity at thiolated Au matrix electrode. Experiment conditions: **(a)** HbS concentration 30 mg cm^{-3} **(b)** HbS concentration 75 mg cm^{-3}; thiol concentration 2mM dissolved in 1.6 mM H_2SO_4; 1.5 M pH 7.0 phosphate buufer; 0.5 M NaCl; T = 38 °C; E = - 0.55V *vs.* Ag/AgCl.

At low protein concentration of 30 mg cm^{-3}, figure **6.10 (a)**, the turbidity profiles showed that changing surface properties seemed to have hardly no effect on the polymerisation process; neither the nucleation nor the growth process changed very much by changing the thiolating agent but all followed a similar aggregation course. Turbidity changes at a bare electrode were minimal compared with thiolated surfaces. All experiments were repeated at least three times and even with multiple repeats similar results were obtained.

Originally it was thought that the similarity in results was due to contamination of one of the thiols, however, the electrode surface was electrochemically cleaned thoroughly with dilute H_2SO_4 between each experiment until the characteristic CV for a clean Au electrode was obtained. Consequently, the similarity of all the turbidity profiles, even when using different thiol functional groups, suggested that

the mechanism of nucleation and growth at low protein concentrations was the same as long as the surface was thiolated.

At high protein concentrations of 75 mg cm^{-3}, figure **6.10 (b)**, the results showed that the initial nucleation phase of protein aggregation did not seem to be affected by changing surface properties; consequently, all turbidity profiles up to 300 s followed a similar course with extremely little growth. However, the turbidity levels from 300 s to 1000 s increased significantly and therefore changing surface properties were seen to affect the growth phase of protein aggregation drastically. This was unexpected as the thiol monolayer was expected to interfere with the nucleation of HbS more than the secondary growth stage.

Furthermore, it was noticeable that charged surfaces, such as cystamine dihydrochloride and 3-mercapto-1-propenesulfonic acid thiolated surfaces, showed the largest turbidity increase whereas the hydrophobic butanethiol surface showed no protein growth at all. This was due to local negative and positive charges on the Hb molecule forming interactions with the charged conducting surface. On the other hand, hydrophobicity negated aggregation of protein as the HbS solution did not interact well with the butanethiol surface. Figure **6.10 (b)** also shows that the early stage of the turbidity profiles of all thiolating agents showed hardly any variation, similar to the results seen at 30 mg cm^{-3}(figure **6.10 (a)**), and changes were only seen in the elongation phase. Consequently, it was shown that changing surface properties had little or no effect on the nucleation but it did affect the rate of polymer growth substantially.

6.6.2 Effect of changing surface properties on the Growth of HbS Aggregates in Au micromesh cell

The effect of altering surface properties on the growth of HbS fibres was also investigated at the Au micromesh cell in the same way as the matrix cell. Consequently, the Au surface was thiolated with the same thiol-based compounds, 3-mercapto-1-propenesulfonic acid, 2-mercaptoethanol, 1-butanethiol and cystamine dihydrochloride. Figure **6.11** shows the rate of turbidity change, a measure of the rate of protein aggregation, at these thiolated surfaces. HbS experiments were performed as normal, consisting of a protein solution with NaCl to aid the conductivity. The results were similar to those seen in figure **6.10 (b)** and showed that changing the surface properties did not seem to affect the initial nucleation phase of protein aggregation, however, the growth phase of polymerisation was significantly altered with the greatest turbidity levels obtained with the charged thiolating surfaces (cystamine dihydrochlorde and mercaptopropene sulfonic acid), whilst the lowest was seen with the hydrophobic surface of butanethiol.

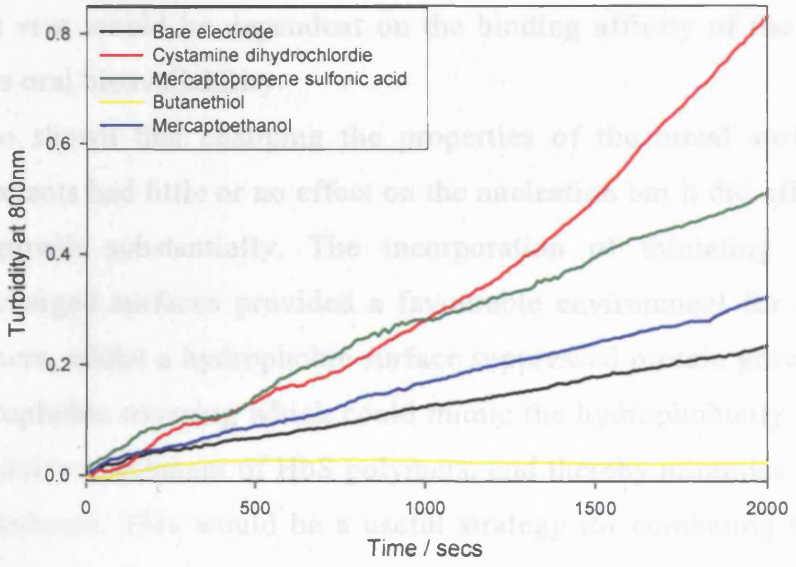

Figure 6.1: UV-visible spectroelectrochemistry time traces showing the effect of different surface properties on changes in turbidity at thiolated Au micromesh electrode. Experiment conditions: HbS 50 mg cm^{-3}; thiol concentration 2mM dissolved in 1.6 mM H_2SO_4; 1.5 M pH 7.0 phosphate buffer; 0.5 M NaCl; T = 38 °C; *E* = - 0.55V *vs.* Ag/AgCl.

6.7 Conclusions

Investigations in this chapter were focussed on using the thin layer electrochemical cell as a novel assay system to investigate the effectiveness of potential anti-sickling agents which cause chemical modification of the HbS structure. It was shown that vanillin and 5-HMF, two naturally occurring cyclic aldehyde compounds whose reported mechanism of action is Schiff base covalent modification of Hb, caused a significant decrease in the polymerisation of HbS aggregates. It was seen that these biological compounds had a pronounced effect on the growth phase of aggregation but not the nucleation phase, as exemplified by the linear regression calculations of phase I and phase III. It was also seen that 5-HMF was more effective than vanillin as equimolar concentrations of vanillin caused a five fold decrease in the turbidity whilst an eight fold reduction was seen with 5-HMF. Furthermore, the addition of vanillin at different points in the polymerisation life cycle was shown to disrupt the subsequent growth of polymers. Consequently, it was demonstrated that a verifiable screening device for investigating compounds as potential agents for disrupting the growth of HbS polymers could be developed. Compounds with a similar mechanism of action could be screened for a reduction in the turbidity levels however any therapeutic efficacy *in vivo* would be dependent on the binding affinity of the compound to HbS and its oral bioavailability.

It was also shown that changing the properties of the metal surface by using thiolating agents had little or no effect on the nucleation but it did affect the rate of polymer growth substantially. The incorporation of thiolating agents which produced charged surfaces provided a favourable environment for the growth of HbS polymers, whilst a hydrophobic surface suppressed protein growth suggesting that a hydrophobic covering which could mimic the hydrophobicity of butanethiol would minimise attachment of HbS polymers, and thereby minimise damage to the plasma membrane. This would be a useful strategy for combating the cascade of events associated with the pathophysiology of this disease. In future it is hoped that a similar set-up can be used to screen multiple compounds for potential efficacy against polymerisation of HbS fibres and even different stages of polymerisation.

Chapter 7: Direct Electrochemistry of HbS Polymers

7.1 Introduction

Hb contains two α subunits and two β subunits, each of which has an electroactive Fe haem group. Although, Hb does not function physiologically as an electron carrier, it is an ideal molecule for the study of electron transfer reactions of haem proteins because of its commercial availability, moderate cost and a known and documented structure. Furthermore, Hb has enzyme like oxidative and reductive catalytic activities, similar to the haem enzyme cytochrome P_{450} [136].

Great efforts in the field of protein electrochemistry have led to a number of studies concerning heterogeneous electron transfer and electrochemical behaviour with Hb being performed at bare electrodes, such as silver [137] and boron doped diamond [138], as well as using mediators and promoters which enhance the electron transfer for Hb. However, only a handful of publications have actually described a behaviour which is consistent with the physiological function: a redox potential around – 70 mV *vs.* SCE and electron transfer rates exhibiting slow irreversible heterogeneous kinetics [139 - 141]. The Hb molecule behaves quite "redox inert" as is reflected by the rate constant of the self exchange of 3×10^{-3} mol^{-1} s^{-1} and the relatively slow oxidation of ferricyanide ($k = 7 \times 10^4$ mol^{-1} s^{-1}) [142, 143].

The facilitation of direct electron transfer between Hb and electrodes is difficult since Hb is a globular oligomeric protein, which may easily poison the electrodes, and the large size of the protein means that the rates of electron transfer between Hb and naked electrodes are extremely slow. Furthermore, proteins are generally irreversibly adsorbed at solid electrodes and to be effective, the native structural and reactivity characteristics of the protein must be retained in the adsorbed state [136, 144]. For large protein molecules such as Hb, the active sites are generally well separated from those in neighbouring molecules so although kinetics of direct electrochemistry tend to be slow due to inaccessibility of the haem active site, the bulkiness of Hb means that no significant changes should occur upon adsorption. However, the structural state of adsorbed bio-macromolecues is still subject to considerable debate.

On the other hand, use of modified electrodes by entrapment within a polymer matrix or thiolation of the surface tends to cause drastic structural changes which are not physiologically relevant as reflected by a fast electron transfer and a

dramatic cathodic shift of the electrode potential. Examples of studies on the electrochemistry of Hb in stable films include the use of bovine Hb-coated polystyrene latex bead films which were prepared and deposited on PG electrodes, showing a pair of well-defined, quasi-reversible CV peaks at about - 360 mV vs. SCE [145] as well as several other studies using ionomer films of Eastman AQ, [146] dimyristoyl phosphatidylcholine [147] and of DDAB-clay [148]. For an excellent review on the topic of direct electrochemistry of Hb the reader is directed to a paper by Scheller *et. al.* titled "Thirty years of Haemoglobin Electrochemistry" [136].

However, although numerous studies have demonstrated direct electron transfer between Hb monomers, to the best of our knowledge there have been no studies performed on the direct electrochemistry of HbS polymers. In this chapter, the direct electrochemistry or the electron conducting properties of HbS aggregates, formed by an *ex-situ* isothermal method, is investigated at a number of different electrodes. In theory, electrochemistry of HbS polymers should be easily achieved with no need for mediators as the spatially linked haem groups and closely aligned HbS active sites in the fibrous state should aid electron transfer.

7.2 Experimental

7.2.1 Materials, Instrumentation and Procedures

Proteins HbS, HbA and haemin were used as supplied. Ag metal wire (grade 1, diameter 0.05 mm), Au metal wire (diameter 0.1 mm, hard temper, 99.99 % purity) and Pt metal wire (diameter 0.1 mm, hard temper, 99.99 % purity) were employed for the fabrication of microelectrodes. A number of bare and modified WE were used to investigate direct electrochemistry of Hb. These can be listed as follows: Au microelectrode; Ag microelectrode; poly-L-lysine (PLL) modified Au microelectrode, 3-mercapto-1-propenesulfonic acid modified Au microelectrode, cystamine dihydrochloride modified Au microelectrode; iota-carrageenans modified Au microelectrode; and Au disk macroelectrode (surface area 0.78 mm^2). The microelectrodes were fabricated by placing an Au or Ag wire through a 5 µl pipette and cleaving the end of the wire to obtain a clean electrode surface. The pipette was subsequently covered with epoxy resin. The PLL-modified electrode was obtained by immersing the electrode in neat PLL for 15 minutes at room temperature and thoroughly rinsing with double distilled water, whilst the thiol-modified electrodes were obtained by immersing the electrodes in an acid solution (1.6 mM H_2SO_4) containing 2 mM thiol compound for two hours, and then rinsing with double distilled water to remove any physisorbed materials. The iota-carrageenan modified electrode was obtained by incubating for 15 minutes in a solution of 0.5 mg cm^{-3} carrageenan and 10 mM KCl dissolved in pure water. All solutions were thoroughly degassed with Ar gas prior to use. Before each modification and experiment the WE was cleaned by electrochemical cycling of H_2SO_4 until no further changes in the voltammetric response could be seen and then it was carefully polished to a smooth surface on silica impregnated with aluminium oxide powder suspensions of decreasing particle sizes of 1 µm, 0.3 µm and 0.05 µm. Finally, the electrodes were cleaned by ultrasonication in double distilled water. CV was performed using a PC operated potentiostat controlled by GPES software, in a three-electrode system with a Pt auxiliary electrode and an Ag/AgCl (3M KCl) reference electrode. Absorption spectra were recorded in a 1 mm glass cuvettes and the temperature was maintained and controlled with the use of a small peltier device. Refer to chapter 2 for a general description of the experimental.

7.2.2 HbS Polymer Formation and Experimental Preparation

HbS polymer formation was achieved using the *ex-situ* isothermal salting out method (experimental procedure **4**) described in chapter **2.5** Degassed phosphate buffer solution (2.42 ml, 2.52 M, pH 7.0) at 38 °C was quickly added to 0.17μM HbS dissolved in 0.025 M phosphate buffer solution also at 38 °C causing HbS protein aggregates to be formed. HbS polymer formation was followed spectroscopically in the UV-visible spectrometer. Spectra's which did not show an increase in absorbance, indicating polymer formation, were not used any further. All solutions were stored under Ar in the fridge until use and used within one day of its initial preparation.

The electrodes were prepared by drop coating small amounts of the fibre solution on to the tip of a clean electrode using a half cut pipette to reduce shear forces. This step was performed several times under an inert atmosphere. The drop coated fibre solution was left in contact with the electrode for 30 minutes and then washed by slowly dipping in deoxygenated pure water and dried by placing the electrode in an Ar environment. It was imperative that the electrode, either before or during the experiment, was not in contact with atmospheric O_2 for long periods, consequently, all solutions were thoroughly degassed prior to use and care was taken to ensure all procedures were performed in an inert environment. During the experiments, Ar gas was bubbled slowly through the buffer solution at a rate which ensured that the solution remained deoxygenated but did not cause vibrations which affected the results. CV potentials ranged from -0.7 V to + 0.8 V for the forward and reverse cycle and were scanned at a rate in the range of 25 mV s^{-1} to 250 mV s^{-1} *vs.* the quasi-reference electrode.

7.3 Direct Electrochemistry of HbS Polymers

Direct Electrochemistry at Bare Electrodes:

Figure **7.1 (a)** shows the CV of HbS polymers at a bare Au microelectrode of diameter 50 μm in a 1.5 M pH 7 phosphate buffer solution at a scan rate of 200 mV s^{-1}. A well-defined reduction peak at around – 184 mV *vs.* Ag/AgCl is observed on the forward scan but no oxidation peak is observable on the reverse scan. The lack of an anodic peak indicates that electron transfer rate is low representing an almost irreversible process. A cathodic shift of more than a 100 mV, compared with the redox potential generally seen for direct Hb monomer electrochemistry (– 70 mV vs. SCE) is observed in our experiments. This shift is slightly less than that expected for a gel-like polymeric material such as HbS polymers as normally, a shift of more than 200 mV is associated with the use of stable polymeric films which immobilise the Hb protein and mediate electron transfer [136]; although ω-hydroxyalkane thiols modified Au electrodes investigating the electrochemical properties of Hb have shown a peak at – 170 mV *vs.* SCE using sodium trifluroacetate as electrolyte at pH 7.1 [149].

Control experiments performed with free HbS monomers at the same electrode surface and under the same conditions did not show any reduction peak in this region confirming that the peak was a result of direct electron transfer between HbS polymers and the Au surface. Control experiments, performed with free HbA and free haemin (CVs not shown) also did not show any peaks whilst the blank phosphate buffer scan showed that this peak was not due to the presence of O_2. All sample preparations and electrochemical measurements were performed under a strict anaerobic environment. These experiments, however, did not allow the mechanism of electron transfer to be investigated in detail and so further work is required in this area.

Figure **7.1 (b)** shows CV's of the same solution of HbS polymers performed one after the other with the latter CV (HbS fibres 2) being performed after a delay of twenty minutes. The reduction peak was present in the first CV but a repeat CV of the same solution performed after twenty minutes showed the disappearance of the peak. This indicated that the polymers adsorbed to the electrode were either breaking away from the surface due to oxidation or were being rendered electrochemically inactive thus blocking the electrochemical response.

SPECIAL NOTE

ITEM SCANNED AS SUPPLIED
PAGINATION IS AS SEEN

increased with more basic solutions compared to acidic ones as a result of more favourable interactions at the electrode surface.

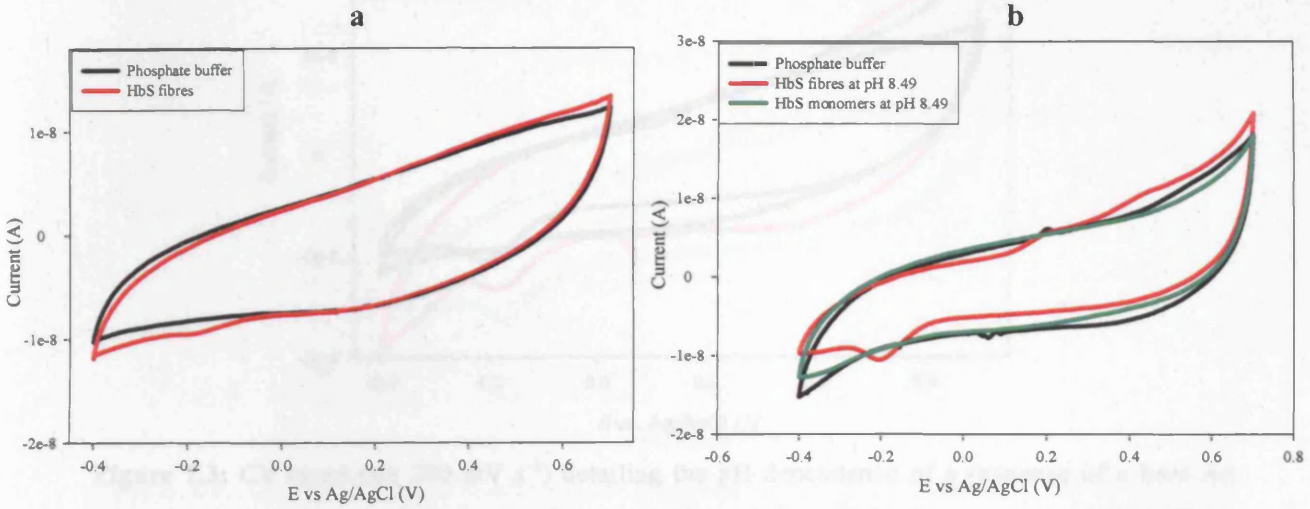

Figure 7.2: CV (scan rate 200 mV s^{-1}) detailing the response of a bare Au microelectrode (diameter 250 µm; surface area 4.91 x 10^4 μm^2) in **(a)** the presence of HbS fibres formed using the *ex-situ* isothermal method in blank pH 6.1, 1.5 M phosphate buffer; and **(b)** in the presence of HbS fibres formed using the *ex-situ* isothermal method and HbS monomers in blank pH 8.49, 1.5 M phosphate buffer. Experimental conditions: HbS concentration 20 mg cm^{-3}, 1.5 M, (pH 6.1 and 8.49) phosphate buffer, temperature 38 °C, dithionite 10 mg ml^{-1}; potential window + 0.7 V to – 0.4 V. All solutions and experiments were thoroughly degassed.

Another interesting point was that increasing the pH of the buffer solution led to a cathodic shift in the potential of the reduction peak, as indicated in figure **7.3** which shows CVs of HbS polymers performed in solutions of pH 6.1, pH 7.0 and pH 8.49. This peak shift was probably due to polymers orientating themselves on the electrode surface in slightly different ways as a result of variances in the surface charge of the polymers at different pHs (pI of HbS = 7.2). Furthermore, the peak shift was another indication of the pH dependence.

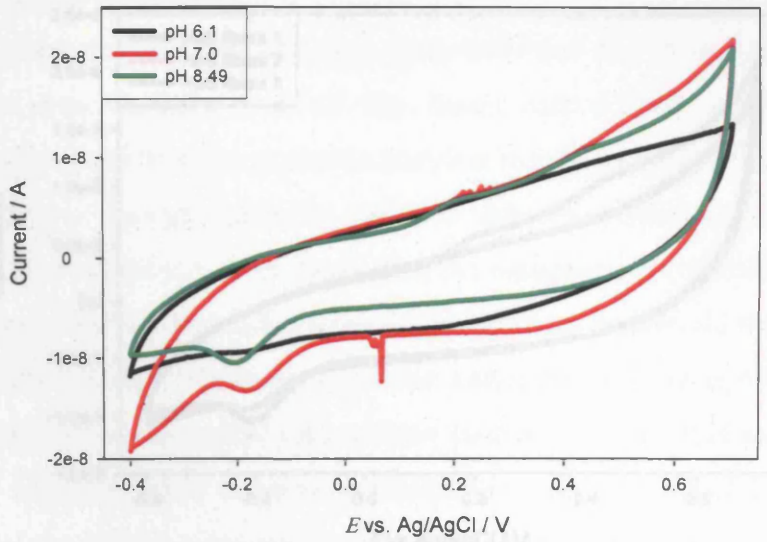

Figure 7.3: CV (scan rate 200 mV s^{-1}) detailing the pH dependence of a response of a bare Au microelectrode (diameter 250 μm; surface area 4.91 x 10^4 μm^2) in the presence of HbS fibres formed using the *ex-situ* isothermal method in blank pH 6.1, pH 7.0 and pH 8.49 (1.5 M) phosphate buffer. Experimental conditions: HbS concentration 20 mg cm^{-3}, 1.5 M, (pH 6.1 and 8.49) phosphate buffer, temperature 38 °C, dithionite 10 mg ml^{-1}; potential window + 0.7 V to – 0.4 V. All solutions and experiments were thoroughly degassed.

Furthermore, figure **7.4** shows a set of three CVs of HbS polymers run in 1.5 M basic phosphate buffer mixture of pH 8.49. These CVs were run straight one after other with the same electrochemical conditions (i.e. the same potential window, + 0.7 V to – 0.4 V, as well as the same scan rate, 200 mV s^{-1}) and showed that over time there was a reduction of 0.2 x 10^{-10} A in the peak size from the first scan to the second scan. No peak shift was noticeable. These results were similar to those seen in figure **7.1 (b)** as they showed a reduction in the peak current over time.

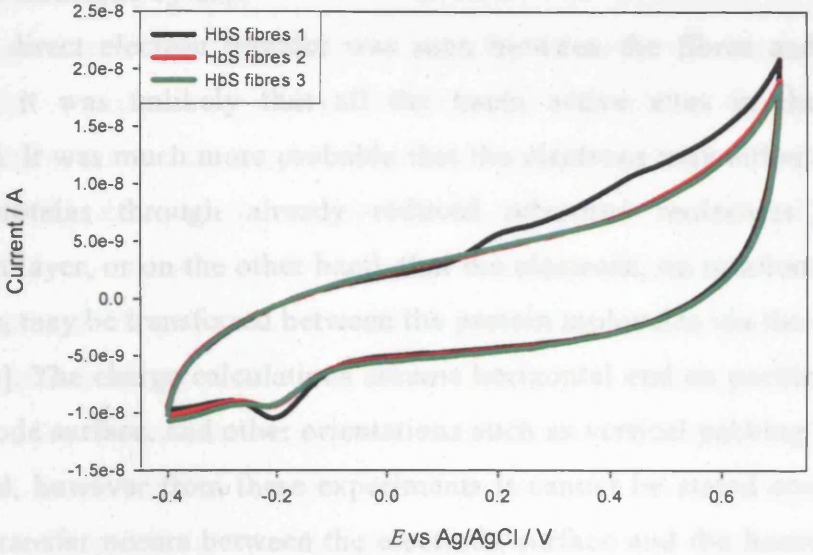

Figure 7.4: CV (scan rate 200 mV s^{-1}) detailing the response of a bare Au microelectrode (diameter 250 μm; surface area 4.91 x 10^4 μm^2) in the presence of HbS fibres at the beginning of the experiment (HbS fibres 1), after 5 minutes (HbS fibres 2) and after 10 minutes (HbS fibres 3) in blank pH 8.49, 1.5 M phosphate buffer. Experimental conditions: HbS concentration 20 mg cm^{-3}, 1.5 M, pH 7 phosphate buffer, temperature 38 °C, dithionite 10 mg ml^{-1}; potential window + 0.7 V to – 0.4 V. All solutions and experiments were thoroughly degassed.

The surface coverage of protein fibres on a Au microelectrode of diameter 250 μm in pH 7 buffer solution (figure **7.1 (a)**) was calculated to be 2.039 x 10^{-5} mol μm^{-2} from the equation:

$$\Gamma = Q / n.F.A$$

where Q is the charge of the peak seen in figure 7.1 (a), calculated to be 5.32 x 10^{-9} C; n is the number of moles of HbS (5.51 x 10^{-14} moles); A is the surface area of the electrode (4.91 x 10^4 μm^2) and F is the Faraday constant.

If HbS fibres (single fibre 21.5 nm wide and 1 μm long) are attached edge on, 178 molecules will be in contact with the electrode (5.4 x 10^{-3} μm per molecule) and therefore for a monolayer, 2289719 x 178 electrons are expected per fibre translating to a value of 6.77 x 10^{-16} moles or a charge of 6.50 x 10^{-11} C. A much higher HbS fibre charge than corresponds to the reduction of one monolayer was obtained by us (5.32 x 10^{-9} C), either due to a very rapid exchange of adsorbed molecules occurring or the charge transfer occurring through several adsorption layers (if the Fe centres were close enough in the fibre to have fast electron

transfer then a charge of 3.3 x 10^{-9} C would be obtained for a bi-layer, similar to the charge measured by us).

Although direct electron transfer was seen between the fibres and the bare Au electrode, it was unlikely that all the haem active sites in the fibres were connected. It was much more probable that the electrons may either be transferred to the proteins through already reduced adsorbed molecules reaching the adsorption layer, or on the other hand, that the electrons, on rotation of the protein molecules, may be transferred between the protein molecules via the exposed haem edge [136]. The charge calculations assume horizontal end on packing of fibres on the electrode surface, and other orientations such as vertical packing have not been considered, however from these experiments it cannot be stated conclusively that electron transfer occurs between the electrode surface and the haem group. Some studies performed previously have suggested that the electrode reaction with haemoproteins involves electron transfer from the electrode to the prosthetic group and not the iron protoporphyrin redox centre [150]. A detailed mechanism of electron transfer between aggregated HbS structures and a naked electrode surface cannot be elucidated with the CV experiments performed in this chapter and further work is required on the direct electrochemistry of HbS polymers to carry forward the work demonstrated in this chapter. Direct electrochemistry experiments were also performed at a bare in-house built Ag microelectrode, similar to the fabrication of the Au microelectrode, but the results did not show any electrochemical behaviour.

Direct Electrochemistry at modified electrodes:

Numerous modified electrodes were fabricated to investigate if facilitation of electron transfer between HbS polymers and the electrode surface is achieved through the use of mediators and promoters. In literature, many studies of Hb electrochemistry have shown that the use of modified electrodes, be it mediator-modified [151], nanoparticle-modified [148] or polymer-modified [152] helps the transfer of electrons but no such studies have been performed for HbS polymers.

Consequently, HbS polymers, formed through the same isothermal salting out method, were drop coated onto Au and Ag microelectrodes modified with PLL, iota-carrageenans and thiolating agents such as cystamine dihydrochloride and 3-mercapto-1-propenesulfonic acid, however, no electrochemical response was observed with any of the modified electrodes. Cystamine dihydrochloride and 3-mercapto-1-propenesulfonic acid were used, as these two thiolating agents had shown the largest increases in protein growth with the Au matrix cell in chapter **6**. Many different conditions were also employed such as dip coating the electrodes into the polymer solution instead of drop coating, using lower salt concentrations and higher temperatures as well as different pH values but again no electrochemistry was observed.

Further work is required to achieve electrochemistry between HbS polymers and modified electrodes. The use of different types of electrodes, such as carbon electrodes, need to be incorporated into these studies, whilst more experiments need to be performed with different thiolating agents. One such study describing the electrochemistry of Hb at L-cysteine modified Ag electrodes, has obtained cathodic and anodic peaks for Hb at potentials around 70 mV and 270 mV vs. Ag/AgCl [150].

7.4 Conclusions

It was demonstrated that the direct electrochemistry of HbS aggregates could be observed at a bare Au microelectrode, confirmed by control experiments with free HbS monomers. A distinct reduction peak was seen but no oxidation peak was present indicating that the electron transfer rate was low representing an almost irreversible process. It was shown that the observation of a cathodic peak was pH-dependent as alkaline pH of 8.49 showed a prominent peak at – 207 mV vs. Ag/AgCl whilst a weak peak at – 182 mV vs. Ag/AgCl was seen in pH 6.1 phosphate buffer. A cathodic shift in the potential of the reduction peak at different pHs was also observed, most probably due to variances in the orientation of polymers on the electrode surface. Furthermore, it was shown that the reduction peak slowly disappeared over time indicating that adsorbed polymers were breaking from the surface or polymers were dissolving as a result of O_2 leakage into the system. Charge and surface coverage calculations indicate either the presence of more than one fibrous layer on the electrode surface or rapid exchange between adsorbed molecules. As a result it cannot be conclusively stated that reduction of haem group as opposed to prosthetic groups is occurring. Experiments performed with modified electrodes did not provide an electrochemical response.

These experiments which exhibited the direct transfer of electrons between polymeric Hb active sites and Au electrode could have a potential application as molecular nano-wires which could undergo reversible and controlled switching between a globular protein and the fibrous state by electrochemical modulation of O_2 partial pressures.

Chapter 8: Concluding Remarks

8.1 Conclusions

A method was devised for monitoring the aggregation of HbS at a conducting surface by electrochemical depletion of O_2 in a series of specially constructed thin layer electrochemical cells. The electrochemical cells consisted of a three electrode system and provided optical transparency and small solution volumes whilst the geometry of the working electrode was found to be essential for the growth of HbS aggregate structures. A matrix geometry composed of an array of small holes was found to deplete O_2 more efficiently than other cells with full depletion occurring within a 100 seconds of the start of the experiment as shown by theoretical modeling. The conditions for reproducible growth of HbS aggregated structures at the Pt electrode were obtained and shown to consist of a high protein concentration (*ca.* 300 mg cm^{-3}) when using the Pt coil cell but much lower (*ca.* 30 mg cm^{-3}) with the Pt matrix cell. High phosphate buffer of 1.5 M (pH 7) with the addition of 0.5 M NaCl salt was also used. NaCl was found to be an important additive as it increased the ionic strength and the conductivity of the solution and also provided a salting-out effect for solubility purposes and the electrode was held at a potential of E = - 0.55 V versus Ag/AgCl, demonstrated by cyclic voltammetry to be situated in the O_2 reduction shoulder.

An understanding of the factors which affect polymerisation at the surface and an insight into the dynamics and mechanism of polymer aggregation was provided by monitoring the extent of polymerisation at an optically transparent electrode using turbidity measurements. The presence of any aggregated protein structures formed at the electrode surface due to electrochemical reduction of O_2 *in situ* was detected as a result of wavelength independent light scattering. The Pt matrix electrochemical cell was employed to investigate the effect of protein concentration, temperature, pH and ionic strength on the gelation of HbS at a conducting surface and the results showed that the kinetics of HbS nucleation and elongation were linearly dependent on the concentration, temperature and ionic strength; an increase in these factors saw a reduction in the time delay and an increase in the growth of aggregation, whilst the protein aggregation was also shown to be favoured by a slightly alkaline pH. Furthermore, most profiles followed the double nucleation mechanism and demonstrated a sigmoidal rate of change in turbidity with an initial lag period where little increase in turbidity was

apparent before large increases were observed. However, experiments performed at certain conditions showed the presence of an intermediary Phase II process in the turbidity profile, consisting of a large decrease in turbidity after the initial nucleation step. This was postulated to be as a result of intermediary aggregates.

The kinetics of polymerisation were investigated using a model for fibrillogenesis describing a two-step process of nucleation followed by elongation and the rate constants at monomer concentration of 300 mg cm^3 were determined to be 9.45 (± 0.08) x 10^{-6} s^{-1} and 1.22 (± 0.03) x 10^{-3} s^{-1} respectively, showing that nucleation was far slower than the growth and thus the rate limiting step.. A similar difference between the rate constants for the nucleation (2.99 (± 0.4) x 10^{-8} s^{-1}) and growth (1.08 (± 0.2) x 10^{-3} s^{-1}) was seen at monomer concentration of 50 mg cm^{-3} HbS. These results obtained from a Au micromesh electrode showed that nucleation was monomer concentration dependent, however growth was largely independent of monomer concentration. A similar pattern was seen with rate constants obtained with the Pt matrix cell; the nucleation rate constant was several orders of magnitude smaller than the elongation rate constant showing that the nucleation process was slower than the growth process. Activation energies for the nucleation and elongation stages of HbS polymerisation were calculated (81.6 (± 1.2) kJ mol^{-1} and 148.2 (± 20.6) kJ mol^{-1} respectively) and compared with the activation energies of another protein polymerising system, β-amyloid fibrillation (311.2 kJ mol^{-1} and 95.3 (± 4.6) kJ mol^{-1} respectively). The ß-amyloid fibril nucleation activation energy was nearly three times larger than the value obtained for HbS protein due to the amyloid monomer undergoing activation through a slow conformational transition. Larger elongation activation energy indicated that nucleation at the surface was more favourable than elongation; however, this could have been due to the initiation of aggregation before the start of the experiment. The Gibbs free energy was also calculated for the nucleation (97.8 (± 20.6) kJ mol^{-1}) and elongation phases (70.3 (± 1.2) kJ mol^{-1}).

Optical microscopy was also coupled with chronoamperometry to visualise the growth of HbS aggregates at a Pt coil electrode. The optical images showed that aggregation occurred only at the surface initially and not in the bulk solution indicating that growth at the surface was thermodynamically more favourable than in solution, whilst polymerisation at the surface was demonstrated to occur in three stages: a time delay when no structures were observed was followed by growth of

fibrous hair-like strands and then globular and gel-like aggregation in the latter stages of the experiment. The optical microscope allowed direct visualisation of the growth of aggregated structures at the electrode, however, the absorption spectroscopy technique permitted a more quantitative approach to monitoring growth compared with optical microscopy, and the increased sensitivity of the absorption spectroscopy technique also allowed the detection of aggregate formation at far lower concentrations.

This methodology was also used as a screening method for drugs that act to alleviate sickle cell crisis by disrupting the nucleation and/or growth of HbS polymerisation *in vivo*. Two naturally occurring cyclic carbonyl compounds, vanillin and 5HMF, were tested in this system and were shown to have a large effect on the elongation phase of polymerisation, demonstrated by a four fold decrease with the addition of vanillin and a nine fold reduction with 5HMF, but no effect was seen in the nucleation phase. Both of these compounds reportedly act by covalently modifying the N terminal of Hb monomers and so should have had a pronounced effect on the nucleation phase, however, the nucleation rate with the addition of vanillin (31.3 ($\pm$ 0.54) x 10^{-3} s^{-1}) and 5HMF (23.7 ($\pm$ 0.66) x 10^{-3} s^{-1}) was found to be similar to a HbS only solution. Similarly, changing the surface properties of the electrode by using thiolating agents was shown to have little or no effect on the nucleation but a substantial effect on the rate of polymer growth. The incorporation of thiolating agents which provided negatively or positively charged surfaces provided a favourable environment for the growth of HbS polymers, whilst a hydrophobic surface suppressed protein growth. The effect of surface properties on protein aggregation was investigated to identify the conditions which cause minimal protein growth and therefore reduce interaction between the surface and polymers.

Direct electrochemistry of HbS fibres was also demonstrated at a Au microelectrode with a reduction peak being observed for the fibres in the region of – 200 mV versus Ag/AgCl. No peak was seen in the background solution or HbS monomer control experiment. A pH dependence on the reduction peak was observed whilst charge and surface coverage calculations indicated a multi-layer deposition of fibres on the electrode. The mechanism of electron transfer could not be elucidated in this study.

This methodology has been used to gain an understanding of the parameters which affect the kinetics and dynamics of HbS polymerisation at a surface compared with free in solution. It has also demonstrated the ability to provide a better understanding of the pathophysiology of SCD *in vivo* and been employed as a screening method for drugs that disrupt nucleation and growth of HbS aggregates and thus could help improve current as well as lead to novel therapeutic strategies for this common and frequently disabling disorder. The electrochemical cell will be utilised to investigate new potential compounds, whose mode of action is specific to the disruption of fibre formation

8.2 Future Work

8.2.1 Characterisation using AFM

There is still a lot of work to be done regarding further characterisation of HbS polymerisation, in particular the dynamics and orientation of polymer growth at a surface. AFM is one technique which can be used to characterise the growth in further detail as the nanometre resolution of this technique allows individual fibres of diameter 21.5 nm to be imaged *in situ* thus allowing the process of polymerisation to be followed in real-time. Although numerous experiments have been performed regarding *ex-situ* AFM imaging of HbS aggregates during the course of this work, further work is required to develop an electrochemical system in which the nucleation and growth of individual HbS fibres, grown through the electrochemical depletion of O_2 at a surface, can be monitored using the AFM. *In-situ* HbS polymerisation imaging with AFM at a surface would allow the fundamental mechanism of polymerisation to be investigated and compared to the established double nucleation mechanism, as well as allow the fundamental properties of HbS nucleation (at short time processes of less than 200 s), such as induction times to be explored in greater detail. Furthermore, AFM would also allow the intermediary phase II seen in chapter 5 to be investigated and any accompanying structural changes at the surface as a result of this phase to be defined. An electrochemical AFM cell for *in-situ* imaging, incorporating a three electrode system similar to those fabricated in this thesis would need to be constructed, requiring a flat conducting surface as the working electrode. The imaging surface needs to be flatter than the sample being imaged, therefore, materials such as atomic gold sputtered on mica or highly orientated pyrolytic graphite (HOPG) surface would be used. The cell would need to be enclosed like a well to keep the HbS solution in constant contact with the electrodes.

The optical microscope experiments have served as a foundation and basis for the visualisation of the growth of HbS fibres, however, further AFM experiments will provide a system in which the reversible and controlled switching between a globular protein and fibrous state by electrochemical modulation can be achieved. Consequently, the kinetic and thermodynamic properties of the fibres grown at an electrode will be determined much more accurately, whilst the investigation of the dynamics and orientation of growth will be augmented using AFM, most probably

through the covalent modification of a gold working electrode. Further characterisation of the kinetics and growth dynamics of HbS polymerisation and a detailed knowledge of polymerisation mechanisms at different interfaces are crucial not only towards the identification of new drug therapies for SCD but also for those processes which have a similar mechanism such as ß-amyloid fibrillisation which is implicated in the development of many neuro-degenerative diseases.

In-situ AFM imaging of sickled RBCs from a normal bi-concave state to the sickled state will also be performed to investigate different aspects of the pathophysiology of the disease such as plasma membrane damage and the increased adhesion of the cells to each other and surfaces. A modified electrochemical cell, fabricated to mimic the narrow capillaries found in the body, will be used for the screening of therapeutic drugs and the analysis of the mechanism of action of biological agents which modify or disrupt the structure of HbS polymers or decrease the adhesion of RBCs to the conducting surface.

8.2.2 Screening for SCA and Anti-sickling Agents

In this thesis, the observation of HbS polymerisation by O_2 depletion in a thin layer electrochemical cell has been demonstrated. Future work in this field would be directed towards developing a medical device in which this system could be used as a diagnostic tool for the detection of the HbS variant and even the severity of the disease, in other words testing whether the subject is a carrier of SCA or has more severe traits. The device would incorporate a three electrode system comprised of indium tin oxide (ITO) conducting glass as the base and working electrode, providing the cell with optical transparency and include a fluorescent tag which would cause fluorescence upon sickling to aid visual detection. The device would hold a thin layer of solution and so would be similar in design to the electrochemical cells fabricated previously; however, lot of work will be required to design a commercially viable cell. Further work will also be performed on finding physiologically relevant conditions for reproducible growth of fibres upon electrochemical deoxygenation.

Currently, newborn babies in England are given screening for sickle cell blood disorders within two weeks of birth using a heel-prick test. However, as it takes approximately twelve weeks for the HbF to be replaced in HbA in newborns this device could be used as a pre-screening test for the parents to establish whether a baby has an increased risk of SCD. This application would be far more useful in developing countries such African countries where there is such a high proportion of babies born with SCD. This method would be far cheaper and quicker than the traditional method of genetic screening.

Another future application of this assay could be to act as a high-throughput screening device where many different compounds are tested simultaneously. The device would be an electrochemical cell similar to the one described above, however, instead of using ITO the working electrode would be composed of multi-well plates with each of the wells acting as individual cells for the testing of different compounds simultaneously. The wells could be pre-treated with compounds such as thiolating agents to increase the extent of HbS aggregation to determine efficacy of the different compounds being tested whilst the metal plates could be heated to change the conditions to physiological temperature. Current fluorescence techniques could be modified to act as a sophisticated and practical

detection method where labelled flourophores could be emitted upon interaction of HbS molecules, causing colouration, whilst the fluorescence could be quenched upon disaggreagation. The effectiveness of current therapeutic compounds that specifically target the aggregation of HbS monomers would be assessed in greater detail and subsequently new potential compounds will be tested in the hope of finding a cure for this debilitating disease. Naturally occurring five-membered heterocyclic aldehydes and its analogues and those compounds which form Schiff base adducts in a symmetrical fashion with the N-terminal αVal1 nitrogens of Hb would be targeted initially. The preliminary work performed in this regard in chapter 6 will aid future studies in this area.

8.2.3 Direct electrochemistry

Further work will also be pursued in investigating the direct electrochemistry of HbS fibres at a number of bare and modified electrode surfaces to determine the electron conducting properties of the fibres. Furthermore, the dependence of fibre conductivity on the conditions of growth will also be investigated in more detail to provide insights into the mechanism of complex biological electron transfer reactions *in-vivo*.

The direct electrochemistry of HbS will be coupled to the orientation of fibre growth work performed using the AFM and the manipulation of growth will be investigated using the incorporation of connecting groups to achieve connectivity and functionality at the fibre ends. A future application for this could be molecular nano-wires which conduct electrical current and be used in molecular electronic devices. The added advantage of HbS fibres as molecular nano-wires is that switching between the globular protein and the fibrous state is relatively easy to achieve through depletion of O_2. Further work regarding the electrochemical characterisation of different surface properties will also be performed. This will be achieved by using thiols and the relevance of this system to a physiological environment will be investigated.

8.3 Summary

Overall, a lot of progress has been made regarding the characterisation of the nucleation and elongation of HbS polymerisation at an electrode surface and also in understanding how they are formed and affected by a number of conditions at a conducting surface. Furthermore, a screening device has also been presented which could be useful to the pharmaceutical industry. However, there is a lot of information still to be obtained and a lot of interesting work yet to be done on utilising the electrochemically modulated growth of HbS polymers in investigating the pathophysiology of SCA in greater detail as well as improving current therapeutic strategies and finding new ones which could aid in finding a cure for this disease.

Chapter 9: References

[1] R.S. Olney. (1999). *Am. J. Prev. Med.*, **16** (2), 116.

[2] F. Haurowtiz. (1938). *Z. physiol. Chem.*, **255**, 264.

[3] http://www.chemistry.wustl.edu/~edudec/LabTutorials/Hemoglobin/MetalComplexinBlood.html

[4] K. Sheng, M. Shariff, R. P. Hebbel (1998). *Blood*, **9**, 3467.

[5] L. Puling, H. A. Itano, S. J. Singer, I. C. Wells. (1949). *Science*, **111**, 543.

[6] V. M. Ingram. (1956). *Nature*, **178**, 792.

[7] L. Sokolov, I. Mukerji. (2000). *J. Phys. Chem. B*, **104**, 10835.

[8] B. C. Wishner, K. B. Ward, E. E. Lattman, W E. Love. (1975). *J. Mol. Biol.*, **98**, 179.

[9] E. A. Padlan, W. E. Love. (1985). *J. Bio. Chem.*, **260** (14), 8280.

[10] D. J. Harrington, K. Adachi, W. E. Royer Jr. (1997). *J. Mol. Biol.*, **272**, 398.

[11] A. Malavalli, B. N. Mansura, J. M. Freidman, A. S. Acharya (2000). *J. Protein Chem.*, **19** (4), 255.

[12] R. Josephs, H. S. Jarosch, S. J. Edelstein (1976). *J. Mol. Biol.*, **102**, 409.

[13] R. H. Crepeau, G. Dykes, R. Garrell, S. J. Edelstein. (1978). *Nature*, **274**, 616

[14] Z. Wong, G. Kishchenko, Y. Chen, R. Josephs. (2000) *J. Struct. Bio.*, **131**, 197

[15] G. Dykes, R. H. Crepeau, S. J. Edelstein. (1979). *J. Mol. Biol.*, **130**, 451.

[16] B. Carragher, D. A. Bluemke, B. Gabriel, M. J. Potel, R. Josephs. (1988). *J. Mol. Biol.*, **199**, 315.

[17] S. J. Watowich, L. J. Gross, R. Josephs. (1993). *J. Struct. Biol.*, **111**, 161.

[18] S. J. Watowich, L. J. Gross, R. Josephs. (1989). *J. Mol. Biol.*, **209**, 821.

[19] I. J. Sherman. (1940). *Bull. Johns Hopkins Hosp.*, **67**, 309.

[20] J. G. Pumphrey, J. Steinhardt. (1976). *Bio. Biophys. Chem. Comm.*, **69** (1), 99

[21] J. G. Pumphrey, J. Steinhardt. (1977). *J. Mol. Biol.*, **112**, 359.

[22] T. E. Wellems, R. Josephs. (1979). *J. Mol. Biol.*, **135**, 651.

[23] W. A. McDade, R. Josephs. (1993). *J. Struct. Biol.*, **110**, 90.

[24] T. E. Wellems, R. J. Vasser, R. Joseph. (1981). *J. Mol. Biol.*, **153**, 1011.

[25] J. Hofrichter, P. D. Ross, W. A. Eaton. (1976). *Proceedings of the Symposium on Molecular and Cellular Aspects of Sickle Cell Disease*, **185**. DHEW Publ. No. (NIH) 76-1007, Bethesda, Maryland.

[26] H. R. Sunshine, J. Hofrichter, F. A. Ferrone, W. A. Eaton. (1982). *J. Mol. Biol.*, **158**, 251.

[27] C. T. Noguchi, D. A. Torchia, A. N. Schechter. (1980). *Proc. Natl. Acad. Sci. USA*, **77**, 5487.

[28] M. A. Goldberg, M. A. Husson, H. F. Bunn. (1977). *J. Bio. Chem.*, **252** (10), 3414.

[29] R. W. Briehl, S. Ewert. (1973). *J. Mol. Biol.*, **80**, 445.

[30] W. A. Eaton, J. Hofrichter. (1990). *Adv. Protein. Chem.*, **40**, 63.

[31] K. Adachi, T. Asakura.(1979). *J. Bio. Chem.*, **254**, 12273.

[32] K. Adachi, T. Asakura.(1980). *J. Mol. Biol.*, **144**, 467.

[33] G. R. Sergeant. (1985). "Sickle Cell Disease". Oxford Univ. Press, London and New York.

[34] N. N. Poillon, B. C. Kim, G. P. Rodgers, C. T. Noguchi, A. N. Schechter. (1993). *Proc. Natl. Acad. Sci. USA*, **90**, 5039.

[35] B. Magdoff-Fairchild, W. N. Poillon, T. Li, J. F. Bertles (1976). *Proc. Natl. Acad. Sci. USA,* **73** (4), 990.

[36] P. D. Ross, A. P. Minton. (1977). *J. Mol. Biol.*, **112**, 437.

[37] F. A. Ferrone, J. Hofrichter, E. A. Eaton. (1985). *J. Mol. Biol.*, **183**, 591.

[38] A. Mozzarelli, J. Hofrichter, W. A. Eaton. (1987). *Science*, **237**, 800.

[39] D. Pletcher, S. Sotiropolous. (1995). J. *Chem. Soc. Faraday Trans.*, **91** (3), 457.

[40] M. S. Turner, J. Wang, C. W. Jones, F. A. Ferrone, R. Josephs, R. W. Briehl. (2002). *Langmuir*, **18**, 7182.

[41] O. Galkin, K. Chen, R. L. Nagel, R. E. Hirsch, P. G. Vekilov. (2002). *Proc. Natl. Acad. Sci. U.S.A.*, **99** (13), 8479.

[42] R. E. Samuel, E. D. Salmon, R. W. Briehl. (1990). *Nature*, **345**, 833.

[43] R. M. Bookchin, T. Baloze, Z. Wang, R. Josephs, V. I. Lew. (1999). *J. Bio. Chem.*, **274** (10), 6689.

[44] K. Adachi, T. Asakura.(1983). *J. Bio. Chem.*, **144**, 467.

[45] O. Galkin, P. G. Vekilov. (2004). *J. Mol. Biol.*, **336**, 43.

[46] J. D. Corbett, W. E. Mickola, M. F. Maestre. (1995). *J. Bio. Chem.*, **270** (6), 2708.

[47] R. W. Briehl. (1995). *J. Mol. Biol.*, **245**, 710.

[48] G Agarwal, J. C. Wang, S. Kuong, S. M. Cohen, F. A. Ferrone, R. Josephs, R. W. Briehl. (2002). *J. Mol. Biol.*, **322**, 395.

[49] A. C. Allison. (1957). *Biochem. J.*, **65**, 212.

[50] J. F. Bertles, R. Rabinowitz, J. Dobler. (1970). *Science*, **169**, 375.

[51] H. R. Sunshine, J. Hofrichter, W. A. Eaton. (1979). *J. Mol. Biol.*, **133**, 435.

[52] P. D. Ross, J. Hofrichter, W. A. Eaton. (1975). *J. Mol. Biol.*, **96**, 239.

[53] G. C. Thompson, M. R. Waterman, G. L. Cottam. (1975). *Arch. Biochem. Biophys.*, **166**, 193.

[54] W. A. Eaton, J. Hofrichter, P. D. Ross, R. G. Tschudin, E. D. Becker (1976). *Biochem. Biophys. Res. Commun.*, **69**, 539.

[55] K. Malfa, J. Steinhardt. (1974). *Biochem. Biophys. Res. Commun.*, **59**, 887.

[56] J. W. Harris,H. B. Bensusan. (1975). *J. Lab. Clin. Med.*, **86**, 564.

[57] S. Kowalczykowski, J. Steinhardt. (1977). *J. Mol. Biol.*, **115**, 201.

[58] K. Moffat, Q. H. Gibson. (1974). *Biochem. Biophys. Res. Commun.*, **61**, 237.

[59] S. J. Gill, R. Spokane, R. C. Benedict, L. Fall, J. Wyman. (1980). *J. Mol. Biol.*, **140**, 299.

[60] S. Basak, F. A.Ferrone, J. T. Wang. (1988). *Biophys. J.*, **54**, 829.

[61] R. W. Briehl, G. W. Christoph. (1987). Exponential progress curves and shear in the gelation of haemoglobin S. In "*Pathophysiological Aspects of Sickle Cell Vaso-Occlusion*" (R. L. Nagel, ed.), **129**. Liss, New York.

[62] M. R. Waterman, G. R. Cottam. (1976). *Biochem. Biophys. Res. Commun.*, **73**, 639.

[63] J. Hofrichter, P. D. Ross, W. A. Eaton. (1974). Kinetic and thermodynamic investigation of deoxyhemoglobin S gelation. In "*Proceedings of the First National Symposium on Sickle Cell Disease*" (J. I. Hercules, A. N. Schechter, W. A. Eaton, R. E. Jackson, eds.), **43**. DHEW Publ. No. (NIH), 75. Bethesda, Maryland.

[64] J. Hofrichter, P. D. Ross, W. A. Eaton. (1974). *Proc. Natl. Acad. Sci. U.S.A.*, **71**, 4864.

[65] F. A. Ferrone, J. Hofrichter, E. A. Eaton. (1976). *Proc. Natl. Acad. Sci. U.S.A.*, **73**, 3034.

[66] F. A. Ferrone, J. Hofrichter, E. A. Eaton. (1985). *J. Mol. Biol.*, **183**, 611.

[67] R. Mircher, F. A. Ferrone. (1997). *J. Mol. Biol.*, **265**, 475.

[68] J. G. Louderback, S. K. Ballas, D. B. Kim-Shapiro. (1999). *Biophys.*, **76**, 2216.

[69] F. A. Ferrone, M. Ivanovu, R. Jasuja. (2002). *Biophys.*, **82**, 399.

[70] P. A. Altman, D. S. Ditmer. (1971). *Resp. Circul.*, **498**, 417.

[71] A. Shirayayev, X. Li, J. D. Gunton (2006). J. Chem Phys., 125, 024902

[72] J. D. Corbett, W. E. Mickols, M. F. Maestre (1995). J. Bio. Chem., 270 (6), 2708.

[73] R. W. Briehl, A. E. Guzman. (1994). *Blood*, **83** (2), 573.

[74] H. Wroblowa, Y. L. Pan, J. Razumney. (1976). *J. Electroanal. Chem.*, **69**, 195.

[75] P. P. Birkin, J. M. Elliot, Y. E. Watson. (2000). *Chim. Commun.*, 1690.

[76] N. M. Markovic, T. J. Schmidt, V. Stamenkovic, P. N. Ross. (2001). *Fuel Cells*, **1** (2), 105.

[77] D. Pletcher, S. Sotiropolous. (1995). J. *Chem. Soc. Faraday Trans.*, **91** (3), 457.

[78] R. W. Zurilla, R. K. Sen, E. Yeager. (1978). *J. Electrochem. Soc.*, **125** (7), 1103.

[79] Southampton Electrochemistry Group, Southampton University. *Instrumental Methods in Electrochemistry*: 2nd Edition (1993) Ellis Horwood Limited. Ashford Press: Southampton.

[80] A.C. Fisher. Electrode Dynamics: 1st Edition (1996) Oxford University Press: Oxford.

[81] K. Adachi, T. Asakura. (1981) *J. Biol. Chem.*, **256** (4), 1824.

[82] Anderson et al (1994) *Art. cells, blood subs., and Immob. Biotech*, **22** (3), 753.

[83] L. Stryer, *Biochemistry*, 4th Edition, (1995). W. H. Freeman and Company, New York.

[84] D. Barham and P. Trinder (1972) *Analyst*, **97**, 142.

[85] W. N. Poillon, J. F. Bertles. (1979). *J. Biol. Chem.*, **254**, 3462.

[86] http://www.nlm.nih.gov/medlineplus/ency/article/003648.htm

[87] R. G. Bates, C. A. Vega, D. R. White, Jr, (1978) *Anal. Chem.*, **50** (9), 1295.

[88] M. Kamihira, A. Naito, S. Tuzi, A. Y. Nosaka, H. Saito, (2000) *Protein Sci.*, **9**, 867.

[89] http://www.rsc.org/suppdata/AN/b6/b613381a/index.sht

[90] K. Adachi, T. Asakura (1979) J. Bio. Chem., 254 (16), 7765.

[91] L. O. Tjernberg, A. Tjernberg, N. Bark, Y. Shi, B. P. Ruzsicska, Z. Bu , J. Thyberg, D. J. E. Callaway (2002) *Biochem. J.*, **366**, 343.

[92] T. Arai, G. Freddi, R. Innocenti, M. Tsukada (2004). *J. Appl Polym Sci.* **91**, 2383.

[93] R. Sabate', M. Gallardo, J. Estelrich (2003) *Biopolymers (Peptide Sci.)*, **71**, 190.

[94] M. Kamihira, A. Naito, S. Tuzi, A. Y. Nosaka, H. Saito (2000) *Protein Sci.*, **9**, 867.

[95] A. C. Allison. (1957). *Biochem. J.*, **65**, 212.

[96] P. J. Mcquilney, P. W. Kuchel (1999) *Biochem. J.*, **342** (3), 597.

[97] A. Fick (1855) Phil Mag., **10**, 30.

[98] A. Fick, (1855) *Poggendorffs Annel. Physik.*, **94**, 59.

[99] J. A. V. Butler (1924). *Trans. Faraday Soc.* **19**, 734.

[100] T. Erdey Gruz, M. Volmer (1930), *Z. Physik. Chem.*, **150A**, 203

[101] D. Lide (editor). *CRC, Handbook of Chemistry and Physics*, 75th Ed. (1994/95), CRC Press: Cleveland, OH.

[102] S. Arrhenius (1889). *Zeitschrift für physikalische Chemie* **4**, 226ff

[103] R. Sabate, M. Gallardo, J. Estelrich (2005) *Int. J. Bio. Macromol.* **35**, 9.

[104] Y. Kusumoto, A. Lomakin, D.B. Teplow, G.B. Benedek, (1998) Proc. Natl. Acad. Sci. USA. 95, 12277.

[105] B.M. Taylor, R.W. Sarver, G. Fici, R.A. Poorman, B.S. Lutzke, A. Molinari, T. Kawabe, K. Kappenman, A.E. Buhl, D.E. Epps (2003). *J. Protein Chem.* **22**, 31.

[106] W.P. Esler, A.M. Felix, E.R. Stimson, M.J. Lachenmann, J.R. Ghiraldi, Y.A. Lu, H.V. Vinters, P.W. Mantyh, J.P. Lee, J.E. Maggio, (2000). *J. Struc. Biol.* **130**, 174.

[107] J.C. Rochet, P.T. Lansbury Jr., (2000). *Curr. Opin. Struct. Biol.* 10, 60.

[108] T.R. Serio, A.G. Cashikar, A.S. Kowal, G.J. Sawicki, J.L. Moslehi, L. Serpell, M.F. Arnsdorf, S.L. Lindquist, (2002). *Science*, **289,** 1317.

[109] J. M. Hempe, R. D. Craver (2000). *Electrophoresis*, 21, 743.

[110] M. Manno, P. L. San Biagio, M. U. Palma (2004). *Proteins: Structure, Function & Bioinformatics*, 55, 169.

[111] F. Hook, M. Rodahl, B. Kasemo, P. Brezezinski (1998). *Proc. Natl. Acad. Sci. USA*, **95**, 12271.

[112] W. Pan, O. Galkin, L. Filobelo, R. L. Nagel, P. G. Vekilov (2007). *Biophys. J.*, 92, 267.

[113] W. Pan, A. B. Kolomeisky, P. G. Vekilov (2005). *J. Chem. Phys.* **122**, 174905.

[114] O. Abdulmalik, D. Obeng, T. Asakura., (2005). *Expert Opin. Ther. Patents.* **15** (11), 1497.

[115] M. H. Steinberg (2006). *Trends in Pharmalogical Sciences*, 27 (4), 204.

[116] P. S. Frenette, G. F. Atweh (2007). *The Journal of Clinical Investigation*, **117** (4), 850.

[117] R. Hoover, R. Rubin, G. Wise, R. Warren (1979). *Blood.*, **54**, 872.

[118] C. C. Johneskiss, R. L. Ackley, E. P. Orringer, E. A. Wayner, L. V. Parise (1993). *Blood.*, **82**, 3548.

[119] A. I. Khan, C. Drew, S. E. Ball, V. Ball, J. C. Ellory, J. S. Gibson (2004). *Bioelectrochem.*, **62**, 141.

[120] D. Chiu, B. Lubin, B. Roelofsen, L. L. Van Deenan (1981). *Blood.*, **58**, 398.

[121] C. D. Ritter (2002). *Nat. Med.*, 8, 1383.

[122] D. N. Levasseur, T. M. Ryan, M. P. Reilly, S. L. McCune, T. Asakura, T. M. Tornes (2004). *J. Bio. Chem.*, **279** (26) 27518.

[123] M. H. Steinberg (2005). Blood, 105 (2), 441.

[124] F. Rosenthal, I. Wislicki, R. Koller (1928). *Klin. Wochenschr.*, **7**, 972.

[125] S. Charache, M. I. Terrin, R. D. Moore (1995). *N. Engl. J. Med.*, **332** (20), 317.

[126] V. P. Cokic, R. D. Smith, B. B. Beleslin-Cockic (2003). *J. Clin. Invest.*, **111** (2), 231.

[127] J. Jiang, S. J. Jordon, D. P. Barr, M. R. Gunther, Maedah, R. P. Mason (1997). *Mol. Pharmacol.*, **52** (6), 1081.

[128] R. H. Zaugg, J. A. Walder, I. M. Klotz (1977). *J. Bio. Chem.*, **252** (33), 8542.

[129] M. K. Safo, O. Abdulmalik, R. Danso-Danquah, J. C. Burnett, S. Nokuri, G. S. Joshi, F. N. Musayev, T. Asakura, D. J. Abraham (2004). J. *Med. Chem.*, **47**, 4665.

[130] D. J. Abraham, A. S. Mehanna, F. C. Wireko, J. Whitney, R. P. Thomas, E. P. Orringer (1991). *Blood.*, **77** (6), 1334.

[131] C. Ziang, X. Li, L. Lian, Q. Chen, O. Abdulmalik, V. Vassilev, C. Lai, T. Asakura (2004). *Br. J. Haemotol.* **125** (6), 788.

[132] O. Abdulmalik, M. K. Safo, Q. Chen (2005). *Br. J. Haemotol.*, **128** (4), 552.

[133] C. Brugnara, (2003). *J. Pediatr. Hematol. Oncol.*, **25** (12), 927.

[134] J. W. Stocker, L. De Francheschi, G. A. Mcnaughton-Smith, R. Corrocher, Y. C. Beuzard Brugnara, (2003). *Blood*, **101** (6), 2412.

[135] E. P. Orringer, J. F. Casella, K. I. Ataga (2001). *JAMA*, **286** (17), 2099.

[136] F. W. Scheller, N. Bistolas, S. Liu, M. Janchen, M. Katterle, U. Wollenberger (2005). *Adv. Coll. Interf. Sci.*, **116**, 111.

[137] X. Chen, C. Ruan, J. Kong, R. Yang, J. Deng (1998). *Electroanalysis*, **10**, 695.

[138] O. Nekrassova, N. S. Lawrence, R. G. Compton (2004). *Analyst*, **129**, 804.

[139] G-J. A. Vidugiris, V. J. Razumas, A. A. Drungiliene, J. J. Kulys, (1988). *Bioelectrochem Bioenerg*, **19**, 513.

[140] F. Scheller, H. J. Prumke, H. E. Schmidt, P. Mohr (1976). *Bioelectrochem. Bioenerg.*, **3**, 328

[141] K. L. Hanrahan, S. M. MacDonald, S. G. Roscoe (1996). *Electrochim. Acta.*, **41**, 2469.

[142] A. Mauk, H. Gray, (1979). *Biochem. Biophys. Res. Commun.*, **86**, 206.

[143] G. Dryhurst, K. M. Kadish, F. W. Scheller, R. Rennenberg. Biological Electrochemistry, vol. 1. New York: Academic Press; (1982), 398.

[144] F. A. Armstrong (2002). *J. Chem. Soc., Dalton Trans.*, 661.

[145] H. Sun, N. Hu. (2004). *Biophys. Chem.*, **110**, 297.

[146] J. Yang, N. Hu, J. F. Rusling. (1999). *J. Electroanal. Chem.*, **463**, 53.

[147] J. Yang, N. Hu, J. F. Rusling. (1999). *Bioelectrochem. Bioenerg.*, **48**, 117.

[148] X. Chen, N. Hu, Y. Zeng, J. F. Rusling, J. Yang. (1999). *Langmuir*, **15**, 7022.

[149] J. I. Blankman, N. Shahzad, C. J. Miller, R. D. Guiles (2000). *Biochemistry*, **39**, 14806.

[150] M. Katterle, U. Wollenberger, F. W. Scheller (1997). *Electroanalysis*, **9** (18), 1393.

[151] H. Ju, L. Dong, H. Chen (1996). *Anal. Lett.*, **29**, 587.

[152] L. Wang, N. Hu (2001). *Bioelectrochemistry*, **53**, 205.

Appendices

Appendix A: Publication

Electrochemical modulation of sickle cell haemoglobin polymerisation†

Zeshan Iqbal,[a] Rachel McKendry,[b] Michael Horton[b] and Daren J. Caruana*[a]

Received 14th September 2006, Accepted 2nd November 2006
First published as an Advance Article on the web 17th November 2006
DOI: 10.1039/b613381a

Appendix B: Colour enhanced HbS polymer Images published on the front cover of The Analyst

SPECIAL NOTE

THIS ITEM IS BOUND IN SUCH A MANNER AND WHILE EVERY EFFORT HAS BEEN MADE TO REPRODUCE THE CENTRES, FORCE WOULD RESULT IN DAMAGE

The Analyst

Interdisciplinary detection science

www.rsc.org/analyst

Volume 132 | Number 1 | January 2007 | Pages 1–84

ISSN 0003-2654

RSC Publishing

0003-2654(2007)132:1;1-N

Appendix C: "Sickle cell microcell": Article published in Chemical Biology

SPECIAL NOTE

THIS ITEM IS BOUND IN SUCH A MANNER AND WHILE EVERY EFFORT HAS BEEN MADE TO REPRODUCE THE CENTRES, FORCE WOULD RESULT IN DAMAGE

Research highlights

Haemoglobin reduced to provide potential drug screening method

Sickle cell microcell

Reference
Z Iqbal *et al*, *Analyst*, 2007, **132**, 27